OPERATION OF ENERGY MICROGRIDS

A THESIS SUBMITTED TO CARDIFF UNIVERSITY
FOR THE DEGREE OF DOCTOR OF PHILOSOPHY

2010

By
Bieshoy Awad Boutros Awad
School of Engineering

ProQuest LLC
789 East Eisenhower Parkway
P.O. Box 1346
Ann Arbor, MI 48106-1346

Contents

List of Tables

List of Figures

Abstract

An Energy MicroGrid comprises a set of energy networks that serve all the energy needs of its local area. These systems include gas, heat, and electricity networks which are linked together at the district heat station. Electricity demand in this Energy MicroGrid is partially served by local generation (MicroSources).

It is difficult to match local electricity generation to local demand in an Energy MicroGrid. The mismatch between generation and demand causes voltage and frequency excursions that often result in generation curtailment or load shedding. Control systems were investigated to reduce voltage and frequency excursions. Moreover, a strategy of operation that reduces the mismatch between generation and demand was studied.

A voltage control system for the MicroGrid was simulated. This voltage control system coordinates the On-Load-Tap-Changer (OLTC) controller with MicroSource Controllers. Where required, it also coordinates MicroGrids and feeders supplied from the same transformer. This voltage control system allowed MicroSources to increase their active power output without causing large voltage rise.

Frequency response from MicroSources, storage, and loads was employed in a frequency control system for an islanded MicroGrid. Intelligent Load Management Controllers were used to provide the load frequency response. Simulations indicated that this frequency control system was able to regulate the frequency in a model MicroGrid network.

Integrated Operation is a strategy to operate the Energy MicroGrid as an integrated system. In this strategy, a Combined Heat and Power (CHP) plant, an electric water heater, and thermal storage were operated to support both electricity and heat networks of the Energy MicroGrid. An Integrated Optimal Power Flow was formulated and was used to investigate the advantages of this Integrated Operation. Simulations indicated that Integrated Operation minimised generation curtailment and load shedding. It also reduced electricity imported from the main grid and the operating cost.

Declaration

DECLARATION

This work has not previously been accepted in substance for any degree and is not concurrently submitted in candidature for any degree.

Signed ...Beshey Awad.... (candidate) Date ..16/11/2010

STATEMENT 1

This thesis is being submitted in partial fulfillment of the requirements for the degree of PhD.

Signed .Beshey Awad..... (candidate) Date ..16/11/2010

STATEMENT 2

This thesis is the result of my own independent work/investigation, except where otherwise stated. Other sources are acknowledged by explicit references.

Signed ..Beshey Awad..... (candidate) Date .16/11/2010

STATEMENT 3

I hereby give consent for my thesis, if accepted, to be available for photocopying and for inter-library loan, and for the title and summary to be made available to outside organisations.

Signed ...Beshey Awad..... (candidate) Date ..16/11/2010

Copyright

Acknowledgements

I would like to express my gratitude to Prof. Nick Jenkins. His suggestions, guidance, and advice were essential to this work. His encouragement and feedback were of great help in developing my research and personal skills. His help made it easy for me to settle in the UK.

I would like to thank Dr. Janaka Ekanayake and Dr. JianZhong Wu for their help and advice. The support I received from them was important. I also would like to thank Dr. Ahmed Shafiu, Dr. Modassar Chaudry, and Mr. Marc Rees for the useful discussions we had.

I would like to acknowledge my sponsors; the Egyptian Government, the Ministry of Higher Education in Egypt, and the Missions Department for their support before and during the course of my PhD studies. I would also like to acknowledge the Egyptian Cultural Bureau in London for their support during my studies.

I would like to acknowledge the support I received from the EU project More MicroGrids, UKERC, and Cardiff University. This support, in the form of travel money and other research related expanses, was of great help to my PhD studies.

I would like to thank all my friends whose advice and encouragement were of great importance to my work. I would like to express my sincere gratitude to Rose King whose friendship I found really priceless. I am grateful to Dr. Nabil Ackladious who was always there when I needed advice. I want to express my deep appreciation for Dr. Mohammed Anwar for him being a great help for my parents with my paperwork at Benha University while I am in the UK. I would also like to thank Nolan Caliao, Gnanasambandapillai Ramtharan, Kane Lok, Sarah Bellew, Sam Weller, and Ian Moore, for all the help I received from them.

Finally, I would like to thank my parents Alice and Awad, my sister Sylvia and my brother Beman for being very supportive.

List of Publications

Journal Papers

1. **B. Awad**, A. Shafiu, and N. Jenkins, "Voltage control in MicroGrids," *International Journal of Distributed Energy Resources*, vol.4, no.2, pp143-157, 2008.

2. **B. Awad**, J. Wu, and N. Jenkins, "Control of distributed generation,"*Elektrotechnik und Informationstechnik*, vol.125, no.12, December 2008, Springer-Verlag Wien.

3. **B. Awad**, J. Ekanayake, and N. Jenkins, "Intelligent load control for frequency regulation in MicroGrids, " *Intelligent Automation and Soft Computing*, vol. 16, no. 2, pp. 299-314, 2010.

Conference Papers

1. **B. Awad**, M. Chaudry, J. Wu, and N. Jenkins, "Integrated optimal power flow for electric power and heat in a MicroGrid," in 20^{th} *International Conference on Electricity Distribution*, (Prague, Czech Republic), CIRED, June 2009.

2. M. Rees, **B. Awad**, and J. Wu, "Steady state flow analysis for integrated urban heat and power distribution networks," in *Proceedings of the* 44^{th} *International Universities Power Engineering Conference*, (Glasgow, United Kingdom), September 2009.

3. P. Papadopoulos, S. Skarvelis-Kazakos, I. Grau, **B. Awad**, L.M. Cipcigan and N. Jenkins, "Impact of residential charging of electric vehicles on distribution networks, A probabilistic approach," in *Proceedings of the* 44^{th} *International Universities Power Engineering Conference*, (Cardiff, United Kingdom), September 2010, paper accepted for presentation.

Nomenclature

List of abbreviations

AC	Alternating Current
AI	Artificial Intelligence
CERTS	Consortium of Electric Reliability Technology Solutions
CCS	Carbon Capture and Storage
CHP	Combined Heat and Power
CIGRÉ	Conseil International des Grands Réseaux Électriques
DC	Direct Current
DG	Distributed Generation
DER	Distributed Energy Resources
DHS	District Heat Systems
DMS	Distribution Management System
DNO	Distribution Network Operator
EM	Energy Manager
EWH	Electric Water Heater
HVDC	High Voltage Direct Current
ILMC	Intelligent Load Management Controller
IOPF	Integrated Optimal Power Flow
LC	Local Controller
LDC	Line Drop Compensation
LP	Linear Programming
LV	Low Voltage

MC	Machine Controller
MGCC	MicroGrid Central Controller
MILP	Mixed Integer Linear Programming
MO	Market Operator
MV	Medium Voltage
OLTC	On-Load-Tap-Changer
OPF	Optimal Power Flow
PI	Proportional Integral Controller
PLL	Phase Locked Loop
PV	Photo-Voltaic
PWM	Pulse Width Modulation
QP	Quadratic Programming
SLP	Successive Linear Programming
TNO	Transmission Network Operator
TN-C-S	An earthing configuration
TT	An earthing configuration
VPP	Virtual Power Plants

List of Symbols

I	Current magnitude (**A**) or (**p.u.**)
$\mathbf{I}$	Current phasor
i	Instantaneous current (**A**) or (**p.u.**)
B	Imaginary part of an element in the bus impedance matrix
C	Cost (**£**)
c	Price (**£/kWh**)
c_p	Specific heat at constant pressure (**J/kg°C**)
$\cos\phi$	Power factor
D	Pipe diameter (**m**)
E	Energy (**J**)
F	Fuel input (**W**)
f	Frequency (**Hz**)
G	Real part of an element in the bus impedance matrix (**p.u.**)
g	Gravitational acceleration($\mathbf{m/s^2}$)
H_t	Total inertia (**s**)

k	Inverse of the V/Q droop line slope (**VAr/V**)
k_s	Gain of the secondary response of a MicroSource or the Flywheel
L	Pipe length (**m**)
$\dot{m}$	Mass flow rate (**kgs**)
n	Normalisation factor for Q_{OLTC} of a MicroGrid
P	Active power (**W**) or (**p.u.**)
P_{i-max}	Sum of the ratings of MicroSources connected to MicroGrid i
p	static pressure (**Pa**)
p_l	static pressure loss (**Pa**)
p_{cf}	Power compensation factor
Q	Reactive power (**VAr**) or (**p.u.**)
R	Resistance (Ω) or (**p.u.**)
	Slope of the Pf droop characteristic of a MicroSource or the Flywheel (in Chapter 4)
R_{Ci}	Difference between the resistance of the path from MS_C to the transformer and the resistance of the common part of the paths from MS_C and MS_i to the transformer
r_l	Hydraulic resistance ($\mathbf{kg^{-1}m^{-1}}$)
RE	Reynolds Number
T	Temperature (**°C**)
	A 15 minute period (For the frequency control system)
t	Time (**s**) or(**min**)
V	Voltage magnitude (**V**) or (**p.u.**)
V_S	Open circuit voltage of a transformer
$\mathbf{V}$	Voltage phasor
v	Instantaneous voltage (**V**) or (**p.u.**)
w	Weighing factor for the MicroGrid
X	Reactance (Ω) or (**p.u.**)
z	Altitude (**m**)
ρ	Density ($\mathbf{kg/m^3}$)
v	Flow velocity (**m/s**)
ϵ	Surface roughness (**m**)
η	Efficiency
Δ	Change, deviation, or excursion
σ	Standard deviation
λ	Overall heat transfer coefficient per unit length of the pipe (**W/m°C**)

Φ	Thermal power (**W**)
ϕ	Angle between voltage and current phasors (**rad**)
$\hat{x}$	A normalised value of a certain variable x
$\overline{x}$	The average value of a group of variables x

List of Subscripts

0	Nominal value
a	Quantity related to the ambient (for temperature)
a, b, c	a,b,and c components of a voltage or a current phasor
av	An average value
$active$	Active component of a current
B_i	Busbar i
CHP	Quantity related to a CHP unit
CHP_P	Quantity related to the electricity output of a CHP unit
CHP_Φ	Quantity related to the thermal output of a CHP unit
c	critical (for demand)
DC or dc	DC voltage or current
EWH	Quantity related to an EWH
$d, q, 0$	Direct , quadrature and 0 components of a voltage or a current phasor
FW	Value related to the electricity storage unit (the flywheel)
$feeder$	Value defined at the end of a passive distribution feeder
G_i	Generator i
i	imaginary part
in	Quantity related to the inlet of a pipe
L	Quantity related to a district heat load
L_i	Electric load i, thermal load i, or Line i
l	Value related to a section of a transmission line or a feeder
MG	Value related to a MicroGrid
MG_i	Value related to the MicroGrid MG_i
MS_i	Value related to the MicroSource MS_i
MS	Value related to a MicroSource
MS_C	Value related to the Control MicroSource
max	upper limit of a value
min	lower limit of a value
N	Total number of MicroSources in the MicroGrid
N_i	Node i
nc	non-critical (for demand)
$OLTC$	Value related to the On-Load-Tap-Changer
out	Quantity related to the outlet of a pipe
P_i	Pipe i
p	Value defined after the primary frequency response

$-R$	Quantity related to the return line in a DHS
rated	Rated value
r	real part
reactive	Reactive component of a current
ref	Reference value
restore	Value related to load restoration
S	Quantity related to a district heat station
S_i	District heat station i
$-S$	Quantity related to the supply line in a DHS
shed	Value related to load shedding
T	Quantity related to a thermal storage tank
T_i	Thermal storage (hot water tank) i
us	unserved (For the historical unserved energy)
V_i	Virtual generator i (used to simulate load shedding)
Pump	Quantity related to a water pump
$\alpha, \beta, 0$	α,β,and 0 components of a voltage or a current phasor
$-$	Charging (for storage)
	In the negative direction (for pipes)
$+$	Discharging (for storage)
	In the positive direction (for pipes)

Sets of Elements

$\mathbb{E}$	Set of elements (such as pipes, valves, or pumps)
$\mathbb{FROM}$	Set of all pipes supplied by water from a node
$\mathbb{G}$	Set of generators (including virtual generators)
$\mathbb{G}_{B_i}$	Set of generators connected at bus B_i
$\mathbb{L}_i$	Set of heat loads connected at node N_i
$\mathbb{L}_{B_i}$	Set of electric loads connected at bus L_i
$\mathbb{MS}$	Set of all MicroSources in a MicroGrid
$\mathbb{P}+_i$	Set of pipes oriented towards node N_i
$\mathbb{P}-_i$	Set of pipes oriented away from node N_i
$\mathbb{S}$	Set of district heat stations
$\mathbb{S}_i$	Set of district heat stations connected at node N_i
$\mathbb{T}$	Set of time periods
$\mathbb{TO}$	Set of all pipes supplying water to a node
$\mathbb{T}_i$	Set of thermal storage tanks connected at node N_i

Chapter 1

Introduction

1.1 Future Energy Supply Systems

Energy supply systems are undergoing a change in their nature. This change is in response to climate change and fuel security concerns. It is influenced by advances in renewable energy technologies, low carbon technologies, metering and communications and is supported by governments energy policies and strategies.

This change will affect electricity, heating and cooling systems, and gas networks. It will increase the coupling between these systems as well. Moreover, it is likely to increase the need for energy storage.

1.1.1 Electric Power Systems

In the UK, the mix of central electric power generation will be influenced by the Large Combustion Plant Directive [1], the EU Emissions Trading Scheme [2], and the UK Renewables Obligation [3]. Many large coal fired power stations will be shut down. Others will have to be fitted with Carbon Capture and Storage (CCS) facilities [4]. New nuclear power stations are to be built and old ones replaced [4]. Large capacity of renewable generation such as wind farms, tidal power, and large solar generation is to be connected to the network [3, 4].

Most of this generation mix is not flexible. Nuclear power stations and coal power stations with CCS are operated at constant output. The output of renewable generation is largely influenced by weather. Hydro power plants are required to maintain a specified rate of river flow [5].

This limited flexibility will reduce the capability of the central generation to

follow changes in load. It will also increase the difficulty of scheduling reserve and frequency response. Such services will have to be provided partially by storage facilities [6] or by demand side management.

The installed capacity of Distributed Generation (DG) and Micro Generation is expected to increase in response to incentives such as the Feed-In Tariffs in several European countries and the UK Renewables Obligation [3].

Currently, DG is connected to the network and treated as a negative load. It replaces energy generated from central generators but it does not replace their capacity [7]. This leads to a large capacity of central generation running just to provide ancillary services.

DG is tripped after distant faults or disturbances [8] and is then automatically restored once its terminal voltage has been restored [9]. Moreover, under-frequency load shedding relays will trip DG as well as loads [8].

The lack of knowledge about the DG output and the variation in renewable generation reduces the accuracy of security analysis. Networks with high penetration level of DG are expected to suffer security problems [8].

1.1.2 Heat Supply Systems

District Heat Systems (DHSs) are systems where heat is produced at central district heat stations and supplied to consumers through a pipe network. They are in use in several countries [10].

Heat is produced at some district heat station by boilers, Combined Heat and Power (CHP) units, or heat pumps. Other district heat stations use waste heat recovered from large power plants.

DHSs have several advantages compared to domestic heat production. Central production of heat allow the use of fuels such as biomass [11,12] and energy from waste. Boilers and CHP of high ratings are usually more efficient than domestic units. Economics of operation of CHP systems favours the use of a single unit to supply several consumers rather than the use of individual CHP units for each consumer [13].

Derived by the higher efficiency, CHP economics [13], incentives for both alternative fuels and renewable heat [3], DHSs will have an increasing potential in the future energy system.

1.1.3 Energy Storage

There are several drivers for the use of energy storage in power systems [6]. Energy storage facilitates the integration of renewable and intermittent energy resources in power systems. It provides a low emissions solution for spinning reserve. It may be used to relieve congested networks and reduce the need of network reinforcement. It increases security of supply.

Several storage technologies were reviewed in [6]. Pumped hydro and compressed air storage are limited to specific locations. Compressed air storage has low energy storage density. Batteries, super-conducting storage, hydrogen electrolysis/fuel cells systems, and flywheels are expensive. The round trip efficiency of compressed air storage and hydrogen electrolysis/fuel cells systems is limited.

Thermal storage, both hot and cold, was identified to be cost effective [6]. It is relatively cheap and has high energy density. It is suitable for use in locations where heat, or cold, can be consumed locally within a suitable time frame.

1.1.4 Coupling between Different Energy Networks

Energy networks are interlinked. Some items of equipment remove energy from one network, convert it to a different form, and inject it into another energy network. A gas fired CHP unit, for example, links the gas network to both heat and power networks. Other equipment, such as gas compressors in a gas network, consumes energy from one energy network to control another energy network. Figure 1.1 shows some possible links between gas, heat, and electric power systems.

The increase in the number of gas turbines, micro turbines, CHP units, and DHSs increases the coupling between heat, gas, and electricity systems. This increases the potential of alternative storage, such as thermal storage. It also increases the mutual interactions between the different energy systems.

1.2 Operation of Future Energy Supply Systems

Several concepts are being investigated in order to operate the future energy supply systems. Some of these concepts, such as MicroGrids [14–19] and Cells [8], deal with sections of an electric power system. Others, such as Virtual Power

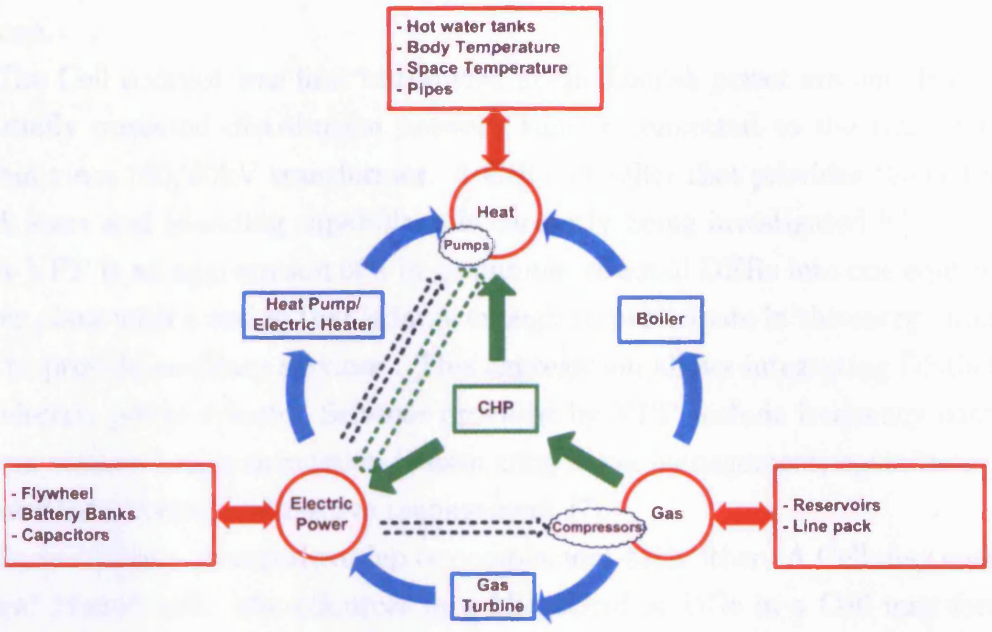

Figure 1.1: Possible links between gas, heat and electric power systems

Plants (VPPs) [7], are concerned with the control of Distributed Energy Resources (DER) which include DG, storage and controllable loads. Finally, the concept of Multi-Carrier Energy Systems [20], deals with the interactions and energy conversion processes taking place at the points were different energy systems in a certain area are coupled.

The concept of Multi-Carrier Energy Systems [20] provides an integrated approach for modelling, optimisation and control of the entire energy supply system. Analysis of these systems emphasises the interactions, mutual effects, and coupling between two or more energy networks.

MicroGrids [14–19] and Cells [8] are sections of an electric power system with high penetration level of local generation. They operate as a part of the whole power system most of the time. If a disturbance occurs, they are able to form an island and carry on supplying their loads. They require black start capabilities in case of a blackout occurs. These emergency functions should increase the supply reliability and system resilience [14, 16].

A MicroGrid is a Low Voltage (LV) network with low rating local generation (MicroSources). It supplies the heat and power needs of the local area [14, 16]. The total demand and the total generation capacity in the MicroGrid are low. The CIGRÉ benchmark MicroGrid [21], for example, has a 100kW peak electric power demand, 63kW of installed MicroSource capacity, and 30kW of electrical

storage.

The Cell concept was first introduced in the Danish power system. It defines a radially operated distribution network that is connected to the transmission system via a 150/60kV transformer. A Cell controller that provides the cell with black start and islanding capabilities is currently being investigated [8].

A VPP is an aggregation of a large number of small DERs into one equivalent power plant with a rating that is large enough to participate in the energy market and to provide ancillary services . This aggregation allows integrating DERs into the electric power system. Services provided by VPP include frequency control, system restoration, transmission system congestion management, optimisation of transmission losses, and reserve management [7].

Some of these concepts overlap or complement each other. A Cell may contain several MicroGrids. MicroSources in a MicroGrid or DGs in a Cell may form a VPP. Also, a MicroGrid may be operated as a Multi-Carrier Energy System. Such combinations allow the exploitation of the complementary advantages and flexibilities offered by the individual concepts.

In this research, an Energy MicroGrid was considered. This Energy MicroGrid is a Multi-Carrier Energy System in which multiple energy networks serve the energy needs of its local area. It is analysed, operated, and controlled using an integrated approach that considers the interactions between the different energy networks. This Energy MicroGrid enjoys the high reliability of a MicroGrid and the flexibility of operation offered by a Multi-Carrier Energy System.

1.3 Electric Power Imbalance in an Energy MicroGrid

In an Energy MicroGrid, some MicroSources use renewables. Others have to follow heat demand rather than electric power demand. They are often unable to provide load following. Moreover, demand variations in a MicroGrid are faster than that in a large interconnected system. This will often cause an imbalance between local generation and local loads. The magnitude of the imbalance will vary with time.

This mismatch between generation and load in a MicroGrid will result in problems such as:

1. Voltage excursions;
2. Frequency excursions during autonomous operation;
3. Generation curtailment when:
   - upper voltage limit is exceeded,
   - generation exceeds demand during autonomous operation, or
   - generation exceeds demand while reverse power flow is not allowed;
4. Load shedding in cases where generation cannot meet the demand during autonomous operation.

In this research, a voltage control scheme for a grid connected MicroGrid was investigated. The purpose of this scheme was to reduce voltage excursions such that MicroSources were able to generate more power without violating the upper voltage limit.

A frequency control mechanism for an islanded MicroGrid was then investigated. This mechanism employed frequency response services from MicroSources, electric storage, and loads.

Finally, the potential of using an integrated approach to operate both heat and electricity networks within the Energy MicroGrid was investigated. The district heat station and the thermal storage were operated to support energy balancing in both networks. This was to improve the utilisation of the energy resources available, reduce power curtailment, and reduce service disruptions.

1.4 Analysis and Decision Making Tools

The research questions outlined were addressed through computer simulations and mathematical models. These models included steady state, optimisation, and transient models. For steady state analysis, Newton-Raphson iterative technique [22] was used. For transient models, the Runge-Kutta based numerical solvers of MatLab Simulink were used.

In all models, some decision making tools were used. Two of these tools use Artificial Intelligence (AI) techniques. These are Rule-Based Systems and Fuzzy Logic Systems. The third tool is Successive Linear Programming (SLP).

1.4.1 Rule-Based Systems

Rule-Based Systems, according to [23], capture the knowledge of a human expert in a specified domain. This knowledge is formulated into an invariant set of "IF ... THEN ... ELSE" rules and implemented in a machine platform. This enables the machine to provide decision support at a level comparable to the human expert.

Rule-Based Systems are suitable for situations where experts are able to create a simple set of rules that explain how they work. More complex systems will often require a larger number of rules which may slow down the speed of the system.

Rule-Based Systems were applied to many areas in power systems [23–27]. These applications include the following:

Planning: AC/DC network design, power plant sitting, and capacitor placement.

Operation: Alarm processing, fault diagnoses, substation switching, daily load forecasting, steady state and dynamic security assessment, maintenance scheduling, network restoration/reconfiguration and load transfer, demand side management, reactive power management and voltage control, distribution automation, protection of HVDC systems, and hydroelectric load dispatching, and automatic fault analysis and fault localization;

Analysis: Control system design, protection coordination, equipment condition monitoring, equipment diagnoses, online plant safety systems, classifying distorted voltage and current waveforms into categories for power quality studies, and harmonic analysis.

1.4.2 Fuzzy Logic Systems

In binary logic, sets and ranges are defined by crisp limits. Variables either belong to or do not belong to a certain range. This undermines the ability of binary logic to deal with systems where ranges are not crisply defined or where they overlap.

Fuzzy logic [23] allows defining ranges where variables can assume partial membership of sets and ranges. This allows fuzzy logic systems to process uncertainties and ambiguities.

Advantages of Fuzzy logic were outlined in [28]. It is efficient in solving problems where functional knowledge is available in terms of heuristic rules. It is suitable for areas in which rules are better described linguistically rather than mathematically or where the assumptions that are made during mathematical modelling obscures the accuracy of the model.

In fuzzy logic systems, raw data inputs are first mapped into fuzzy domain where data is expressed by its degrees of membership in fuzzy sets. Fuzzy rules, which are usually linguistic rules, are then applied and the results are transformed back into real numbers.

Fuzzy logic has several applications in power systems [23, 25, 28, 29]. These applications include the following:

Planning: Generation expansion planning and reliability analysis;

Operation: Reactive power and voltage control, power system stabilizers, frequency control, load forecasting, dynamic generator rescheduling, maintenance scheduling, generation scheduling, unit commitment, economic dispatch, state estimation, optimal power flow, security assessment, fault diagnoses, power system protection and relaying, power system restoration, switching, classifying power quality disturbances and locating their sources;

Analysis: Condition monitoring and control system design, power system stability assessment, load flow studies, diagnosing power quality problems and estimating power quality indices.

1.4.3 Successive Linear Programming

Optimisation is finding the best solution for a certain problem from the domain of all possible solutions. This problem is described mathematically by an objective function and a set of constraints. The objective function defines the optimality criteria while the constraints define the domain of feasible solutions. The objective function and the constraints are functions of the decision variables whose values are the solution of the optimisation problem [5].

A wide range of optimisation techniques is available [5, 30–32]. These techniques are either mathematical or heuristic. Among the mathematical optimisation techniques are Gradient method, Linear Programming (LP), Quadratic Programming (QP), Mixed Integer Linear Programming (MILP) and

Successive Linear Programming (SLP). Example of heuristic techniques include Genetic Algorithms, Simulated Annealing, and Particle Swarm Optimisation. Other AI techniques such as Artificial Neural Networks have some applications in optimisation.

LP [5, 30] is very widely used for problems where the decision variables are real and the objective function and the constraints are linear. MILP is used in cases where some decision variables can only assume integer values. The objective function and the constraints in MILP have to be linear. QP, on the other hand, deal with problems with a quadratic objective function [30].

SLP [32] is used for optimisation problems with nonlinear constraints. In SLP, the nonlinear constraints are linearised around an initial operating point and an LP problem is solved. The results are then validated against the original nonlinear equations. These two steps are repeated till the solution converges.

SLP has been used in power systems in the fields of operational planning and optimal power flow studies as well as in asset planning [33, 34].

1.5 Research Questions Addressed in the Thesis

The main research question addressed in this thesis is the balancing of local generation and local demand in the Energy MicroGrid. This was investigated on three levels.

1.5.1 Voltage Control in MicroGrids

A voltage control system for the MicroGrid was investigated. This control system was based on the availability of a vacuum-switch OLTC for LV transformers. This voltage control system coordinates between the OLTC control and the reactive power control of the MicroSources such that voltage excursions are reduced. This allows MicroSources to inject more power into the MicroGrid without causing a large increase in voltage.

1.5.2 Frequency Control in an Islanded MicroGrid

During an emergency conditions taking place while the MicroGrid is islanded, balance between power generation and demand has to be achieved rapidly in order to maintain frequency at an acceptable level. A frequency control system

for the islanded MicroGrid was investigated. This control system uses frequency response from MicroSources, storage, and non-critical loads to balance generation and demand and maintain frequency within acceptable limits.

1.5.3 Integrated Operation of an Energy MicroGrid

An approach to minimise the imbalance between local generation and local demand was investigated. This approach is based on scheduling the equipment coupling the DHS to the LV network in the Energy MicroGrid as well as thermal storage. An Integrated Optimal Power Flow model was built to assess the effectiveness of this approach.

1.6 The Structure of the Thesis

1.6.1 Energy MicroGrids

Chapter 2 starts with a review of MicroGrids. The different concepts of a MicroGrid, elements constituting them, their management, their operation and their safety were summarised. This concept was further developed into an Energy MicroGrid where all energy networks are coupled together.

As this research investigates the interactions between the power and the heat networks within the Energy MicroGrid, a review of DHSs was undertaken. This review included the various elements of a DHS and their steady state mathematical models.

Finally, the Energy MicroGrid test system that was used for the case studies in this research is described.

1.6.2 Voltage Control in MicroGrids

Chapter 3 is a study of the voltage control in a MicroGrid during grid connected operation. It starts with a brief review of voltage control in distribution networks. A voltage control system for MicroGrids is then discussed. The use of a simple rule-based system in cases where multiple MicroGrids and passive distribution feeders are supplied from the same transformer is explained.

1.6.3 Frequency Control in MicroGrids

Chapter 4 is a study of a frequency control system for an islanded MicroGrid. The frequency targets of this control system is defined. Contribution of MicroSources and storage into frequency response services are discussed. An Intelligent Load Management Controller that uses Fuzzy Logic to control non-critical loads such that they provide frequency response is described.

1.6.4 Integrated Operation of an Energy MicroGrid

Chapter 5 is a study of the benefits offered by using a Multi-Carrier Energy System approach in operating an Energy MicroGrid. A model of an Integrated Optimal Power Flow (IOPF) for heat and electric power in the MicroGrid is formulated. Integrated Operation of the Energy MicroGrid was defined. The advantages of this Integrated Operation was investigated using the IOPF.

1.6.5 Conclusion and Future Work

Chapter 6 concludes this research. It summarises the results of the different chapters. It describes the relation between the outcomes of this research in relation to the current state-of-the-art and in relation to previous research. Research questions that arose from analysing the results and findings of other chapters are listed and future research that complements this study is described.

Chapter 2

Energy MicroGrids

2.1 Introduction

MicroGrids have been investigated in many research projects in Europe, United States, and Japan. These projects have addressed the topology, operation, control, and safety issues. To date, the benefits and potential of MicroGrids have not been fully exploited in public electricity systems.

In this research, a review of the various MicroGrid research projects was undertaken with particular emphasis on the European MicroGrid concept. This review included control, management, and operational aspects of a MicroGrid.

The concept of a MicroGrid was further developed into an Energy MicroGrid that comprises electrical power, gas, and district heat systems. As interactions between heat and electrical power systems were studied in this research, a review of the elements of district heat systems and their modelling was undertaken.

A model test system for the Energy MicroGrid is described. This model was used in later chapters to assess the performance of the control systems investigated in this research.

2.2 MicroGrids Concepts

MicroGrids [14–19] are small power networks to which low power generating units and loads are connected. They supply the local area with heat and electric power. MicroGrids operate either as an island or connected to a main electrical grid. The majority of generating units in the MicroGrid, MicroSources, are connected via power electronic interfaces.

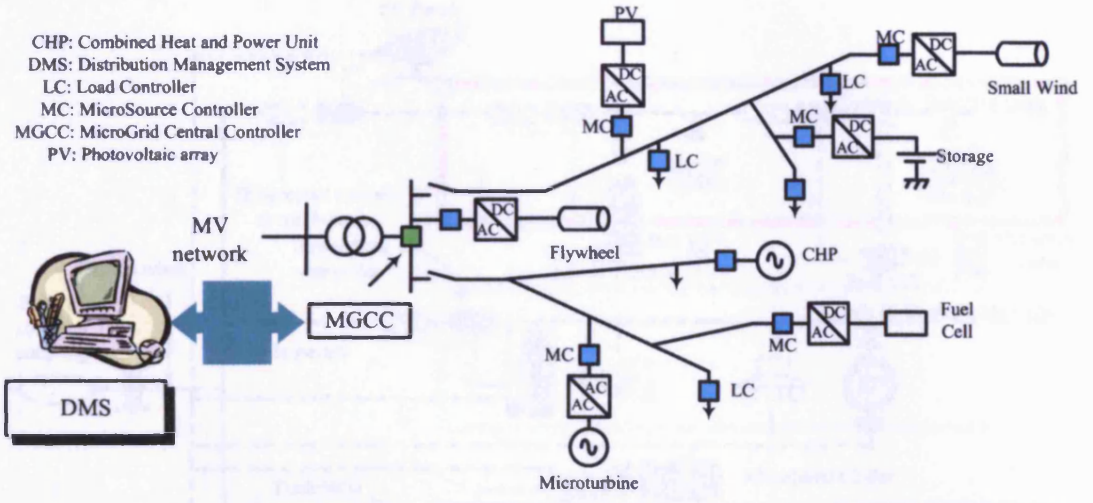

Figure 2.1: The EU MicroGrid [14].

A number of research projects have been conducted with each project having its own concept of a MicroGrid.

2.2.1 The EU Concept of a MicroGrid

Two research projects, MicroGrids [14, 15] and More MicroGrids [15], were funded by the European Commission to investigate MicroGrids. The objectives were to increase the penetration level of renewable generation and distributed energy resources, increase the supply reliability through allowing islanding, reduce the overall system losses, and enhance power quality.

The EU MicroGrid architecture is shown in Figure 2.1. It contains a set of MicroSources and controllable loads connected to the LV network. A central energy store, a flywheel, is assumed to be available at all times. Supervisory functions such as economic dispatch are provided by a MicroGrid Central Controller (MGCC).

If multiple MicroGrids are operating in the same distribution network, a Distribution Management System (DMS) is used to coordinate between the MGCCs of the different MicroGrids.

2.2.2 The CERTS Concept of a MicroGrid

In the US, the Consortium of Electric Reliability Technology Solutions (CERTS) has its own definition of a MicroGrid. The CERTS MicroGrid allows

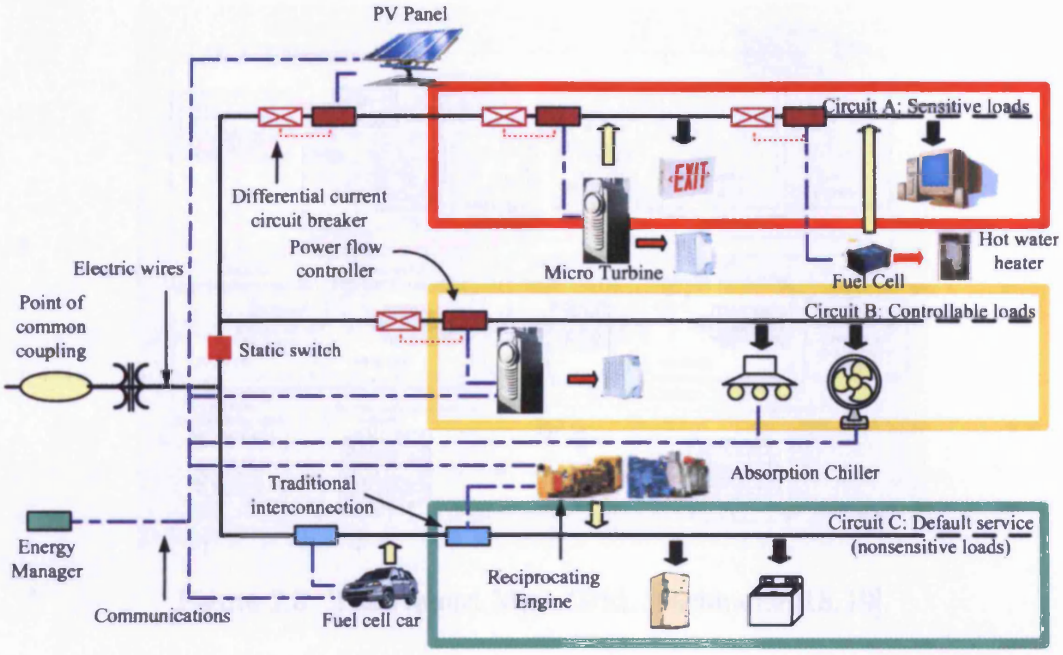

Figure 2.2: The CERTS MicroGrid [35].

local generation connected to a small power network to form an island and carry on supplying the sensitive loads connected to this network in case of any disturbance in the main grid [16, 17].

In the CERTS MicroGrid, Figure 2.2, loads are divided into sensitive, adjustable, and shedable loads. Each of these three sets of loads is connected to an independent feeder. MicroSources are connected to the feeders supplying sensitive and adjustable loads. These two feeders are connected to the rest of the network via a static switch.

If any disturbance occurs in the main network, the static switch isolates the two feeders to which MicroSources, sensitive loads and adjustable loads are connected. This forms an island and allows the MicroSources to supply the sensitive loads and some of the adjustable loads.

All components in the CERTS MicroGrid are plug and play to allow easy expansion of the system. Peer-to-peer control guarantees high reliability. An energy manager (EM) is used for slow economic dispatch of the power generation of MicroSources. All MicroSources have storage at their DC busbar and no central storage is necessary.

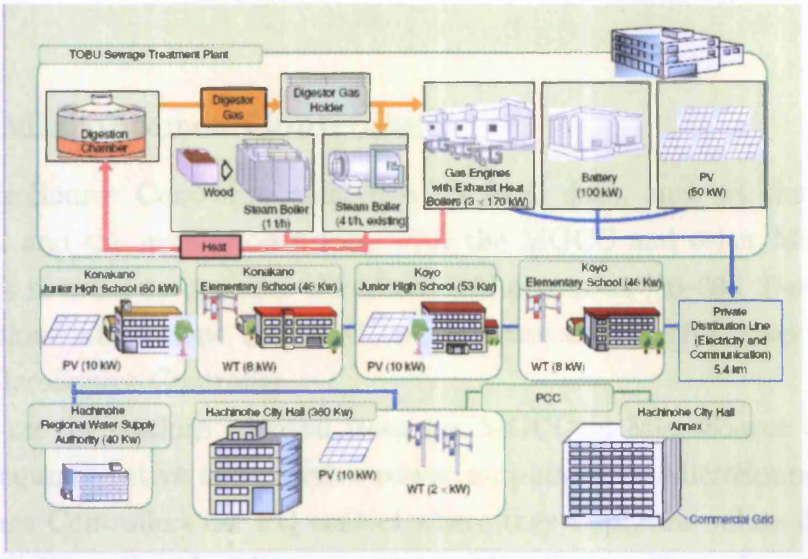

Figure 2.3: The Aomiri MicroGrid, Hachinohe [18, 19].

2.2.3 The Japanese Concept of a MicroGrid

Several demonstration MicroGrid projects are being conducted in Japan. Their main objective is to balance fluctuations in load and intermittent generation in the MicroGrid by means of energy storage and controllable generation [15]. The MicroGrid is then viewed by the main network as a constant load.

A schematic diagram for one of the projects, the Aomori project in Hachinohe, Japan, [18, 19] is shown in Figure 2.3. In this project, an energy management system was used for 7 days ahead operational planning, 2 hours ahead optimal dispatching, and real time tie line control and frequency regulation [19].

2.3 Elements of a MicroGrid

2.3.1 The MicroGrid Central Controller

In the EU MicroGrid, the Microgrid Central Controller (MGCC) optimises the operation of the MicroGrid [14]. It provides supervisory and management functions such as scheduling, forecasting, and security assessment [36]. It dispatches active and reactive power generation to MicroSource controllers and the load shedding to load controllers.

Similar functions are provided by the Energy Manager (EM) in the CERTS MicroGird [17] and the energy optimisation system in the Japanese MicroGrid

[19].

2.3.2 MicroSource Controllers

A MicroSource Controller exchanges its local data, such as the available generation and the generation prices, with the MGCC and other MicroSource Controllers in order to optimise the MicroGrid operation [36–38]. Based on the results of these interactions, the MGCC sends active and reactive power set points to each MicroSource Controller.

Based on the settings received from the MGCC, a MicroSource Controller sets the required active and reactive power outputs of its MicroSources. Some MicroSource Controllers use PQ control where they apply the values dispatched by the MGCC to the MicroSources. Other MicroSource Controllers use droop control to provide voltage and frequency support to the MicroGrid.

i) PQ Control

PQ control is used in cases where MicroSources are not required or not able to provide voltage or frequency support. With PQ control, the MicroSource Controller does not change the output settings of its MicroSource in response to fluctuations in the MicroSource terminal voltage or the MicroGrid frequency [39, 40].

MicroSources with PQ control require a reference frequency signal to operate. During grid connected operation, this reference frequency is supplied by the main grid. During autonomous operation, it has to be supplied by another MicroSource that operates on droop control.

ii) Droop Control

Droop control [41] is originally used to regulate frequency in transmission networks where the network frequency is related to the kinetic energy stored in the rotors of synchronous machines. In these networks, a sudden shortage of power will be supplied from this energy. This reduces the speed of the rotors and, subsequently, the network frequency. The frequency drop is detected by speed governors which respond by increasing the power generation based on linear droop characteristics, Figure 2.4(a).

Droop control is also used to regulate voltage in transmission networks. Due to the high X/R ratio in these networks, voltage is largely affected by reactive power. For this reason, voltage is regulated by controlling the reactive power output of shunt compensators and generators. Linear reactive power/voltage droop characteristics, Figure 2.4(b), are used to determine the amount of reactive power injected to the network.

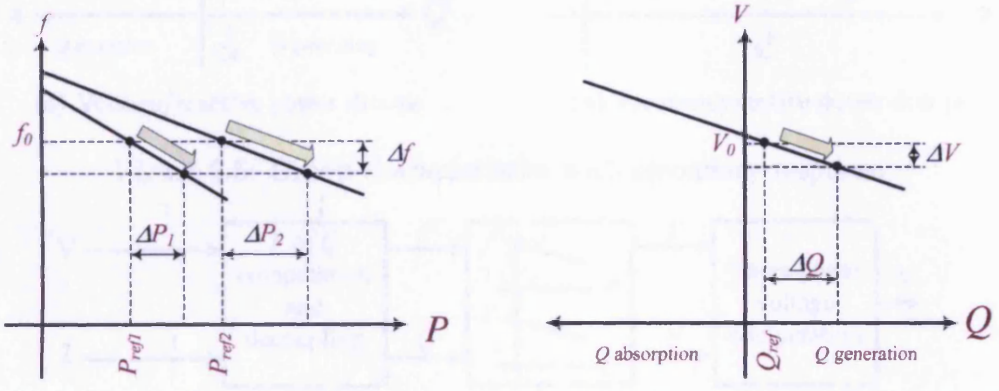

(a) Frequency/active power droops (b) Voltage/reactive power droops

Figure 2.4: Typical droop characteristics

A MicroGrid, unlike transmission networks, has low X/R ratio and low inertia. Despite this difference, droop control was found suitable for MicroGrids [42]. It was used by many authors [16, 17, 40, 43–45] to regulate voltage and frequency in islanded MicroGrids.

This primary droop response is able to contain disturbances and reduce voltage and frequency excursions. On the other hand, it not able to restore the original voltage and frequency.

In order to restore the nominal voltage and frequency, some MicroSource controllers have a secondary control loop. This loop slowly moves the droop characteristic such that active and reactive power required are supplied at nominal frequency and voltage [39]. This response is illustrated by Figure 2.5.

For MicroSources with power electronic converters, another approach for droop control was used [40, 42, 45]. This approach is illustrated by Figure 2.6 where the output voltage and current values are used to calculate the active and reactive power outputs. These values are then used to set the required voltage and frequency reference signals for the converter.

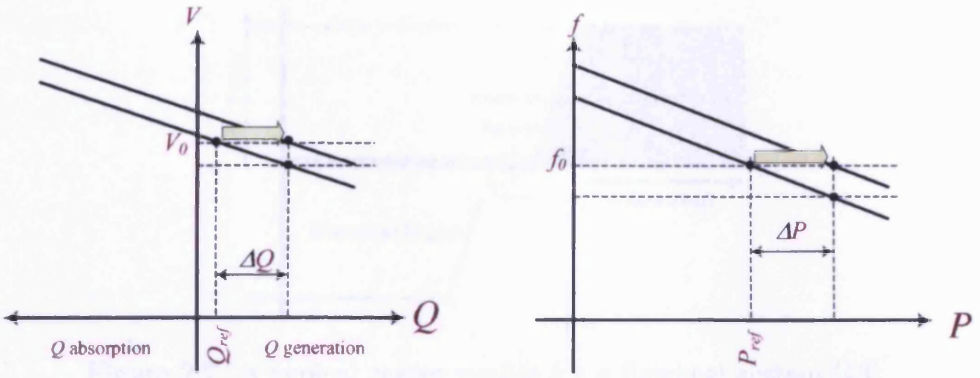

(a) Voltage/reactive power droops (b) Frequency/active power droops

Figure 2.5: Droop characteristics with secondary response

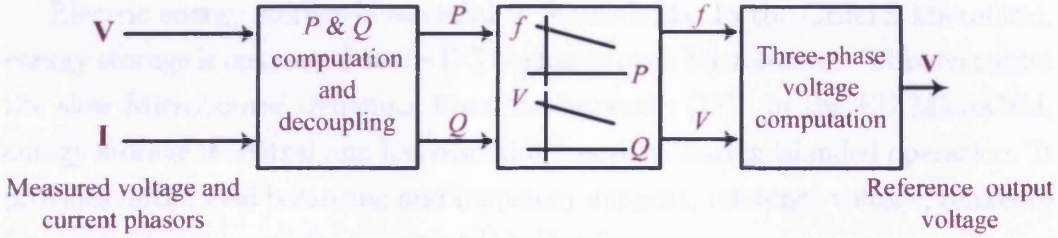

Figure 2.6: Alternative approach for droop control [40].

2.3.3 Load Controllers

Load Controllers perform similar functions to MicroSource Controllers. They exchange their required load demand, possible load shedding, and load shedding prices with each other, with MicroSource Controllers and with the MGCC. This information is used to optimise the settings of the controllable loads [36, 38].

Load Controllers should participate in frequency control during islanded operation [40].

2.3.4 MicroSources

MicroSources are low power generating units (≤100kW) [16]. They serve the heat and electrical power demand of the MicroGrid. MicroSources do not contribute much to network losses as they are located close to the loads. They require no investment in transmission systems. The carbon emissions of MicroSources that use CHP or renewable resources are low compared to that of central generation.

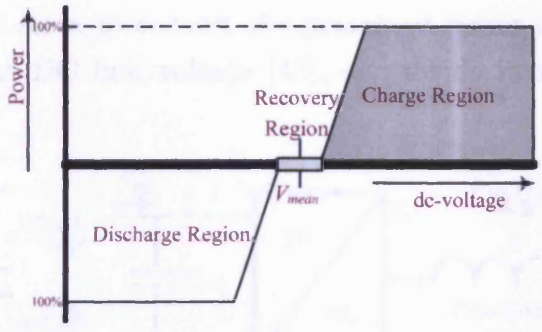

Figure 2.7: A typical power profile for a flywheel system [43].

2.3.5 Electric Energy Storage

Electric energy storage is essential in MicroGrids. In the CERTS MicroGrid, energy storage is connected at the DC busbar of each MicroSource. This decouples the slow MicroSource dynamics from the networks [17]. In the EU MicroGrid, energy storage is central and has essential functions during islanded operation. It provides initial load balancing and frequency support, reference voltage, reference frequency, inertia, and fault current [14, 43, 46].

Storage options include batteries, super-capacitors, superconducting magnetic energy storage, and high speed flywheels. Because of costs, energy and power densities, and cycling capability; high speed flywheels were used in the EU MicroGrid [43].

The flywheel is connected to the MicroGrid via a DC-link. The grid side converter is used to set the flywheel output power. The other converter charges or discharges the flywheel to maintain a constant DC-link voltage [43].

A typical power profile of a flywheel is shown in Figure 2.7. The flywheel is able to increase its power output from zero to full power in 4.5ms [43]. This fast response compensates for the low inertia of the MicroGrid.

2.3.6 Power Electronic Interfaces

Many MicroSources generate DC power. Others generate AC power with frequency that is different from the power frequency. This power is injected to the MicroGrid via a power electronic interface as shown in Figure 2.8.

The generator side converter may have different configurations depending on the technology of the generator [47]. Examples of these configurations are diode rectifiers, thyristor rectifiers, voltage source converters, and DC/DC converters.

This converter may serve to convert the generated power into DC power [47], maintain a constant DC link voltage [43], or provide maximum power point tracking [47].

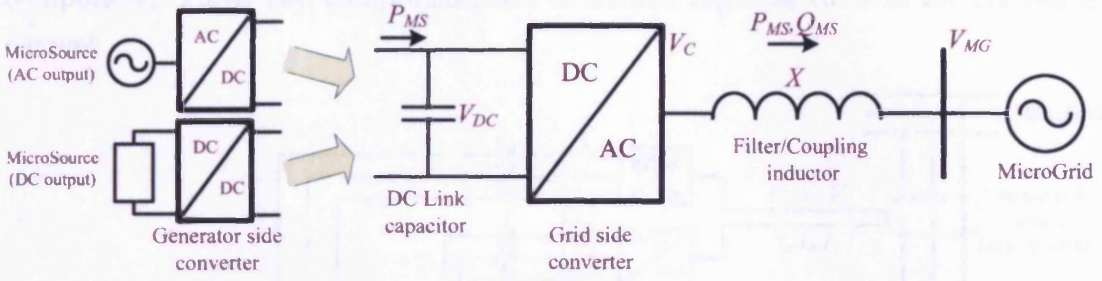

Figure 2.8: Power electronic interface.

The grid side converter is usually a voltage source converter with a coupling inductor or an inductive output filter [16,17,43]. The MicroSource reactive power output is always controlled at this converter. Active power output control, on the other hand, has two options.

Some converters are controlled to maintain a constant DC-link voltage [40, 44]. Doing this, they inject the power generated by the MicroSource into the MicroGrid. Others are controlled to supply the active power output required by the MicroSource Controller [16, 17, 43]. In this case, the DC-link must be able to compensate for the difference between the speed of response of the grid side converter and that of the MicroSource.

Two configurations for the control system of the grid side converter are shown in Figure 2.9. In both configurations, output voltage and current are measured. The measured current is compared to a reference current. The difference between the two currents is scaled and added to the measured voltage. The result is used as a carrier signal for the Pulse Width Modulation (PWM) [40, 43, 44].

In Figure 2.9(a), the grid side converter operates to supply the active and reactive power outputs specified by the MicroSource controller [43]. The reference current is calculated such that, when injected at the voltage measured, it supplies the active and reactive power outputs set by the MicroSource controller to the MicroGrid .

In Figure 2.9(b), the grid side converter operates to supply the reactive power output specified by the MicroSource controller and maintain a constant DC-link voltage [40, 44]. The measured voltage and current are used to calculate the reactive power output and the active and reactive components of the output

current. The difference between the reactive power output and the reactive power output required is used to control the the reference reactive current component. The error in the DC-link voltage is used to control the reference active current component. These two components are combined together to form the reference current.

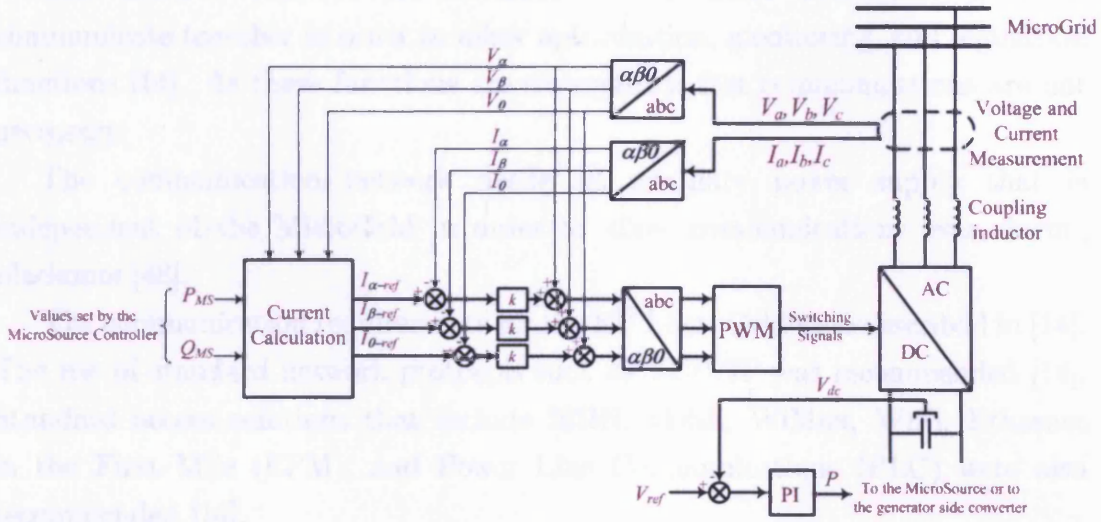

(a)

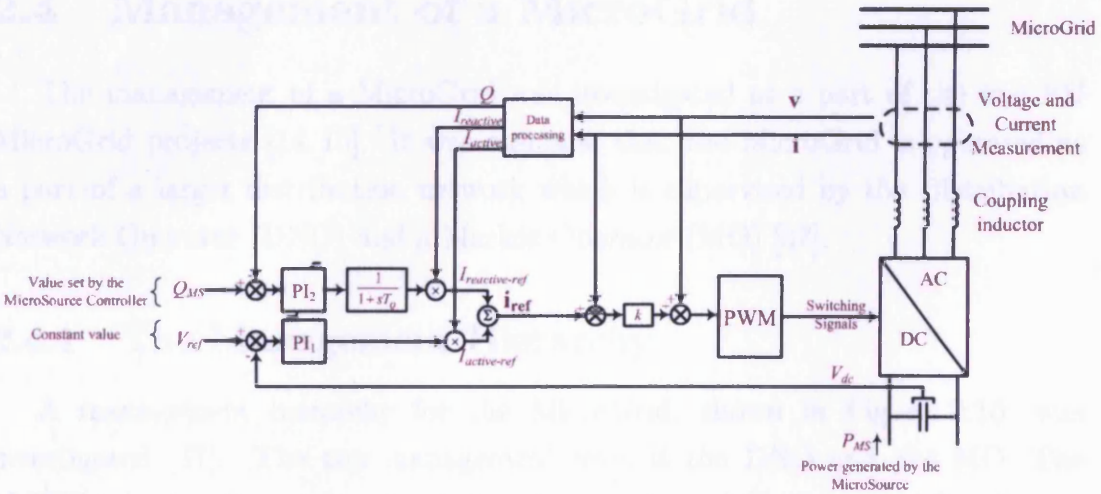

(b)

Figure 2.9: The control system of the grid side converter.

The output frequency of the converter is either set by a phase locked loop (PLL) that measures the MicroGrid frequency [43], or by the MicroSource controller [42].

The power electronic interface allows fast and flexible control of MicroSources [16]. They also decouple the inertia of the rotating machines from the network.

2.3.7 Communication Infrastructure

The MGCC, MicroSource controllers, and Load Controllers need to communicate together in order to allow optimisation, monitoring, and regulation functions [14]. As these functions are supervisory, fast communications are not necessary.

The communication network needs an auxiliary power supply that is independent of the MicroGrid in order to allow communications even during blackouts [48].

The communication requirements for the EU MicroGrid were described in [14]. The use of standard network protocols such as TCP/IP was recommended [14]. Standard access solutions that include ISDN, xDSL, WiMax, WiFi, Ethernet in the First Mile (EFM), and Power Line Communications (PLC) were also recommended [14].

2.4 Management of a MicroGrid

The management of a MicroGrid was investigated as a part of the two EU MicroGrid projects [14, 15]. It was assumed that the MicroGrid is operated as a part of a larger distribution network which is supervised by the Distribution Network Operator (DNO) and a Market Operator (MO) [37].

2.4.1 The Management Hierarchy

A management hierarchy for the MicroGrid, shown in Figure 2.10, was investigated [37]. The top management level is the DNO and the MO. The MGCC is in the intermediate level. Local Controllers (LC), these are MicroSource Controllers and Load Controllers, constitute the lowest level of management.

i) Centralised management of MicroGrids

Centralised management of a MicroGrid was outlined in [14]. The MGCC, in this case, is responsible for managing the MicroGrid. This MGCC ensures that heat and electricity demands are served and that the MicroGrid is running

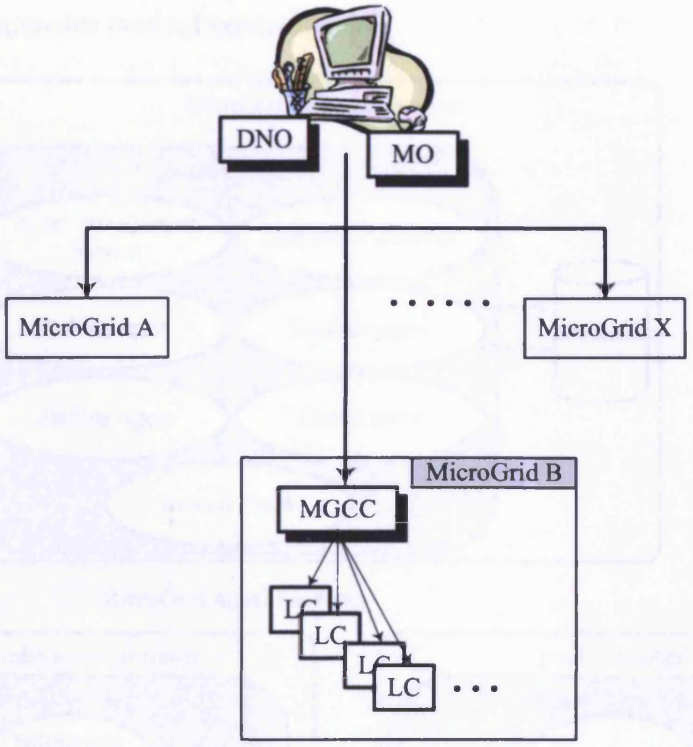

Figure 2.10: Management hierarchy of a MicroGrid [37]

according to the standards set by the DNO. It also dispatches voltage, active power, and reactive power set points to MicroSource Controllers.

ii) Distributed management of MicroGrids - multi-agent systems

Distributed management of the MicroGrid was addressed in [36–38]. In this case, the decision making process involves LCs as well as the MGCC. A multi-agent system, such as the system shown in Figure 2.11 [38], provides monitoring, scheduling, market operation, secondary regulation, and load management functions.

In the multi-agent based management hierarchy shown in Figure 2.11, each control element in the MicroGrid would have a set of agents that provide its functionality. Each of these agents has its own objectives and is capable of taking certain control actions. These agents communicate together to build their knowledge of the network. They then take actions based on this knowledge and their objectives.

The use of this multi-agent system was found to increase the robustness of the system, provide the MicroGrid with plug-and-play capability, and reduce the

need for an expensive central controller [38].

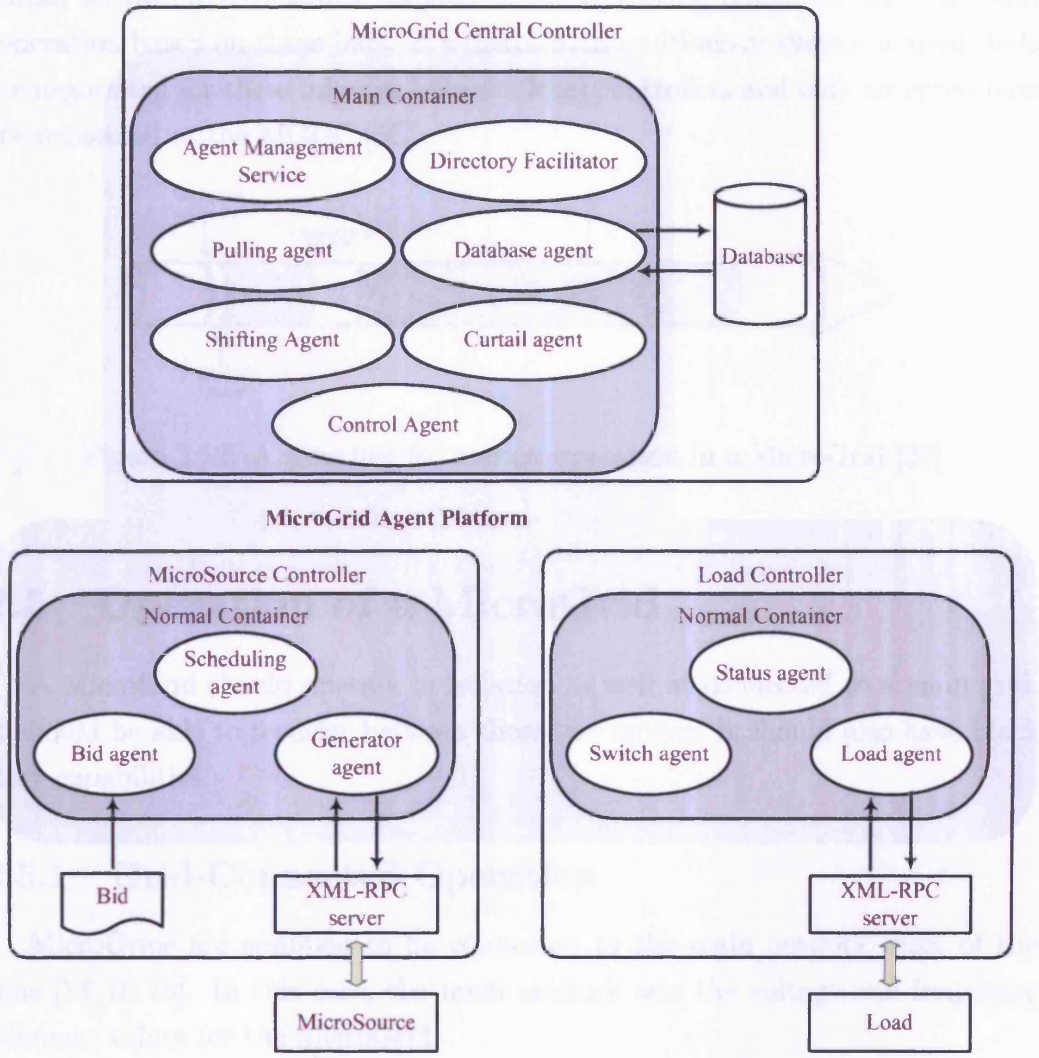

Figure 2.11: The architecture of a multi-agent MicroGrid management system [38]

2.4.2 Market Operation

A structure for the energy market in the MicroGrid was discussed in [14, 36]. This energy market was set to cover 15 to 30 minutes ahead 15-minutes periods [14, 36]. The time line for MicroGrid market operation is shown in Figure 2.12.

In this energy market, the MGCC receives grid prices from the DNO or the MO and announces them to all local controllers. Load controllers and MicroSource controllers place their bids based on the announced prices, forecasted generation,

and expected demand. If a centralised management system is used, bids are placed at the MGCC which dispatches the operating points for all loads and generation based on these bids. If a distributed multi-agent system is used, bids are negotiated for three minutes between local controllers and only accepted bids are registered at the MGCC [36].

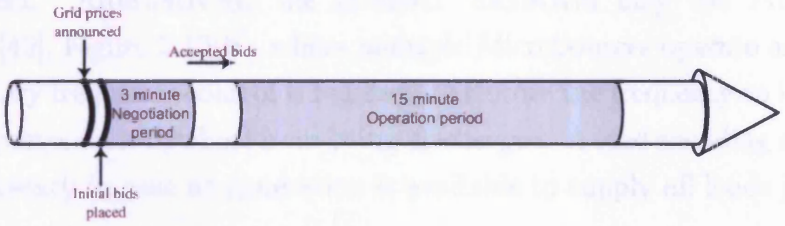

Figure 2.12: A time line for market operation in a MicroGrid [36]

2.5 Operation of a MicroGrid

A MicroGrid should operate in isolation as well as connected to a main grid. It should be able to transfer between these two modes. It should also have black start capabilities.

2.5.1 Grid-Connected Operation

MicroGrids are assumed to be connected to the main network most of the time [14, 16, 19]. In this case, the main network sets the voltage and frequency reference values for the MicroGrid.

During grid connected operation, all MicroSources Controllers may run on PQ control as well as on droop control. In the latter case, voltage/reactive power droop operation will provide limited local voltage support whereas frequency/active power droop operation will not be able to influence the network frequency.

2.5.2 Islanded Operation

The MicroGrid should be able to transfer smoothly from grid-connected operation to islanded operation [17]. It should run safely afterwards within acceptable voltage and frequency limits [17, 40].

MicroSources which provide reference voltage and frequency for the MicroGrid during islanded operation are termed "Master MicroSources". These MicroSources run on droops [40] whereas other MicroSources operate on PQ control. It is possible to operate the islanded MicroGrid with only one Master MicroSource, Single-Master operation [40], Figure 2.13(a). This Master MicroSource is usually the flywheel. Alternatively, the islanded MicroGrid may use Multi-Matser operation [40], Figure 2.13(b), where multiple MicroSources operate as Masters.

Secondary frequency control is required to restore the frequency to its nominal value and prevent the flywheel from being discharged. A load shedding mechanism is also necessary in case no generation is available to supply all loads [40].

i) Stability of an islanded MicroGrid

The stability of a MicroGrid during autonomous operation was studied in [39]. For small disturbances, the MicroGrid was found stable when at least one MicroSource operates on droop control. For short circuit faults, induction motor loads limit the critical clearing time. Under-voltage load shedding of motors is required to increase the transient stability limit.

ii) Protection of an islanded MicroGrid

Due to the thermal limitations of semiconductor devices, controllers of power electronic interfaces can only allow currents that are just above the rated current. This limits the contribution of MicroSources in fault currents [40].

During grid connected operation, the fault current supplied by the main grid will trip overcurrent relays. On the other hand, during autonomous operation, the fault current supplied by MicroSources will not be detected by overcurrent relays.

Unless a radical change in the LV network protection systems is to be made [16,17], one MicroSource, e.g. the flywheel unit, has to supply large fault current that is enough to operate the overcurrent protection [40,46]. The power electronic switches of this MicroSource has to be uprated to 3 to 5 times of its rated current.

A control system to supply short circuit current was investigated in [49]. This control system, by trying to restore the terminal voltage and the frequency to their nominal values, injects a current that is high enough to operate the protection.

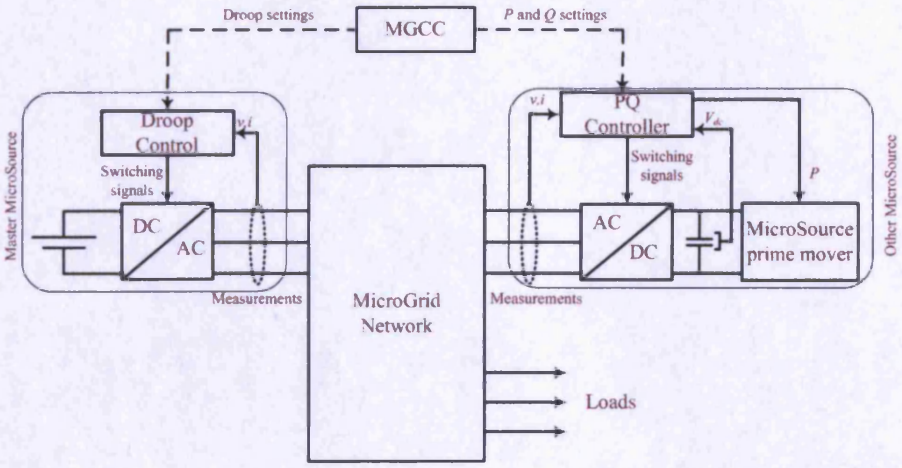

(a) Single-master operation

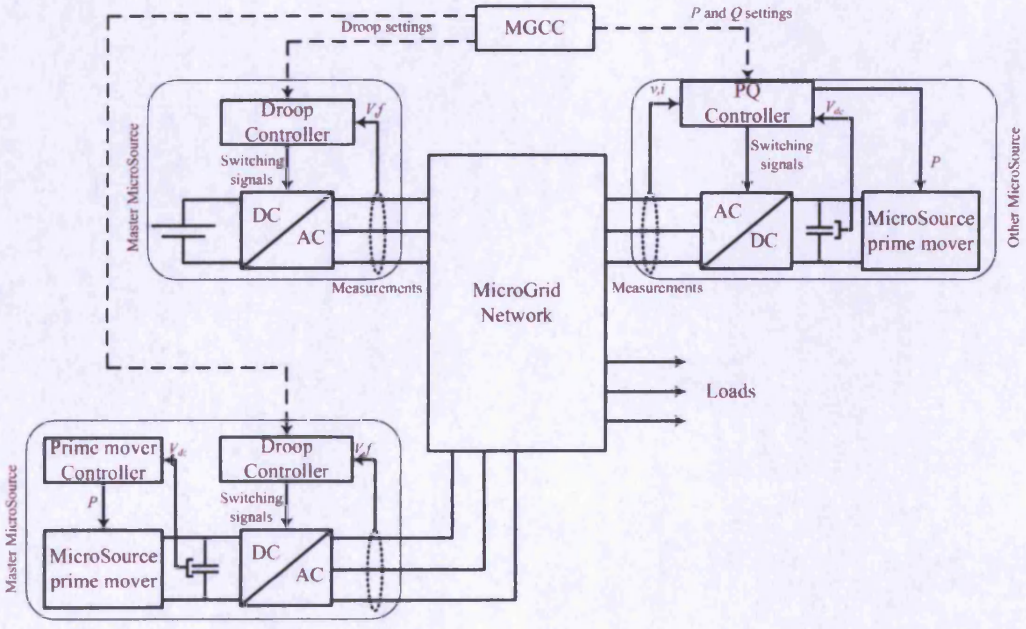

(b) Multi-master operation

Figure 2.13: Islanded operation of a MicroGrid [40].

2.5.3 Black-Start and Service Restoration

A procedure for service restoration and black start of MicroGrids was described in [48]. This procedure is supervised by the MGCC. It is only initiated subsequent to a blackout and after confirming that the main grid connection can not be restored.

The MGCC was assumed to have full knowledge of the MicroGrid status prior to the blackout. This includes data about loads, generation, and the capabilities of MicroSources. As the MGCC needs to communicate with other controllers in the MicroGrid during this process, an axillary power supply that is independent of the MicroGrid has to be available for the communications network.

The service restoration procedure is as follows:

1. Disconnect all loads and MicroSources and isolate the transformer.
2. Allow MicroSources with black start capability to form and island and start supplying their loads.
3. Energise the MicroGrid by the energy storage device and reconnect all the sectionalising switches in steps.
4. Allow the already running islands to resynchronise, in steps, with the MicroGrid.
5. Start restoring as much controllable loads as the available generation allows.
6. Restore non controllable MicroSources and MicroSources with no black start capability.
7. Carry on restoring more loads if the available generation allows so.

2.5.4 Resynchronisation to the Main Grid

The process of resynchronising the MicroGrid to the main network was studied in [43]. The resynchronisation procedure manipulates the reference frequency of the energy storage in order to change the MicroGrid frequency and phase angle.

The block diagram of the resynchronisation controller that was used in [43] is shown in Figure 2.14. It measures the instantaneous phase voltages on both sides of the synchronisation switch and resolves them into direct and quadrature

components. The quadrature voltage error is used to adjust the reference frequency of the energy storage.

The synchronisation switch is closed when the main grid voltage magnitude remains larger than 90% of its rated value for a period of at least 0.2s and the quadrature axis voltage error is less than 5%.

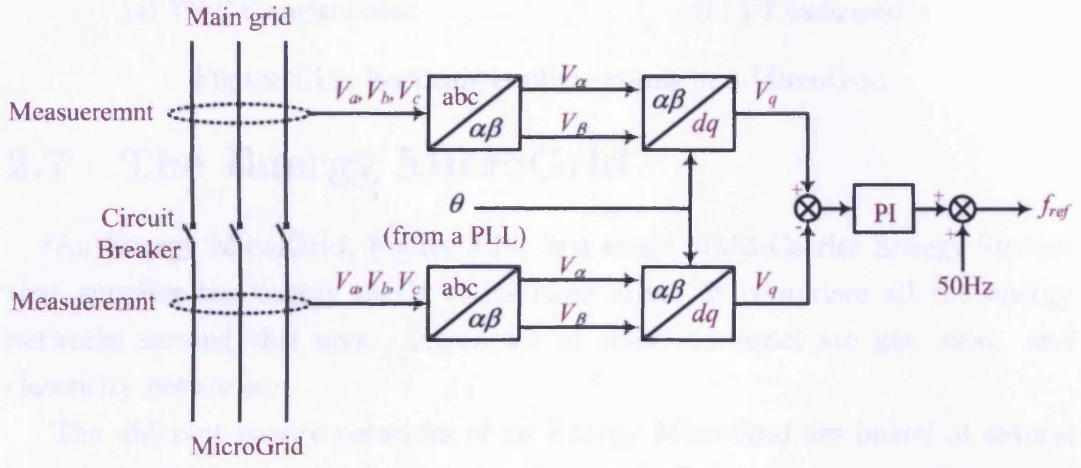

Figure 2.14: A control system to resynchronise a MicroGrid to the main grid [43]

2.6 Safety of a MicroGrid

The TN-C-S earthing configuration, Figure 2.15(a), was found suitable for MicroGrids [46]. In this configuration, the transformer neutral and the transformer are earthed at the substation. One conductor, the protective earth neutral, supplies the consumers installations by both earth and neutral connections. This connection is divided into two independent earth and neutral connections inside the consumer installations.

The TT earthing configuration, Figure 2.15(b), was also found suitable for MicroGrids [46]. In this configuration, consumers have earth electrodes that are independent of that of the transformer neutral.

It was assumed that, during autonomous operation, the transformer remains connected to the LV network to retain its neutral earth [46].

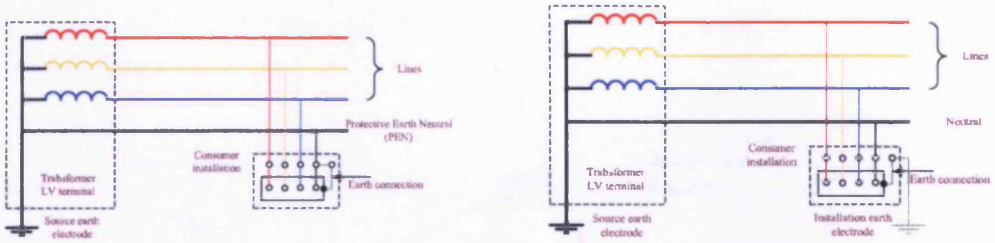

(a) TN-C-S configuration (b) TT configuration

Figure 2.15: Earthing configurations in a MicroGrid

2.7 The Energy MicroGrid

An Energy MicroGrid, Figure 2.16, is a small Multi-Carrier Energy System that supplies the energy needs of its local area. It comprises all the energy networks serving this area. Examples of these networks are gas, heat, and electricity networks.

The different energy networks of an Energy MicroGrid are linked at several points. As these networks interact together and affect each other, an integrated approach is used for planning, operating, and controlling them.

The power network of the Energy MicroGrid was assumed to have the same architecture as the EU MicroGrid. Details of the gas network was not considered in this research. The architecture, the main elements, and the models of the heat network of the Energy MicroGrid are described in Section 2.7.1 and Section 2.7.2.

2.7.1 The District Heat System

Heat needs in the Energy MicroGrid are served by a District Heat System, Figure 2.17. In this DHS, water is heated at a central district heat station and distributed to consumers via a Supply Pipe Network. At consumers' premises, the water temperature drops due to heat consumption. This water is supplied back to the district heat station via a Return Pipe Network.

i) Heat exchangers

Heat exchangers, Figure 2.18, are used in many DHS equipment to transfer heat between two hydraulically isolated systems. Each of these two systems establishes a fluid stream inside the heat exchanger. The two streams are separated by a surface of high heat transfer coefficient. Heat is transferred from

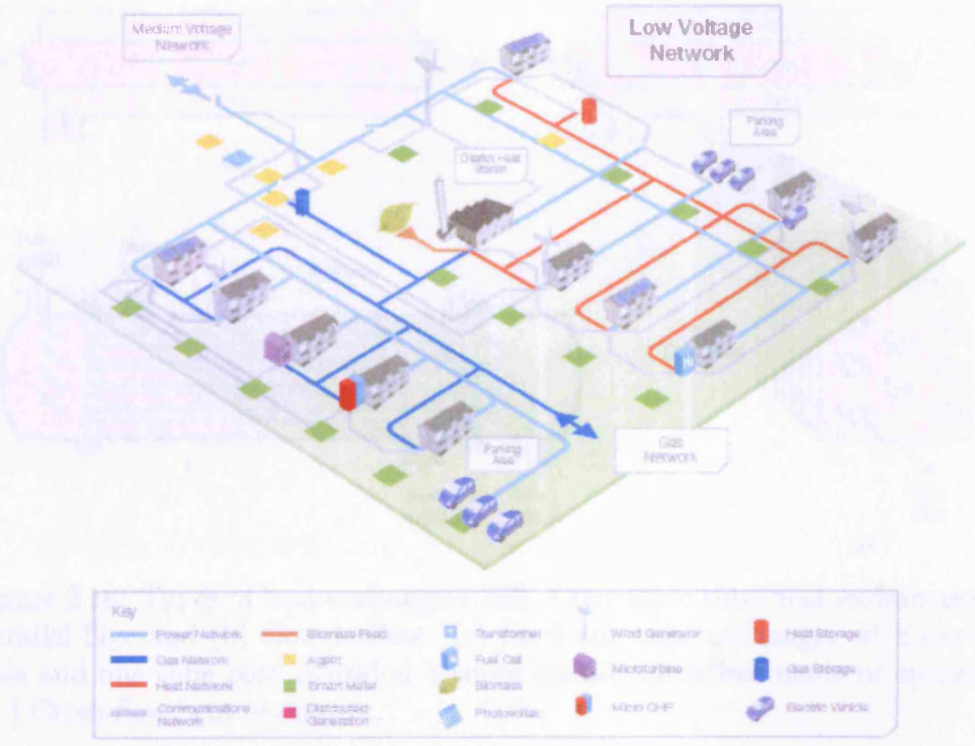

Figure 2.16: An Energy MicroGrid

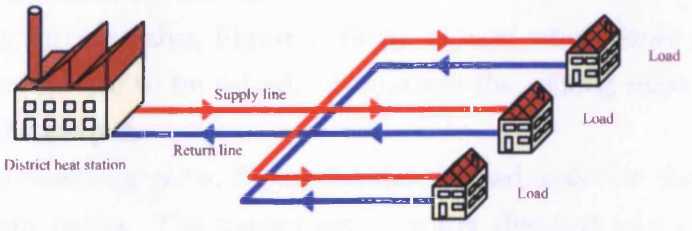

Figure 2.17: A simple district heat system

the fluid at the higher temperature to the fluid at the lower temperature through convection.

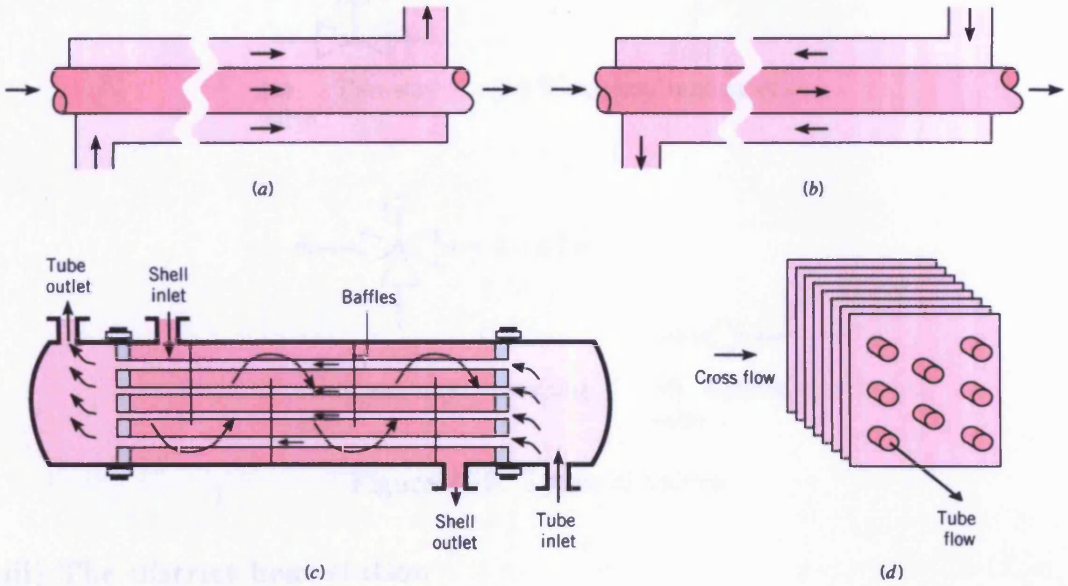

Figure 2.18: Types of heat exchangers [50]. Concentric tube heat exchangers: (a) Parallel flow and (b) Counterflow. (c) Shell-and-tube exchanger with one shell pass and one tube pass (showing 4 tubes cross-counterflow mode of operation). (d) Cross-flow heat exchanger.

ii) Valves

Four types of valves, Figure 2.19, are used in heating systems [51]. These are two-way valves, three-way mixing valves, three-way diverting valves, and balance valves.

A two-way valve, Figure 2.19(a), controls the mass flow rate through changing the hydraulic resistance for the fluid flow.

A three-way mixing valve, Figure 2.19(b), is used when water supplied from two separate inputs are to be mixed. It controls the mixing ratio of any of the two inputs in the output.

A three-way diverting valve, Figure 2.19(c), is used to divide the supply water into two different paths. The percentage of water diverted into any of the two pathes is determined by the valve position.

A balance valve, Figure 2.19(d), is used in some branches to increase their hydraulic resistance [51]. The valve position is set during installation to provide the required resistance. Afterwards, it remains unchanged during operation.

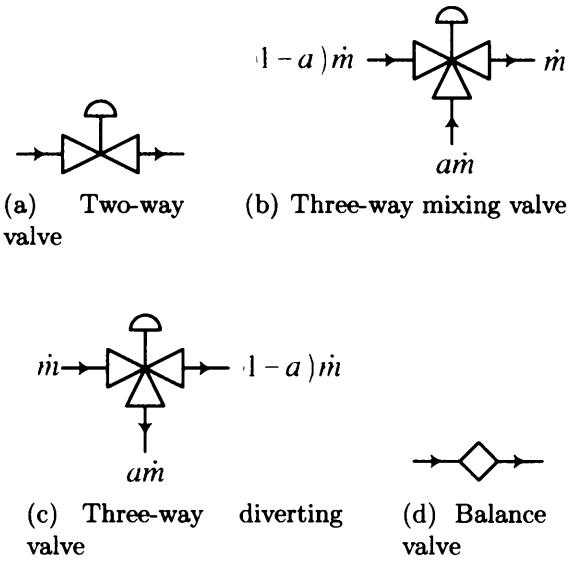

(a) Two-way valve (b) Three-way mixing valve

(c) Three-way diverting valve (d) Balance valve

Figure 2.19: Types of valves

iii) The district heat station

The district heat station supplies heat to the DHS and provides the energy required to maintain the water flow in the DHS pipes [52]. One district heat station in the DHS has to set the reference pressure in both the supply and return networks [52].

In a district heat station, heat may be produced from electricity, gas, coal, biomass, and geothermal energy [53–55]. This is done by boilers, electric heaters, heat pumps or CHP units.

A schematic diagram for the district heat station of the Energy MicroGrid is shown in Figure 2.20. It contains a CHP unit and an electric heater for heat production and an electric water pump to maintain the flow. This station operates in the pressure maintenance mode.

iv) Heat loads

Heat loads are either consumers' space heating and domestic hot water systems or smaller DHSs. They are connected to the DHS either directly or via heat exchangers.

Consumers with a direct connection to the DHS use the hot water supplied by the network as a source of domestic hot water and for central heating. The water pressure and temperature at the supply line have to be suitable for the direct use

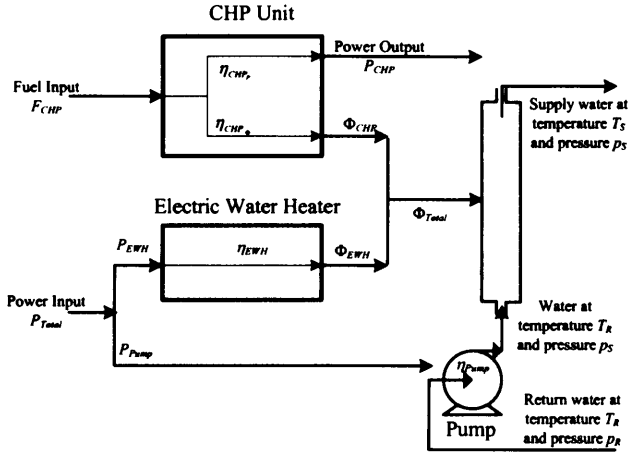

Figure 2.20: District heat station of the Energy MicroGrid

of water. This type of connections was not considered in this research.

Heat exchangers isolate the consumer's installations from the district heat network. This allows high pressure and temperature to be used in the DHS. It guarantees equal flows in the Supply and Return Networks. It also prevents leakages in consumers installations from affecting the DHS. In this research, all consumers were assumed to be connected via heat exchangers.

The controllable parameters at the the DHS side of a heat exchanger are the return temperature and the water flow rate. Power supplied to these loads is controlled by varying one or both of them. This is done using valve combinations as shown in Figure 2.21.

In Figure 2.21(a), a two-way valve is used to adjust the flow rate such that a constant return temperature is maintained. In this configuration, an increase in heat consumption increases the flow rate.

In Figures 2.21(b) and 2.21(c), three-way valves are used. These valves maintain a constant flow rate at the supply side. This flow is divided by the valve between the load and a bypass link. The temperature of the water supplied to the load will drop whereas the water supplied to the bypass link will not change. The return temperature is a function of the percentage of water flowing into the two branches.

In Figure 2.21(d), a three-way mixing valve/pump combination was used to maintain a constant water flow at the load. This flow is partially supplied with hot water at the source supply temperature. The difference between the supply and load flow rates is supplied by circulating some of the load return water. This

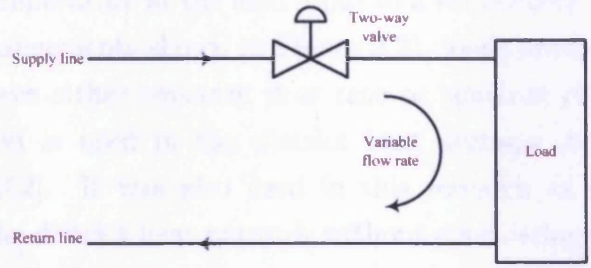

(a) Variable flow rate arrangement with a two-way control valve

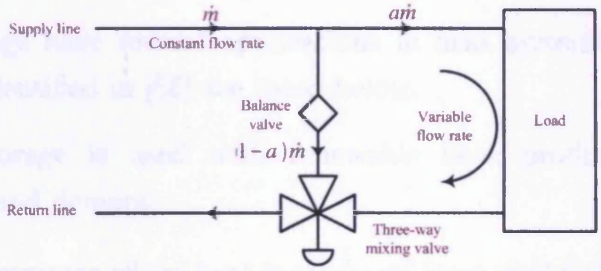

(b) Constant flow rate arrangement with a three-way mixing valve

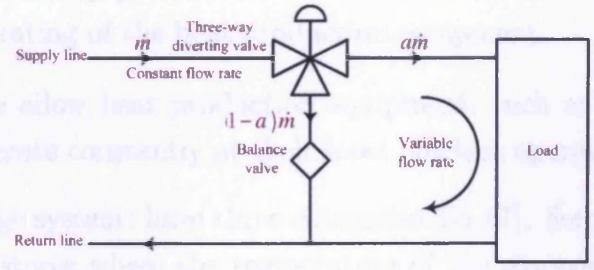

(c) Constant flow rate arrangement with a three-way diverting valve

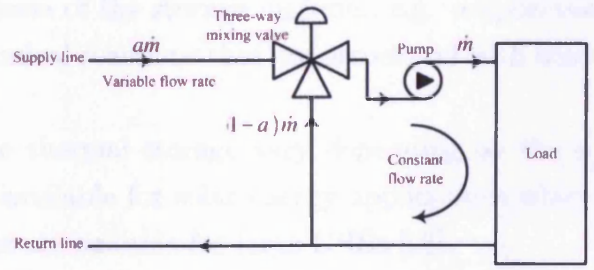

(d) Variable flow rate arrangement with a three-way mixing valve and a load pump

Figure 2.21: Control of heat loads [51]

drops the water temperature at the load input to a value below that of the supply.

In the four arrangements shown in Figure 2.21, loads are seen by the network as devices that have either constant flow rate or constant return temperature. This representation is used in the district heat systems simulation softwares PSS^{TM}-SINCAL [52]. It was also used in this research as it allows studying the operation of the district heat network without considering the control details of individual loads.

v) Heat storage

Thermal storage have several applications in heat systems. Some of these applications, as identified in [56] are listed below.

1. Thermal storage is used with renewable heat production to balance production and demand.

2. It is used in systems where heat is produced from electricity. This is to shift heat production towards periods of low electricity demand.

3. It is used to supply peak heat demand in cases where this peak demand exceeds the rating of the heat production equipment.

4. It is used to allow heat production equipment, such as boilers and CHP units, to operate constantly at their most efficient operating point.

Thermal storage systems have three categories [56,57]. Some thermal storage use sensible heat stores where the temperature of the storage medium and the energy stored are dependent on each other. Other storage systems use latent heat. These are isothermal heat stores in which charging and discharging cause a change in the phase of the storage material, e.g. evaporation. The third type uses reversible chemical reactions that are associated with absorption and release of thermal energy.

The size of the thermal storage vary depending on the application. Small storage tanks are available for solar energy applications whereas Large seasonal underground stores are suitable for large DHSs [56].

An example of sensible heat stores is hot water storage tanks. The energy density of these tanks are in the order of 10kWh/m^3 [56]. Three of the configurations used in hot water tanks are shown in Figure 2.22. Other configurations were described in [58,59].

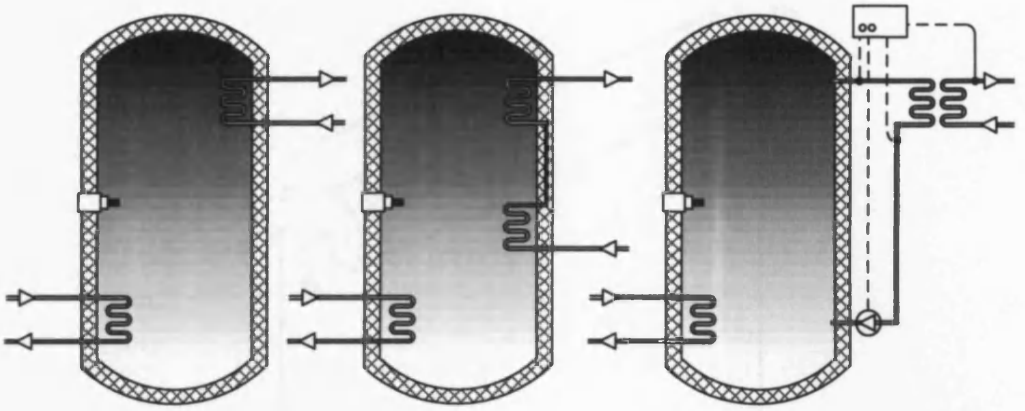

Figure 2.22: Typical configurations of hot water storage tanks [56].

In the Energy MicroGrid, the thermal storage facility was assumed to be a hot water tank. The charging and discharging of this tank is done through two independent heat exchanger coils.

2.7.2 Modelling of District Heat Systems

Models of district heat networks were found in [53] and [52]. These models are based on basic concepts of fluid flow and heat transfer as described in [50].

i) Pipe flow equations

Water flow in a pipe, Figure 2.23, is an incompressible viscous flow. It is governed by the continuity equation, Equation 2.1, and Bernoulli equation, Equation 2.2. In these equations, $\dot{m}$ is the mass flow rate, v is the flow velocity, p is the static pressure, z is the altitude, ρ is the specific weight, and g is the gravitational acceleration. The subscripts 1 and 2, where used, denote the point at which the associated parameter is defined.

$$\dot{m}_1 = \dot{m}_2 \tag{2.1}$$

$$\left(p_1 + \frac{1}{2}\rho v_1^2 + \rho g z_1\right) - \left(p_2 + \frac{1}{2}\rho v_2^2 + \rho g z_2\right) = p_l \tag{2.2}$$

For district heat network applications, the pressure loss term in Bernoulli equation, p_l, is a function of the mass flow rate as shown by equation 2.3 [53, 60] where r_l is the hydraulic resistance of the pipe.

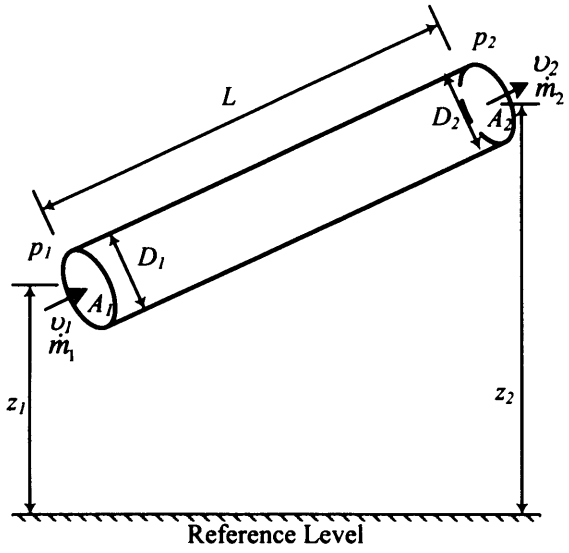

Figure 2.23: Steady incompressible viscous flow in a pipe.

$$p_l = r_l \dot{m}^2 \tag{2.3}$$

Due to the highly turbulent flow in district heat network pipes, the hydraulic resistance, r_l, is almost constant. Its value is calculated by equation 2.4 where L is the length of the pipe, D is its diameter, and ϵ is the roughness of its internal surface. Full derivation of this equation is included in Appendix A.

$$r_l = \left(\frac{1}{-2\log\left(\frac{\epsilon}{3.71D}\right)} \right)^2 \frac{8L}{\pi^2 \rho D^5} \tag{2.4}$$

ii) Analysis of Pipe Networks

A pipe network contains a set of nodes between which network elements are connected. The fluid flow in such network is subject to the energy law, the continuity law and the characteristic of the elements [53].

According to the continuity law, the total mass flow rate into any node must be zero. This is illustrated by Figure 2.24 which depicts a node to which a set $\mathbb{E}$ of elements is connected. Each element, i, in this set has a mass flow rate of $\dot{m}_i$ that is either positive or negative depending on the direction of the flow. The continuity law, applied to the node shown in Figure 2.24, is expressed by Equation 2.5.

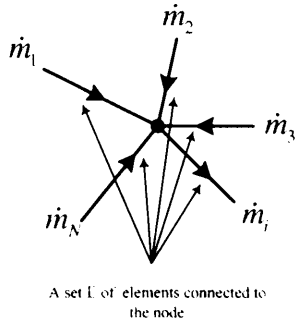

Figure 2.24: Continuity law (Node equations)

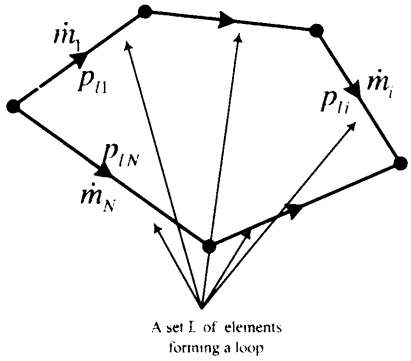

Figure 2.25: Energy law (Loop equations)

$$\sum_{i \in \mathbb{E}} \dot{m}_i = 0 \tag{2.5}$$

According to the the energy law, the total static pressure loss over any closed loop must be zero. The mathematical expression for this law applied at a loop comprising a set $\mathbb{E}$ of elements, shown in Figure 2.25, is given by equation 2.6. In this equation, p_{l_i} is the pressure drop associated with the element i.

$$\sum_{i \in \mathbb{E}} p_{l_i} = 0 \tag{2.6}$$

The characteristic of an element defines the relation between the static pressure loss and the mass flow rate associated with this element. This characteristic is usually in the form of Equation 2.7 where the values of s and r_l are determined by the element type and geometry. This equation for a pipe is equivalent to equation 2.3 with s being equal to 2.

$$p_l = r_l \times \left|\dot{m}^{s-1}\right| \times \dot{m} \tag{2.7}$$

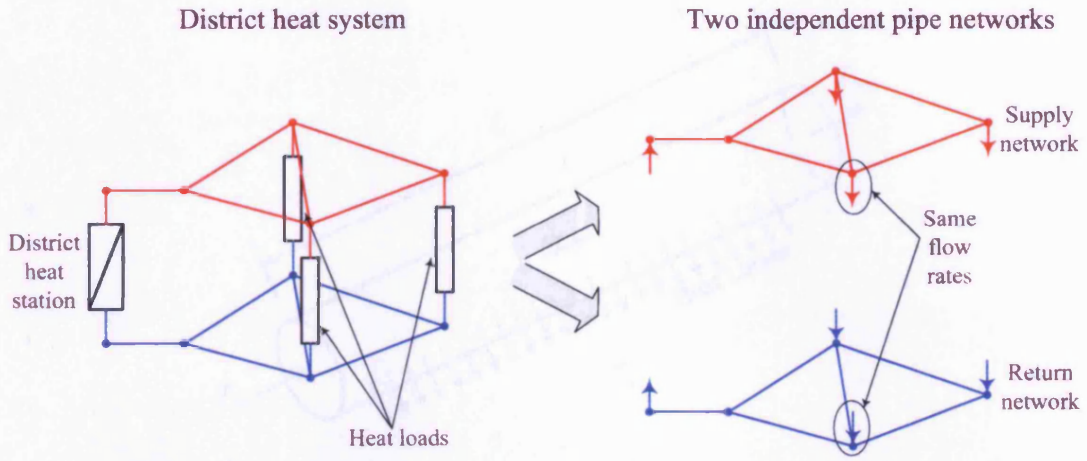

Figure 2.26: The district heat network as two independent pipe networks

Iterative methods are required to calculate the flows in a meshed pipe network. Some of these methods, such as Hardy-Cross, Newton-Raphson, and the basic circuits methods were reviewed in [53].

iii) The Double Pipe Network in District Heat Systems

The DHS contains two identical pipe networks. These are the Supply Network and the Return Network. They are connected together by district heat stations and heat loads.

The pressure difference at the input of the heat exchanger connecting loads should be, at all times, higher than the value required to sustain the flow. The excess pressure is balanced by combinations of valves. This guarantees that the water flow rate and the pressure difference of the load are independent of each other. This causes the two pipe networks to be independent of each other [52,53].

No water is to accumulate either at the district heat station or at loads. The mass flow rate supplied from the Supply Network to a load must be equal to the mass flow rate supplied back from the load to the Return Network. Similarly, mass flow rate supplied from the Return Network to a district heat stations is equal to that returned from the district heat station to the Supply Network.

The double pipe network of the DHS is modelled as two independent pipe networks. The only coupling between them is that the mass flow rate out of one of them at any node is the mass flow rate into the same node in the other network. This is illustrated by Figure 2.26.

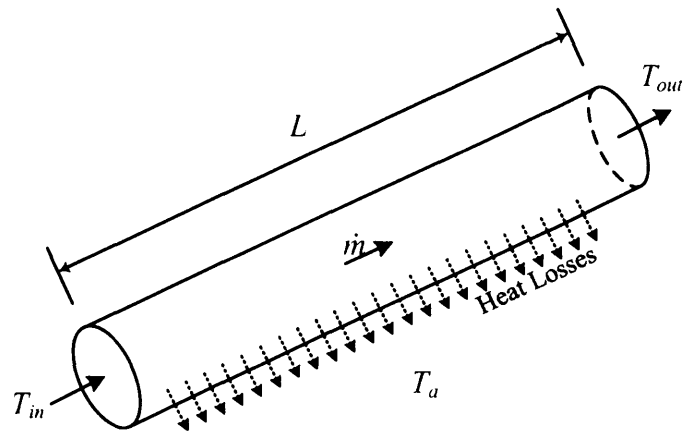

Figure 2.27: Temperature drop in a district heat network pipe

iv) Heat losses from a pipe

As hot water flows in a pipe, Figure 2.27, some heat is lost to the ambient via the pipe walls. This causes the water temperature to drop. The temperature at the pipe outlet is given by Equation 2.8 and the average temperature in the pipe given by Equation 2.9 [52]. Full derivation of both equation is in Appendix A. In both equations, T_{in} is the temperature at the pipe inlet, T_{out} is the temperature at the outlet, T_{av} is the average temperature inside the pipe, $\dot{m}$ is the mass flow rate, L is the pipe length, D is its diameter, λ is the overall heat transfer coefficient in W/m°C.

$$T_{out} = T_a + (T_{in} - T_a)\, e^{-\frac{\lambda L}{c_p \dot{m}}} \tag{2.8}$$

$$T_{av} = \left(T_a - \frac{c_p \dot{m}}{\lambda L}\,(T_{out} - T_{in})\right) \tag{2.9}$$

Equation 2.8 depicts an exponential decay. For losses to remain low, the exponential term has to be close to zero. This allows approximating this exponential decay by the linear relationship given in Equation 2.10.

$$T_{out} = \begin{cases} T_a + (T_{in} - T_a) \times \left(1 - \frac{\lambda L}{c_p \dot{m}}\right) & \text{if } \frac{\lambda L}{c_p \dot{m}} \leq 1 \\ T_a & \text{if } \frac{\lambda L}{c_p \dot{m}} \geq 1 \end{cases} \tag{2.10}$$

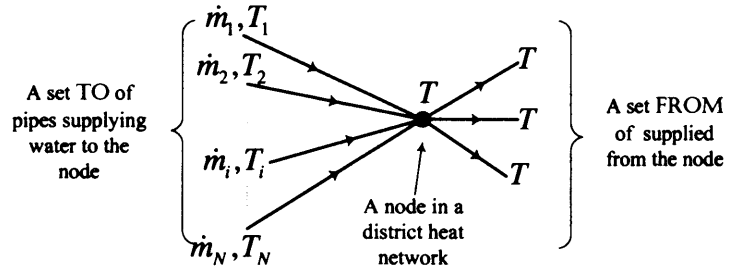

Figure 2.28: Temperature calculation at a node in a district network

v) Node Temperature

Figure 2.28 shows a node in a district heat network. A set $\mathbb{TO}$ of pipes supply water to this node. Each of these pipes supply water at a certain temperature and mass flow rate. Another set $\mathbb{FROM}$ of pipes are supplied by water from this node.

The temperature at the node, TO, is the average temperature of all the water supplied to the node weighted by its mass flow rate. This is shown by equation 2.11 [52].

$$T = \frac{\sum_{i \in \mathbb{TO}} \dot{m}_i T_i}{\sum_{i \in \mathbb{T}} \dot{m}_i} \tag{2.11}$$

The temperature at the inputs of any element j, where $j \in \mathbb{FROM}$, is equal to the temperature at that node. This is illustrated by Equation 2.12.

$$T_j = T \tag{2.12}$$

vi) Heat Exchangers

Figure 2.29 shows a counter flow heat exchanger. At the primary side, hot water enters the heat exchanger at temperature T_{S1} at a rate of $\dot{m}_1$. At the secondary side, cold water enters the exchanger at a temperature of T_{R2} and a rate of $\dot{m}_2$. Heat is transferred from the primary side to the secondary side at a rate of Φ causing the primary water temperature to drop to T_{R1} and the secondary water temperature to increase to T_{S2}.

The changes in temperatures at the primary and secondary sides of the heat exchanger, $T_{S1} - T_{R1}$ and $T_{S2} - T_{R2}$, are related to the mass flow rates, $\dot{m}_1$ and $\dot{m}_2$, and to the rate of heat transfer Φ. These relations are given by Equation 2.13 and Equation 2.14.

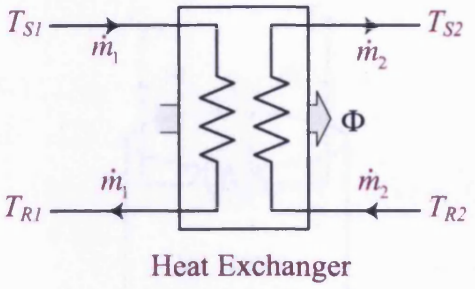

Figure 2.29: A heat exchanger

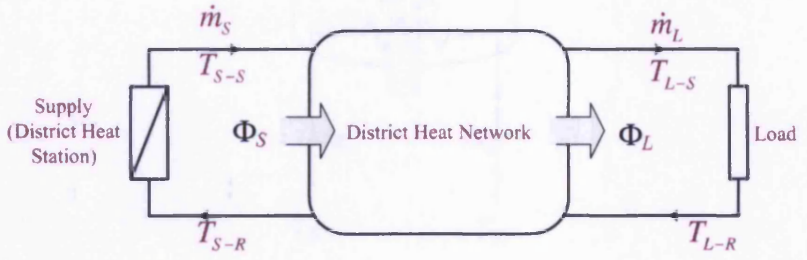

Figure 2.30: A heat source and a heat load connected to a district heat network

$$T_{S1} - T_{R1} = \frac{\Phi}{\dot{m}_1 c_{p1}} \tag{2.13}$$

$$T_{S2} - T_{R2} = \frac{\Phi}{\dot{m}_2 c_{p2}} \tag{2.14}$$

vii) Heating loads and sources

Figure 2.30 shows a district heat station and a load connected to a DHS. The supply and return temperatures at at the terminals of the district heat station and the load and the mass flow rates associated with them are marked on the Figure. The heat supplied by the source Φ_S and the heat supplied to the load Φ_L are given by Equations 2.15 and 5.23.

$$\Phi_S = c_p \dot{m}_S \left(T_{S-S} - T_{S-R}\right) \tag{2.15}$$

$$\Phi_L = c_p \dot{m}_L \left(T_{L-S} - T_{L-R}\right) \tag{2.16}$$

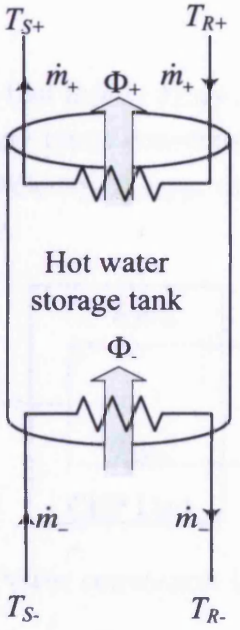

Figure 2.31: A hot water storage tank

viii) Thermal storage

A hot water storage tank with independent charging and discharging coils is shown in Figure 2.31. Hot water enters the charging coils at temperature T_{S-} and with a mass flow rate of $\dot{m}_-$. Heat is transferred from the charging coil to the tank at a rate of Φ_-. This causes the water temperature at the outlet of the charging coil to drop to T_{R-}. Similarly, water enters the discharging coil at temperature T_{R+} and exits it at a temperature T_{S+}. The discharging flow rate is $\dot{m}_+$ and the associated heat transfer is Φ_+.

The charging and discharging rates are given by Equation 2.17 and Equation 2.18. The rate of change of the stored energy inside the storage tank, $\frac{dE}{dt}$, is the difference between these two values as shown by Equation 2.19.

$$\Phi_- = c_p \dot{m}_- \left(T_{S-} - T_{R-}\right) \tag{2.17}$$

$$\Phi_+ = c_p \dot{m}_+ \left(T_{S+} - T_{R+}\right) \tag{2.18}$$

$$\frac{dE}{dt} = \Phi_- - \Phi_+ \tag{2.19}$$

ix) CHP Units

The CHP unit converts the fuel input, F_{CHP}, into electric power, P_{CHP}, and heat, Φ_{CHP}. The fractions of fuel input converted into electricity and power are defined by the CHP electric efficiency, η_{CHP_P}, and heat efficiency, η_{CHP_Φ}. This process is shown by Figure 2.32.

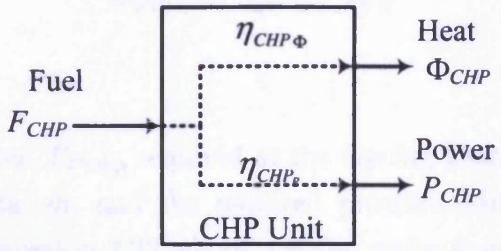

Figure 2.32: Power conversion in a CHP unit

The values of CHP efficiencies depend on the type of the fuel and the CHP technology. They are also affected by some operational parameters such as the percentage loading and the hot water supply temperature T_S [53,61].

In a steam back pressure CHP unit [53], the overall efficiency of the CHP unit, $\eta_{CHP_P} + \eta_{CHP_\Phi}$, is constant. On the other hand, both η_{CHP_P} and η_{CHP_Φ} vary linearly with the T_S as shown in Figure 2.33 and Equations 2.20 and 2.21. In both equations, $\eta_{CHP_{P0}}$, $\eta_{CHP_{\Phi 0}}$ and $\frac{\Delta\eta}{\Delta T_S}$ are all constants.

$$\eta_{power} = \eta_{CHP_{P0}} - \frac{\Delta\eta}{\Delta T_S} T_S \tag{2.20}$$

$$\eta_{heat} = \eta_{CHP_{\Phi 0}} + \frac{\Delta\eta}{\Delta T_S} T_S \tag{2.21}$$

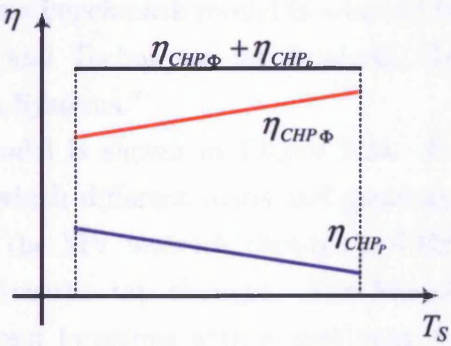

Figure 2.33: Efficiencies of a steam back pressure CHP unit

x) Electric Water Heater

The electric water heater was modelled as a constant efficiency device that converts the input electric power, P_{EWH} into heat, Φ_{EWH}. This is shown by equation 2.22 where η_{EWH} is the heater efficiency.

$$\Phi_{EWH} = \eta_{EWH} P_{EWH} \tag{2.22}$$

xi) Pumps

The pumping power, P_{Pump} required at the district heat station is determined by the mass flow rate, $\dot{m}$, and the required pressure head, Δp [50, 51]. This relation is given by equation 2.23 where ρ is the water density.

$$P_{Pump} = \frac{\dot{m}\Delta p}{\rho} \tag{2.23}$$

2.8 An Energy MicroGrid Test System

An Energy MicroGrid test system was used in the study cases in this research. This system comprises an electric network and a DHS. The electric network is the CIGRE Benchmark MicroGrid system [21]. The DHS system was devised based on the topology of the electric network and the the data for the district heat system pipes described in [62].

2.8.1 The CIGRE Benchmark MicroGrid System

A benchmark model for a MicroGrid was described in [21] as a part of the EU MicroGrids project. This benchmark model is adopted by CIGRE TF C6.04.02, "Computational Tools and Techniques for Analysis, Design and Validation of Distributed Generation Systems."

This benchmark model is shown in Figure 2.34. It includes a main 315m distribution feeder to which different loads and generators are connected. This feeder is connected to the MV network through a 400kVA transformer with a 5 step $\pm 2.5/ \pm 5\%$ off-circuit tap changer. The MiceoGrid has 21 consumers conencted at five different locations with a maximum aggregated load of 116.4 kVA. Five MicroSources with total capacity of 63kW and a 30kW flywheel are connected to the MicroGrid.

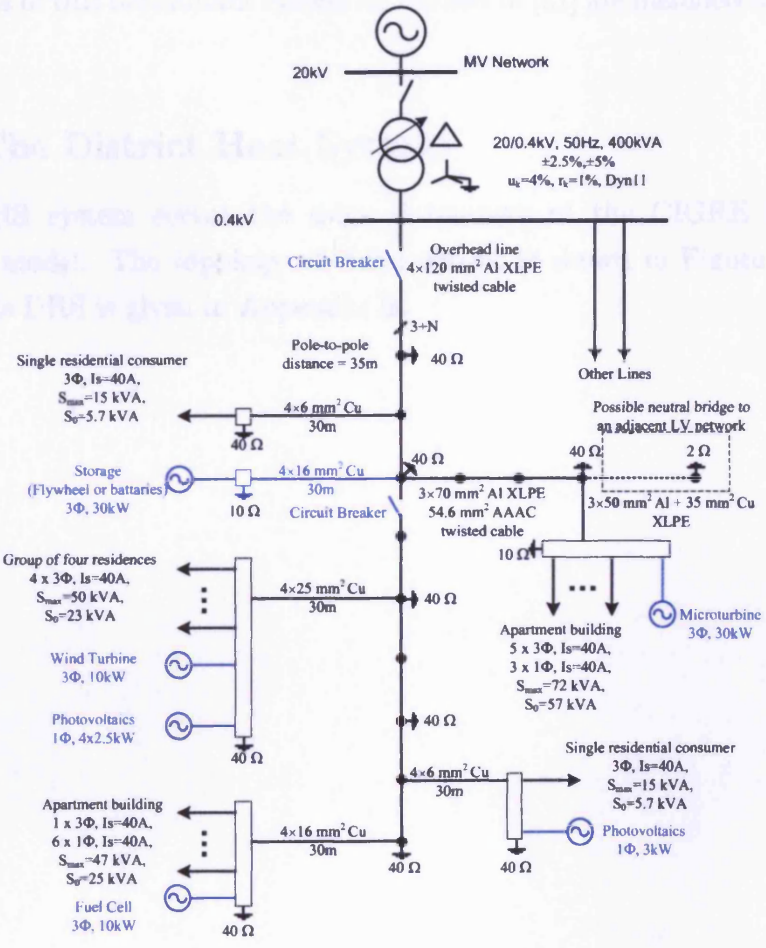

Figure 2.34: The CIGRE benchmark MicroGrid [21].

A larger system comprising this MicroGrid and two distribution feeders supplied from the main transformer, Figure 2.35, was also described in [21]. This system is suitable to investigate the effects of MicroGrids on other LV networks supplied to the same transformer. It also allows the investigation of the control of multiple MicroGrids if some MicroSources were assumed to be connected to any or both of the passive LV feeders.

The data of this benchmark system as defined in [21] are included in Appendix B.

2.8.2 The District Heat System

The DHS system serves the same consumers of the CIGRE benchmark MicroGrid model. The topology of this network is shown in Figure 2.36. The date for this DHS is given in Appendix B.

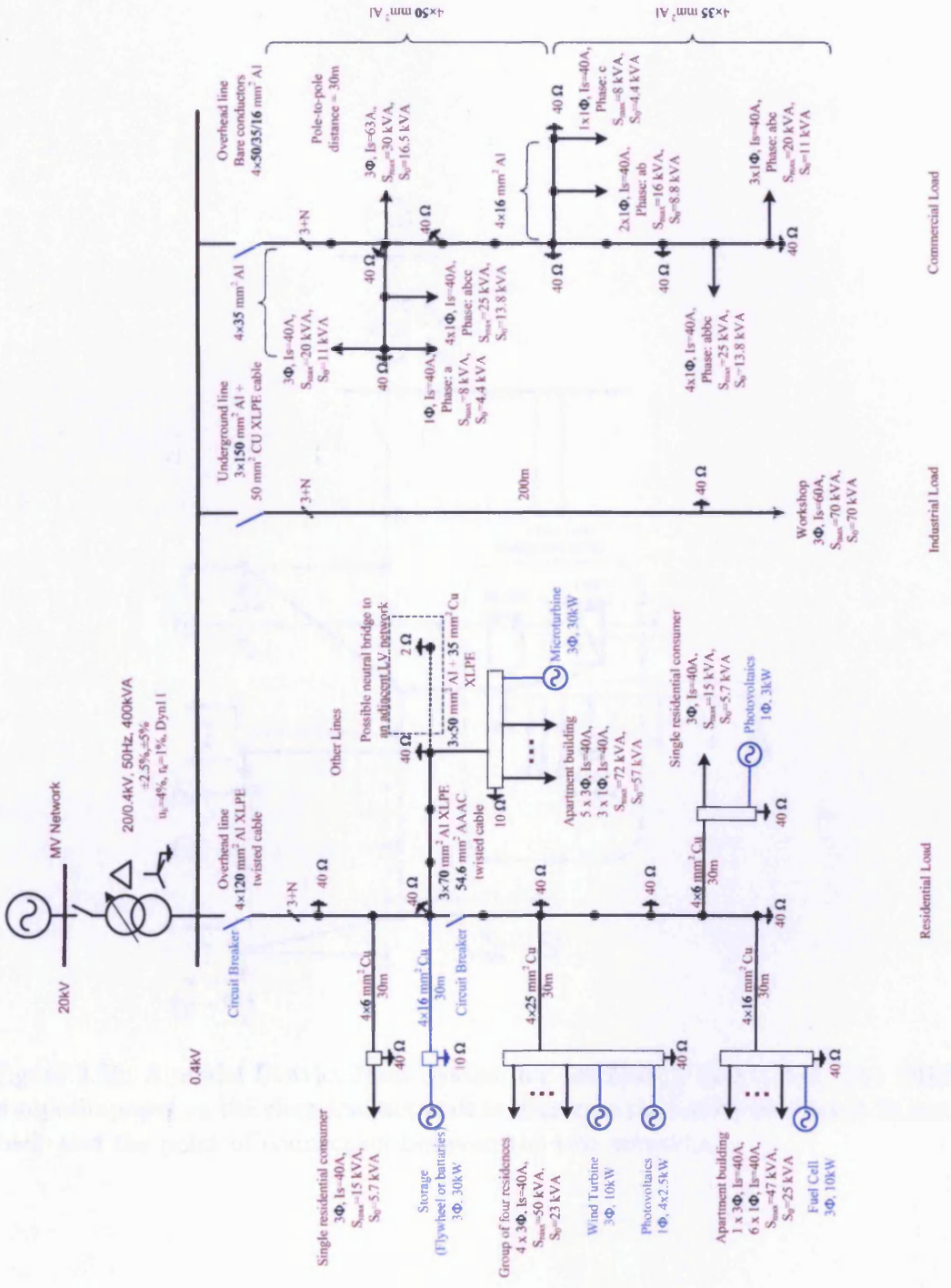

Figure 2.35: The benchmark MicroGrid with multiple distribution feeders [21].

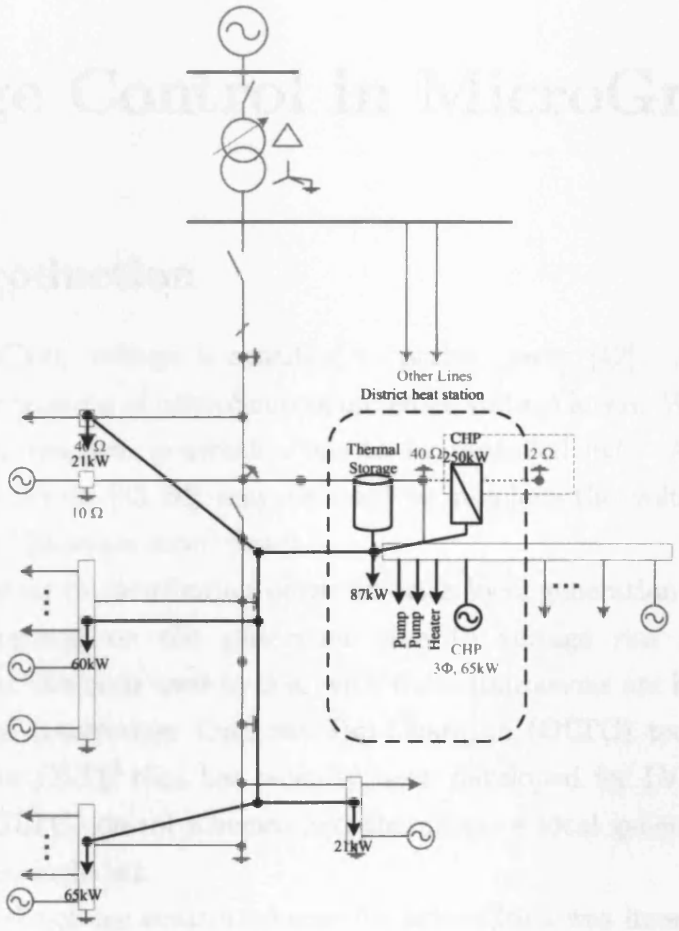

Figure 2.36: A model District Heat System for the Energy MicroGrid. The DHS is superimposed on the electrical network to illustrate the locations of the different loads and the point of connection between the two networks

Chapter 3

Voltage Control in MicroGrids

3.1 Introduction

In a MicroGrid, voltage is sensitive to active power [42]. An increase in active power generation of MicroSources increases voltage levels. When the upper voltage limit is reached, generation has to be curtailed [63]. Active network management schemes [63, 64] may be used to regulate the voltage and allow MicroSources to generate more power.

Voltage control in distribution networks with local generation was reviewed. Limitations imposed on the generation due to voltage rise are described. Techniques that has been used to deal with these limitations are highlighted.

A review of transformer On-Load-Tap-Changers (OLTC) technologies was undertaken. An OLTC that has recently been developed for LV networks [65] is described. OLTC control schemes and the effect of local generation on these schemes are also included.

A multi-level voltage control scheme for MicroGrids was investigated. This scheme coordinates reactive power control of MicroSources and the OLTC control. It was applied to the MicroGrid benchmark network [21] to illustrate its performance.

Application of this voltage control system in networks where multiple MicroGrids and passive distribution feeders are supplied from the same transformer was also investigated. A simple rule-based system was used in the OLTC controller to decide the suitable tap action based on control signals from all MicroGrids and feeders. The operation of this system in a network comprising two MicroGrids and a distribution feeder is illustrated.

3.2 Voltage Control in Distribution Networks

In a simple radial distribution network, Figure 3.1, voltages are determined by active and reactive power flow, P and Q; and by the line parameters, R and X. The per-unit voltage rise in this system , $V_2 - V_1$, is approximately given by equation 3.1 [66].

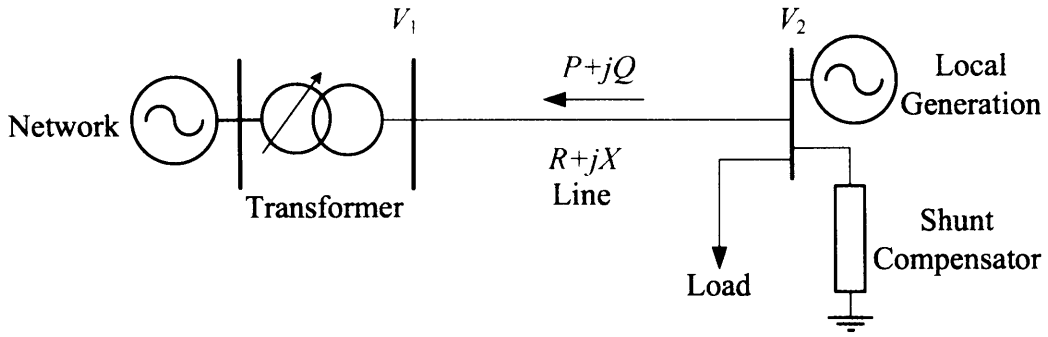

Figure 3.1: A simple radial distribution network.

$$V_2 - V_1 \approxeq PR + QX \tag{3.1}$$

The value of V_2 may be regulated through changing P, Q, or V_1.

3.2.1 Active Power Curtailment

Active power flow, P, has a large effect on the voltage levels in distribution networks due to the low X/R ratio [66]. If the generation is much higher than the load, voltage may exceed its limit. In this case, generation must be curtailed [63]. This often limits the installed generation capacity and the allowable generation of the connected units [63, 66].

3.2.2 Reactive Power Control

Reactive power flow, Q, may be changed using reactive power compensators [41, 67] or generator reactive power control [68]. The effect of reactive power on voltage levels is less than that of active power due to the low X/R ratio. Nevertheless, it has been used by many authors [68–71] to regulate the voltage and reduce generation curtailment.

3.2.3 On-Load-Tap-Changers

Voltage, V_1, is controlled by regulating transformers [41, 67]. These transformers have multiple taps on one of their windings, usually the HV windings. Selecting a different tap position changes the transformer turns ratio, and consequently its voltage ratio. Regulating transformers were used in [63, 64] to reduce voltage excursions and hence increase the power generated.

On Load Tap Changers, OLTCs, change the tap position of regulating transformers without disconnecting the load. They are usually installed where frequent tap changes are required.

Transformers with no OLTC have to be disconnected from the network to change their taps. In this case, taps are changed only to allow load growth or seasonal changes [41].

The most common type of OLTCs use mechanical switches [72]. Some OLTCs that use power electronic switches were found in literature [72–74]. Recently, a vacuum switch OLTC was built for LV networks [65].

Mechanical OLTC

Figure 3.2 shows a mechanical selector-diverter switch mechanism. In this mechanism, a selector switch is used to set the tap position required. This selector switch is not able to make or break the current A mechanical diverter switch is used to transfer the load current to the selected tap. Resistors are inserted in the circuit to limit the current that is circulated between taps during the tap changing process.

Arcing occurs at the contacts of the diverter switch of the OLTC during tap changing. This reduces the lifetime of the contacts and contaminates the insulating oil [72]. The arc is extinguished at the zero current crossing point.

This mechanism is robust and reliable. On the other hand, it is slow, expensive, and bulky [65]. Its life is limited by a total number of tap changing operations [72]. Its current limiting resistors cause voltage sags during tap changing.

Power electronic OLTC

Several attempts were made to use power electronic diverter switches rather than the mechanical one [72–74]. Two of these power electronic diverter switches

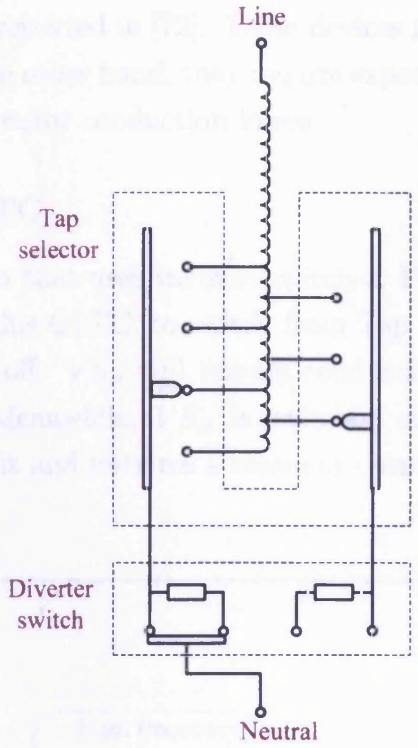

Figure 3.2: Mechanical selector-diverter switch OLTC

are shown in Figure 3.3.

Power electronic diverter switches use thyristor switches to transfer the current between taps. This prevents arcing. Afterwards, mechanical switches [74], or vacuum switches [72] short circuit the thyristors and carry the load current.

In [74] , thyristors were isolated from the circuit after their current is transferred to the mechanical switch.

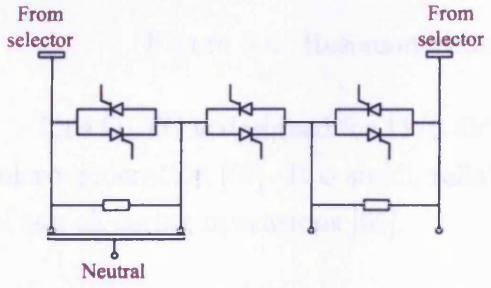

(a) Current is transferred to a mechanical switch [73, 74]

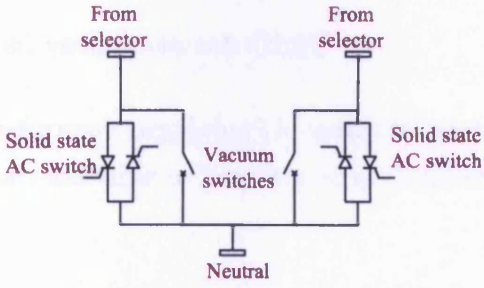

(b) Current is transferred to a vacuum switch [72]

Figure 3.3: Power electronic diverter switches for OLTCs.

Power electronic diverter switches in which thyristors carry the load current

for the whole time were reported in [72]. These devices are fast as no mechanical switches are used. On the other hand, they require expensive thyristor protection and they give rise to thyristor conduction losses.

Vacuum switches OLTC

An OLTC mechanism that uses vacuum switches, Figure 3.4, was developed at Areva T&D [65]. In this OLTC, to switch from Tap A to tap B, the vacuum switch VS_A is switched off. VS_A will remain conducting as arcing takes place between its contacts. Meanwhile, VS_B is switched on. This closes the high frequency resonant circuit and initiates a resonant current that extinguishes the arc in VS_A.

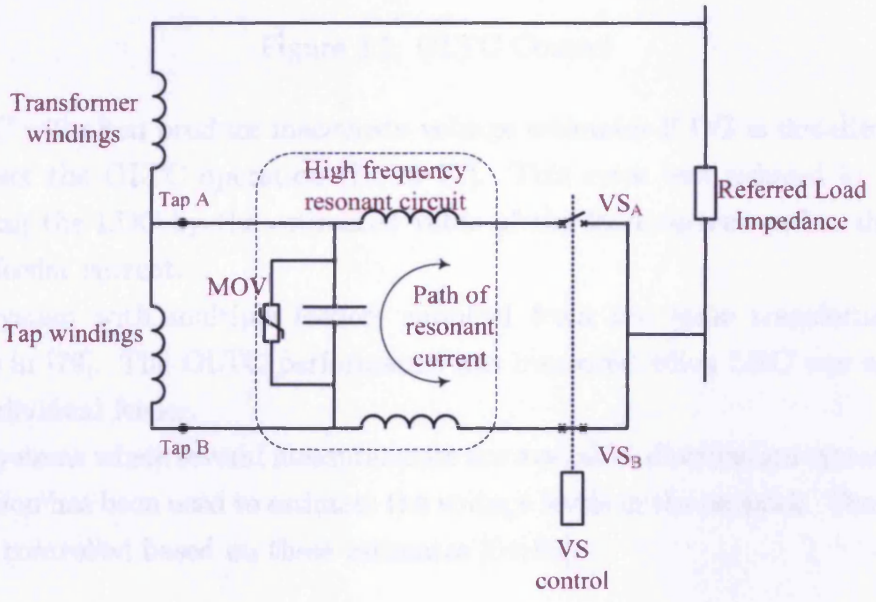

Figure 3.4: Resonant-commutated vacuum-switch OLTC

This OLTC is designed for 11/0.4kV transformers supplying LV networks with micro-generation [65]. It is small, reliable, fast, and able to handle a large number of tap changing operations [65].

OLTC control

Two OLTC control schemes are shown in Figure 3.5. In these schemes, the OLTC maintains the voltage of a certain point within a deadband. This point is either at the transformer secondary, as in Figure 3.5(a), where voltage is measured

directly; or close to the load, as in Figure 3.5(b), where Line Drop Compensation (LDC) is used to estimate the voltage.

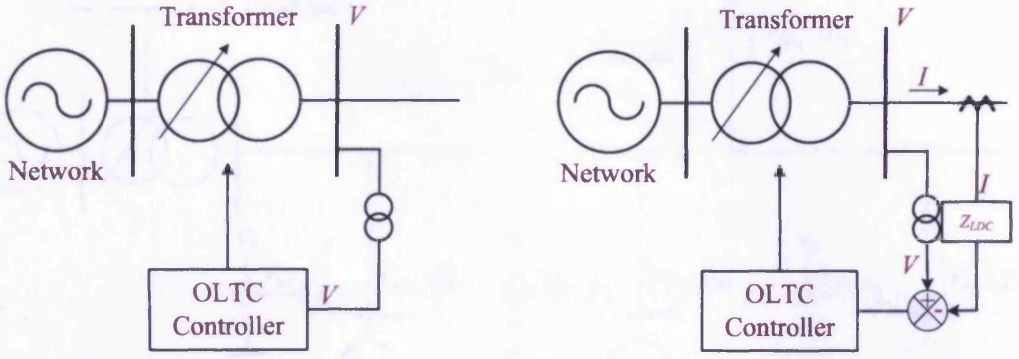

(a) OLTC used to control the voltage of the LV busbar

(b) OLTC used to control the voltage at a remote point

Figure 3.5: OLTC Control

LDC will often produce inaccurate voltage estimates if DG is installed. This will affect the OLTC operation [70, 75–77]. This error was reduced in [78] by supplying the LDC by the estimated value of the load current rather than the actual feeder current.

A system with multiple feeders supplied from the same transformer was studied in [79]. The OLTC performance was improved when LDC was used for each individual feeder.

In systems where several measurements are available, distribution system state estimation has been used to estimate the voltage levels in the network. The OLTC is then controlled based on these estimates [64, 80].

3.3 Multi-Level Voltage Control in a MicroGrid

A multi-level voltage control scheme was used to regulate the voltage in MicroGrids. This scheme, shown in Figure 3.6, coordinates between MicroSource controllers and the OLTC controller. MicroSource controllers respond instantaneously to voltage excursions by changing the reactive power output of their MicroSouces. The OLTC is then controlled to maintain the reactive power output of one MicroSource, hereafter termed the Control MicroSource, MS_C, within a deadband.

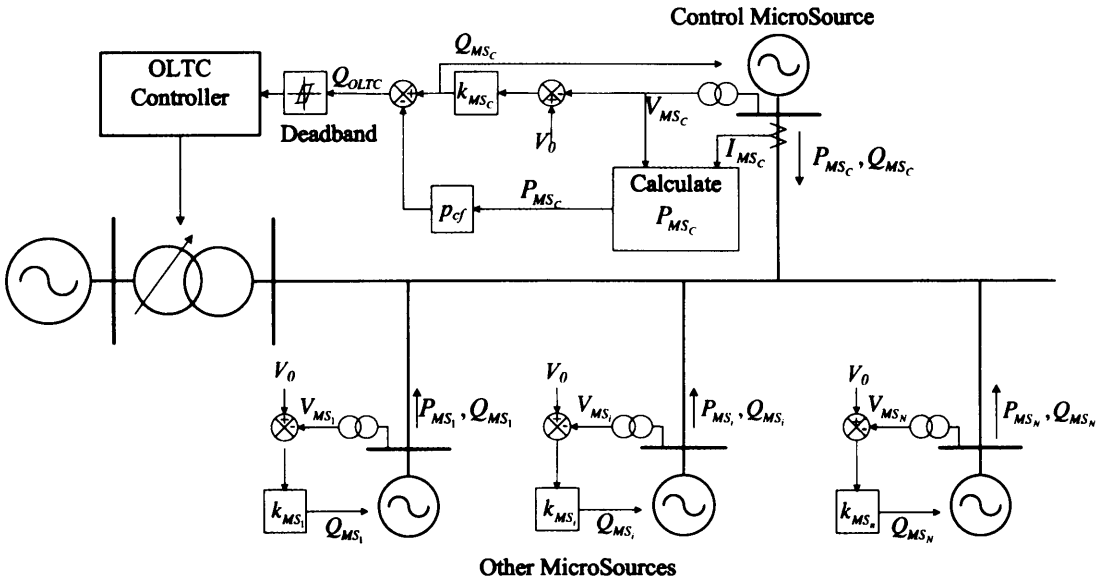

Figure 3.6: A multi-level voltage control scheme for a MicroGrid

3.3.1 Primary Control

The primary voltage control is provided by MicroSource controllers. They use voltage/reactive power droop control, as in [16, 42, 43, 81], to reduce voltage excursions.

The droop characteristic of a MicroSource, MS_i, is shown in Figure 3.7. This characteristic is described by Equation 3.2 where Q_{MS_i} is the reactive power output of MS_i, V_{MS_i} is its terminal voltage, V_0 is 1.0p.u., and k_{MS_i} is a constant. The value of k_{MS_i} is calculated from equation 3.3 where ΔV_{max} is the maximum permissible voltage deviation and Q_{MS_i-max} is the reactive power rating of the MicroSource.

$$Q_{MS_i} = -k_{MS_i}(V_{MS_i} - V_0) \tag{3.2}$$

$$k_{MS_i} = \frac{Q_{MS_i-max}}{\Delta V_{max}} \tag{3.3}$$

Figure 3.8 shows the droop characteristics of the Control MicroSource, MS_C, and another MicroSource, MS_i. Changes in the operating point of both MicroSources following an increase in the output power of MS_i, P_{MS_i}, were tracked on these characteristics.

At the initial operating point in Figure 3.8, point 1, both MS_C and MS_i

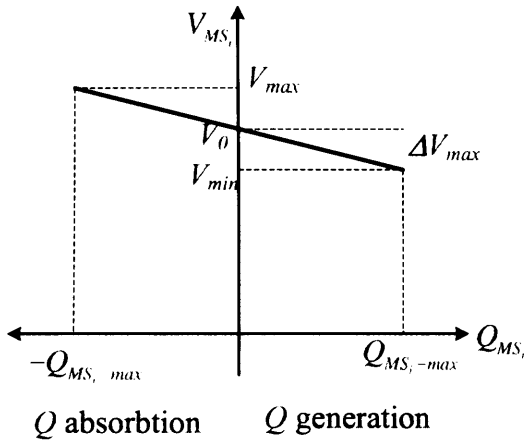

Figure 3.7: A typical voltage/reactive power droop characteristic

were operating at 1.0p.u. voltage and zero reactive power output. The increase in P_{MS_i} increases the voltage at all busbars. This moves the operating point to point 2 in Figure 3.8. All MicroSources, being droop controlled, start absorbing reactive power to reduces the voltage excursion and move the operating point to point 3.

The changes in reactive power output of both MicroSources are of different magnitudes but have the same direction. Therefore, a change in Q_{MS_C} indicates that a similar change in Q_{MS_i} should have taken place.

Due to the high reactance of the transformer, the voltage of the transformer LV busbar is more sensitive to reactive power than active power. Any MicroSource connected to this busbar should work on constant reactive power output to prevent unnecessary reactive power circulation.

3.3.2 Secondary Control

The OLTC controller tries to maintain Q_{MS_C} within a deadband. As point 3 in Figure 3.8 is outside this deadband, the OLTC controller taps to reduce the voltage and the operating point moves to point 4.

The deadband must be wider than the change in Q_{MS_C} associated with any single tap step. This change is approximately calculated by equation 3.4 where V_s is the open circuit transformer voltage at the initial tap position, ΔV_s is the change in the transformer open circuit voltage due to the tap step, X is the total reactance from the control MicroSource to MV network, and $\mathbb{MS}$ is the set of all MicroSources in the MicroGrid . Full derivation of this equation is in

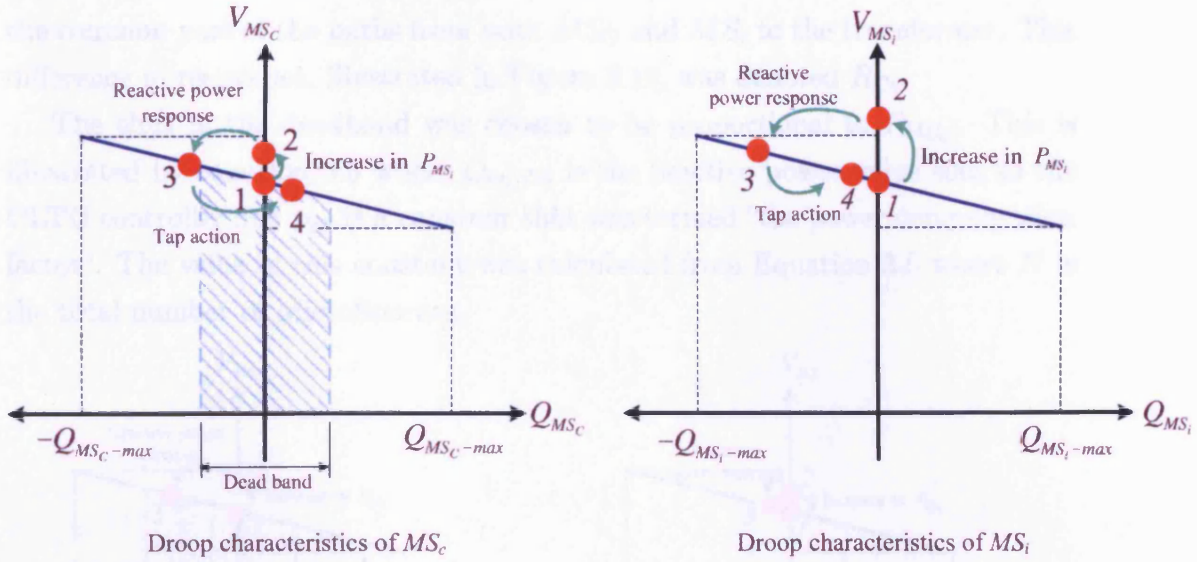

Figure 3.8: The principle of operation of the multi-level voltage control system

appendix C. This deadband was increased by 20% to account for uncertainties and approximations.

$$\Delta Q_{MS_C} = -\frac{k_{MS_C}}{2}\left(1 + \frac{V_s - X\sum_{i\in \mathrm{MS}} k_i}{\sqrt{\left(V_s - X\sum_{i\in \mathrm{MS}} k_i\right)^2 + 4V_0 X\sum_{i\in \mathrm{MS}} k_i}}\right)\Delta V_s \qquad (3.4)$$

3.3.3 The Power Compensation Factor

Figure 3.9 tracks the changes in the operating point of both MS_C and MS_i for an increase in P_{MS_C}. Point 1 is the initial operating point. Point 2 is the operating point with no reactive power response. Point 3 is the operating point after the reactive power response.

At point 3, V_{MS_C} is much higher than V_{MS_i} and Q_{MS_C} is outside the deadband. A tap operation would bring this value inside the deadband and cause a large drop in V_{MS_i}. This tap operation is prevented by shifting the deadband to compensate for the effect of the active power generated by MS_C.

The difference between ΔV_{MS_C} and ΔV_{MS_i} is determined by the difference between the resistance from the MS_C to the transformer and the resistance of

the common part of the paths from both MS_C and MS_i to the transformer. This difference in resistance, illustrated in Figure 3.10, was denoted R_{Ci}.

The shift in the deadband was chosen to be proportional to P_{MS_C}. This is illustrated by equation 3.5 where Q_{OLTC} is the reactive power value sent to the OLTC controller and p_{cf} is a constant that was termed "the power compensation factor". The value of this constant was calculated from Equation 3.6 where N is the total number of MicroSources.

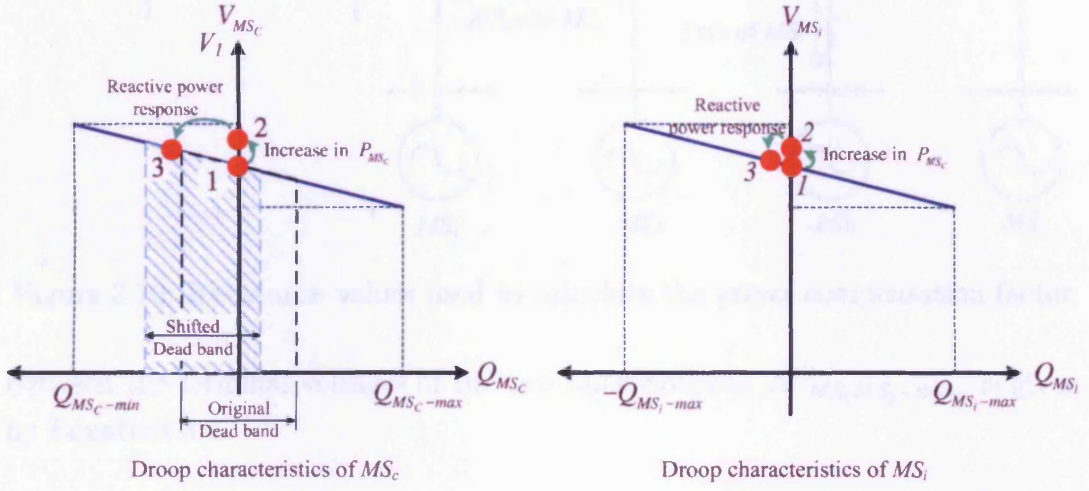

Figure 3.9: Deadband shifting

$$Q_{OLTC} = Q_{MS_C} - p_{cf} P_{MS_C} \tag{3.5}$$

$$p_{cf} = k_{MS_C} \frac{\sum_{i \in \mathbb{MS}} R_{Ci}}{N-1} \tag{3.6}$$

3.3.4 Selection of The Control MicroSources

Each section l of an overhead line or a cable in the MicroGrid, Figure 3.11, has a resistance R_l and a thermal limit P_{l-max}. The maximum per unit voltage drop across this feeder ΔV_{l-max} is calculated by Equation 3.7.

$$\Delta V_{l-max} = R_l P_{l-max} \tag{3.7}$$

The path between any two MicroSources, MS_i and MS_j, is made of a set $\mathbb{E}_{MS_i MS_j}$ of overhead lines/cables sections. The maximum possible difference

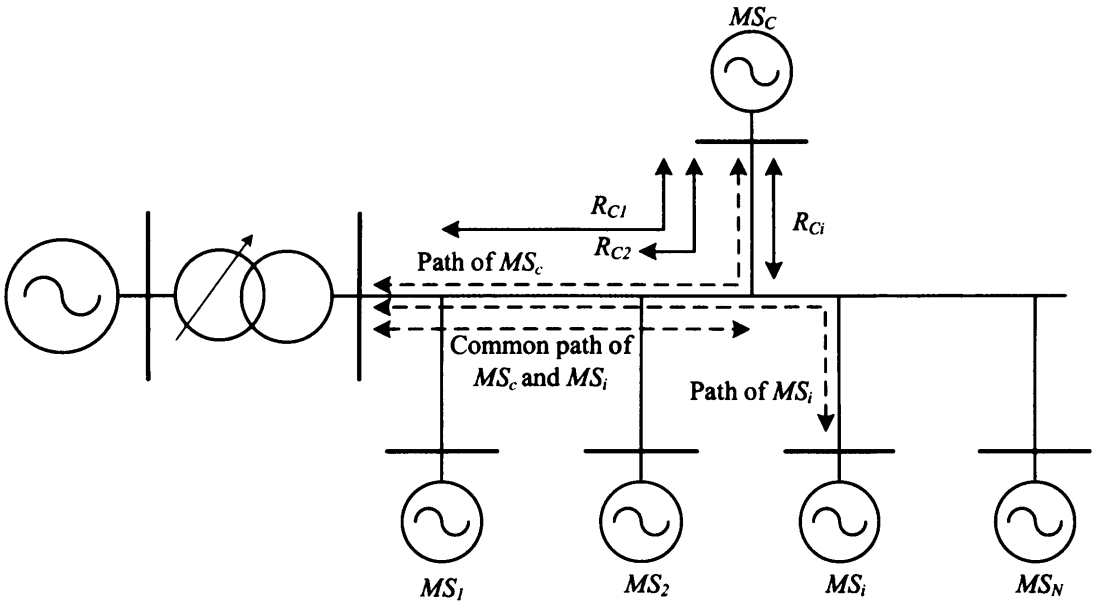

Figure 3.10: Resistance values used to calculate the power compensation factor

between the terminal voltages of the two MicroSources, $\Delta V_{MS_iMS_j-max}$, is given by Equation 3.8.

$$\Delta V_{MS_iMS_j-max} = \sum_{l \in \mathbb{E}_{MS_iMS_j}} \Delta V_{l-max} \tag{3.8}$$

Ideally, the voltage control system would maintain the reactive power output of the Control MicroSource at zero and its terminal voltage, V_{MS_C} at 1.0pu. In this case, the terminal voltage of the MicroSource MS_i, V_{MS_i}, will be within the range of 1.0pu$\pm\Delta V_{MS_CMS_i-max}$ where $\Delta V_{MS_CMS_i-max}$ is the maximum possible difference between the voltage of MS_C and that of MS_i. The smaller the value of $\Delta V_{MS_CMS_i-max}$ is the smaller the voltage excursion at the MicroSource MS_i will be.

$\Delta V_{MS_iMS_j-max}$ was calculated for every two MicroSources, $MS_i \in \mathbb{MS}$ and $MS_j \in \mathbb{MS}$. For every MicroSource MS_i, an average value for the maximum voltage difference between this MicroSource and other MicroSources was calculated using Equation 3.9 where N is the total number of MicroSources. The standard deviation of the same values were then calculated using Equation 3.10.

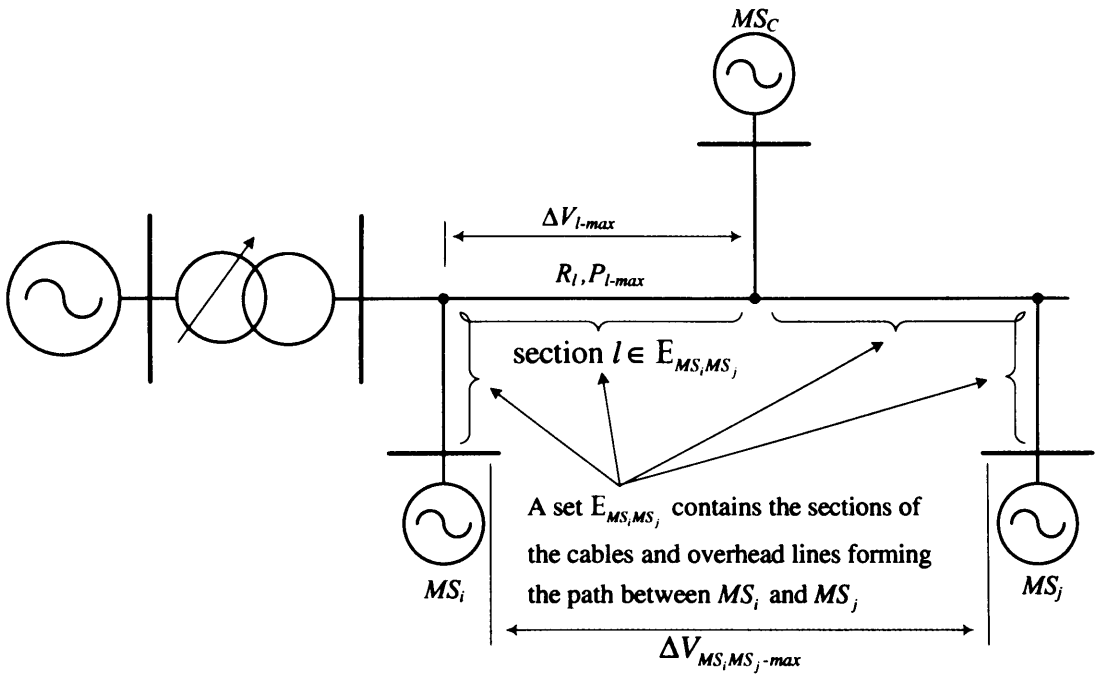

Figure 3.11: Selection of the Control MicroSource

$$\overline{\Delta V}_{MS_i MS_j-max}\big|_{MS_i} = \frac{\sum_{MS_j \in \mathbf{MS}, MS_j \neq MS_i} \Delta V_{MS_i MS_j-max}}{N-1} \tag{3.9}$$

$$\sigma\left(\Delta V_{MS_i MS_j-max}\right)\big|_{MS_i} = \sqrt{\frac{\sum_{MS_j \in \mathbf{MS}, MS_j \neq MS_i} \left(\Delta V_{MS_i MS_j-max} - \overline{\Delta V}_{MS_i MS_j-max}\big|_{MS_i}\right)^2}{N-1}} \tag{3.10}$$

The Control MicroSource was chosen to be the MicroSource which value of $\overline{\Delta V}_{MS_i MS_j-max}\big|_{MS_i} + 2\,\sigma\left(\Delta V_{MS_i MS_j-max}\right)\big|_{MS_i}$ is less than that of all other MicroSources.

3.4 Voltage Control with Multiple MicroGrids and Feeders

In practice, multiple MicroGrids and passive distribution feeders may be connected to the same distribution transformer as shown in Figure 3.12. In

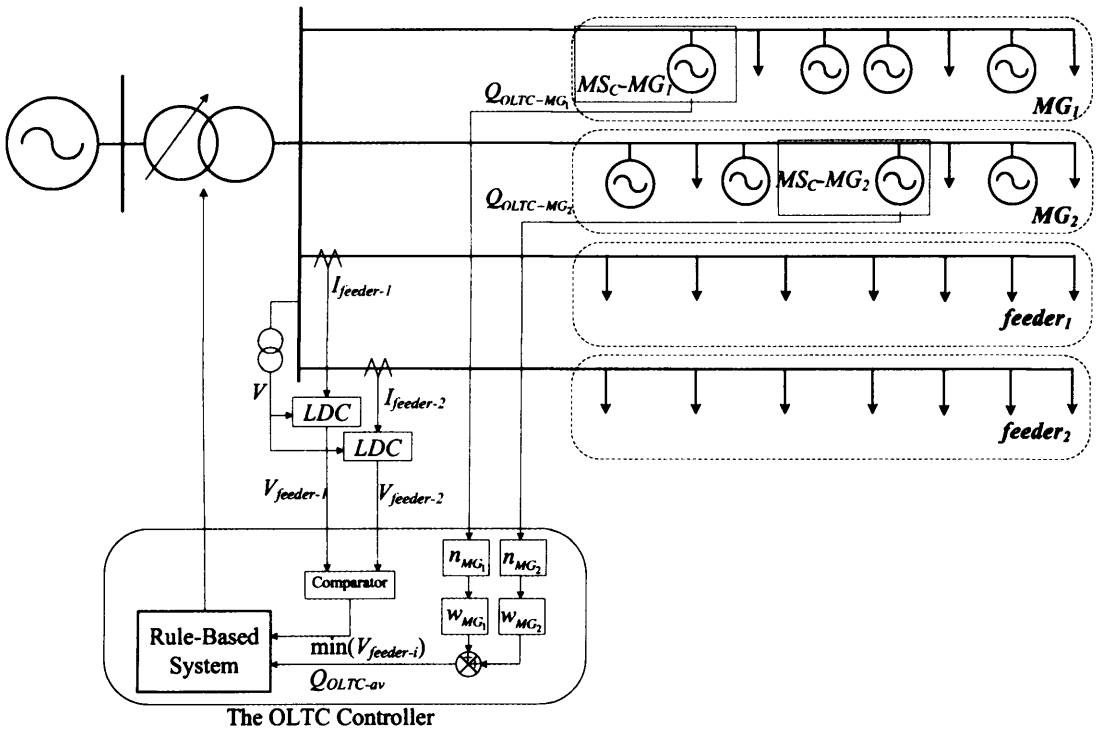

Figure 3.12: Multi MicroGrid/feeder operation

this case, the voltage control scheme should take care of the voltage levels of all MicroGrids and feeders.

Each MicroGrid has its own Control MicroSource. The Control MicroSource of the MicroGrid MG_i sends its reactive power value, $Q_{OLTC-MG_i}$ to the OLTC controller.

Due to the difference in ratings between different Control MicroSources, the individual values of reactive power sent to the OLTC controller will have different ranges. These values are multiplied by normalisation factors to account for these differences.

The normalisation factor for the MicroGrid MG_i, n_{MG_i}, is calculated by equations 3.11. In this equation, $Q_{MS_C-MG_i-max}$ is the reactive power rating of the Control MicroSource of MG_i, $\sum_{MG_i \in \mathbf{MG}} Q_{MS_C-MG_i-max}$ is the sum of the reactive power ratings of all Control MicroSources.

$$n_{MG_i} = \frac{\sum_{MG_i \in \mathbf{MG}} Q_{MS_C-MG_i-max}}{Q_{MS_C-MG_i-max}} \tag{3.11}$$

The resulting value of each MicroGrid is then weighted by the total capacity of MicroSources installed in this MicroGrid. The weighing factor for the MicroGrid

MG_i, w_{MG_i}, is calculated using equation 3.12 where $\mathbb{MG}$ is the set of all MicroGrids connected to the transformer, $\mathbb{MS}_{MG_i}$ is the set of all MicroSources in the MicroGrid MG_i, $P_{MS_j-rated}$ is the active power rating of the MicroSource MS_j.

$$w_{MG_i} = \frac{\sum_{MS_j \in \mathbb{MS}_{MG_i}} P_{MS_j-rated}}{\sum_{MG_i \in \mathbb{MG}} \left(\sum_{MS_j \in \mathbb{MS}_{MG_i}} P_{MS_j-rated} \right)} \tag{3.12}$$

The average value of these weighted values, $Q_{OLTC_{av}}$, is then calculated.

The voltage at the end of each passive feeder, $V_{feeder-i}$, is estimated by LDC. The OLTC controller selects the minimum value of these estimated voltages, $\min(V_{feeder-i})$.

The OLTC controller uses a simple rule-based system to decide the action required. The rules applied are:

1. If $\min(V_{feeder-i})$ is below the minimum allowable voltage, V_{min} then increase the voltage.
2. If $Q_{OLTC_{av}}$ is outside the deadband then
   (a) If reactive power is being generated, then increase the voltage.
   (b) If reactive power is being absorbed, then check the value of $\min(V_{feeder-i})$
      i. If decreasing the voltage will reduce $\min(V_{feeder-i})$ below V_{min} then do nothing.
      ii. If decreasing the voltage will not reduce $\min(V_{feeder-i})$ below V_{min} then reduce the voltage.

3.5 Case Studies

This control scheme was applied to the network shown in Figure 3.13. This system is based on the CIGRÉ MicroGrid benchmark model [21]. It comprises two MicroGrids, MG_1 and MG_2, and a passive distribution feeder connected to the same distribution transformer. All loads and generation were assumed to be balanced across the three phases. MicroSources connected at the same

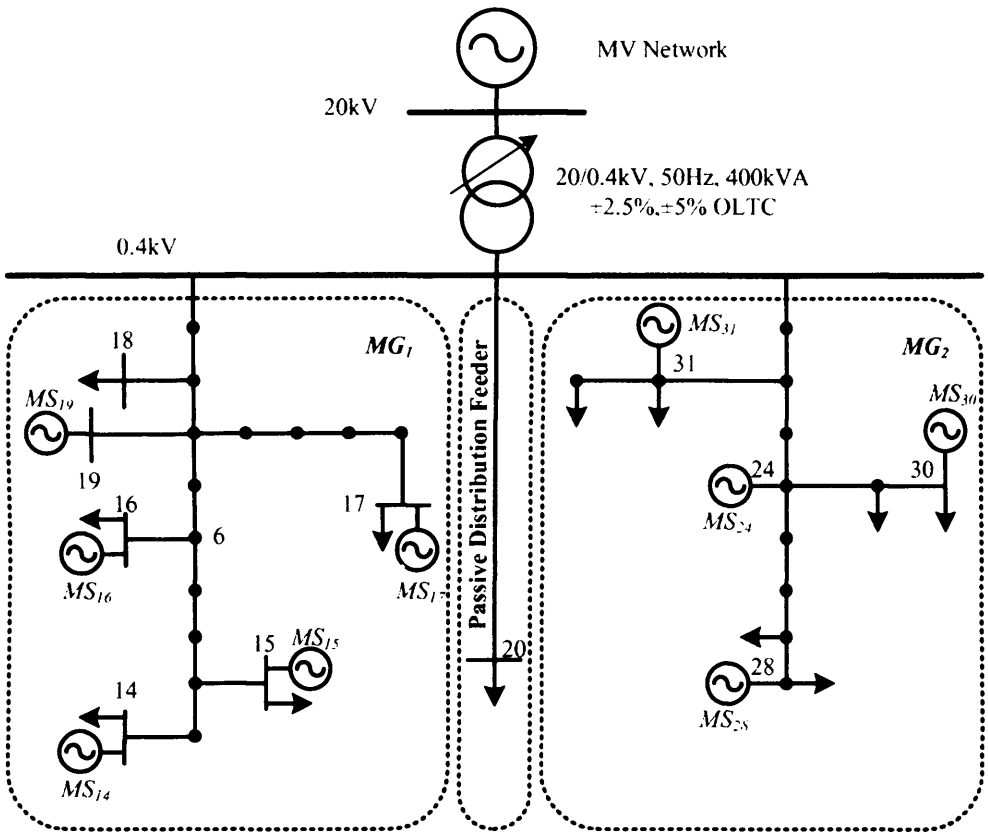

Figure 3.13: Network used to test the voltage control system

busbar were lumped into one MicroSource. The ratings of MicroSources and the parameters of the control system are given in appendix D.

3.5.1 Single MicroGrid Operation

Only MG_1 was considered. The maximum voltage differences between every two MicroSources in this MicroGrid is included in Appendix D. The value of $\overline{\Delta V}_{MS_iMS_j-max}\big|_{MS_{16}} + 2\,\sigma\left(\Delta V_{MS_iMS_j-max}\right)\big|_{MS_{16}}$ was found to be smaller than its equivalent for other MicroSources. Based on this fact,MS_{16} was selected to be the Control MicroSource.

Figure 3.14 shows four cases of the operating point moving along the droop characteristics for the two MicroSources MS_{16} and MS_{19}. The points in this figure are marked as follows:

- Initial point at which the system is operating at no load, no generation, and rated transformer open circuit voltage.

- Operating points after a change in generation or load with no tap change.
- ■ Operating point after a tap change.

The four cases in Figure 3.14 are as follows:

1. The system was fully loaded except at busbar 16. The MicroGrid voltages consequently dropped and the MicroSources responded by generating reactive power. As the reactive power generation by the Control MicroSource, Q_{16}, was outside the deadband, the OLTC increased the voltage by 2.5%.

2. Four MicroSources increased their output power; MS_{14} to 15kW, MS_{15} to 4.5kW, MS_{17} to 45kW, and MS_{19} to 45kW. All MicroSources, due to droop control, started absorbing reactive power to reduce the voltage. The high reactive power absorbed by MS_{16} triggered a tap action that reduced the transformer voltage by 2.5%.

3. The Control MicroSource, MS_{16}, increased its generation to 40kW. The increase in its terminal voltage and the resulting change in its reactive power output were larger than these of any other MicroSource. The deadband was shifted to the left which prevented the tap action.

4. This case is similar to case 3 but the increase in power generation of MS_{16} was 100kW. The voltage rise and the subsequent reactive power absorption of all MicroSources were significant. The deadband shift did not block the tap action and the OLTC reduced the voltage by 2.5%.

The effect of this voltage control scheme on the allowable power generation at the MicroSources' busbars is shown in Figure 3.15 for the cases of:

1. MicroSources operate on zero reactive power output;

2. only reactive power droop control is activated; and

3. the multi-level control is fully deployed.

The thermal limits of the cables connecting the MicroSources to the main feeder are shown by the solid line.

The two sets of results in Figure 3.15 are for the two cases where with thermal limits were not enforced during the simulations, Set (1); and where the thermal

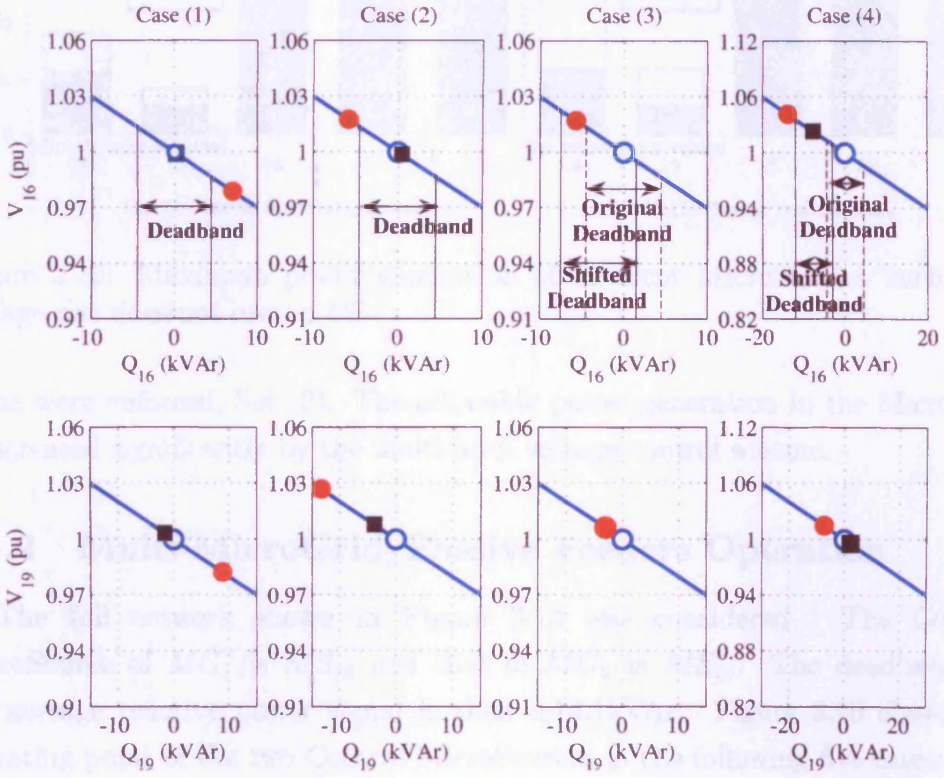

Figure 3.14: Voltage control of a single MicroGrid: Snapshots showing the initial operating point, ○; the operating point after a change in generation or load, ●; and the operating point after a tap step, ■.

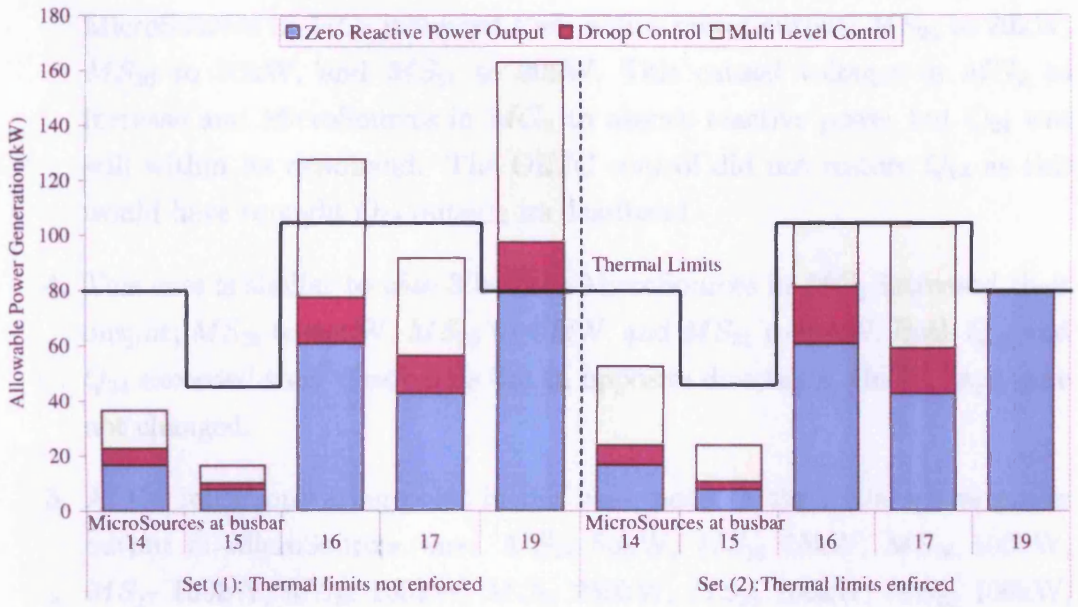

Figure 3.15: Maximum power generation of different MicroSources such that voltage rise does not exceed 6%

limits were enforced, Set (2). The allowable power generation in the MicroGrid is increased significantly by the multi-level voltage control scheme.

3.5.2 Multi-MicroGrid/Passive Feeders Operation

The full network shown in Figure 3.13 was considered. The Control MicroSource of MG_1 is MS_{16} and that of MG_2 is MS_{24}. The deadband for the average reactive power signal is then $\pm$14.1kVAr. Figure 3.16 shows the operating point of the two Control MicroSources in the following five cases:

1. Both MicroGrids were fully loaded except at busbar 16. All voltage levels dropped and all MicroSources started to supply reactive power. As the reactive power output of the two Control MicroSources, Q_{16} and Q_{24}, were outside their deadbands, the OLTC increased the voltage by 2.5%.

2. MG_1 was fully loaded except at busbar 16. Q_{16} exceeded its deadband while Q_{24} did not. The OLTC increased the voltage by 2.5% to bring both values within their deadbands.

3. MG_1 was fully loaded except at busbar 16. As a result, MicroSources in MG_1 started supplying reactive power and Q_{16} left its deadband.

MicroSources in MG_2 increased their active power output; MS_{28} to 20kW, MS_{30} to 20kW, and MS_{31} to 30kW. This caused voltages in MG_2 to increase and MicroSources in MG_2 to absorb reactive power but Q_{24} was still within its deadband. The OLTC control did not restore Q_{16} as this would have brought Q_{24} outside its deadband.

4. This case is similar to case 3 but the MicroSources in MG_2 increased their output; MS_{28} to 40kW, MS_{30} to 40kW, and MS_{31} to 60kW. Both Q_{16} and Q_{24} exceeded their deadbands but in opposite directions. Hence, taps were not changed.

5. At the initial operating point in this case, point $\Diamond$, the initial active power output of MicroSources was: MS_{14} 50kW, MS_{15} 15kW, MS_{16} 100kW, MS_{17} 150kW, MS_{19} 150kW, MS_{24} 250kW, MS_{28} 100kW, MS_{30} 100kW, and MS_{31} 150kW. The initial transformer open circuit voltage was 0.95p.u. A 140kVA load was then connected to the passive distribution feeder. This brought its voltage below 0.94p.u. The OLTC then increased the voltage to 97.5% regardless of the voltage levels in the two MicroGrids.

The effect of this voltage control scheme on the allowable power generation at the busbars where MicroSources are connected is shown in Figure 3.17 for the cases of:

1. MicroSources operate on zero reactive power output;

2. only reactive power droop control is activated; and

3. the multi-level control is fully deployed.

The allowable power generation in both MicroGrids is increased significantly by the multi-level voltage control scheme.

3.6 Conclusion

A multi-level voltage control scheme for MicroGrids was investigated. It is based on the recent availability of a vacuum switch OLTC that has been developed for MV/LV transformers, and the flexible operating capabilities of MicroSources with power electronic interfaces. It uses reactive power for primary control and

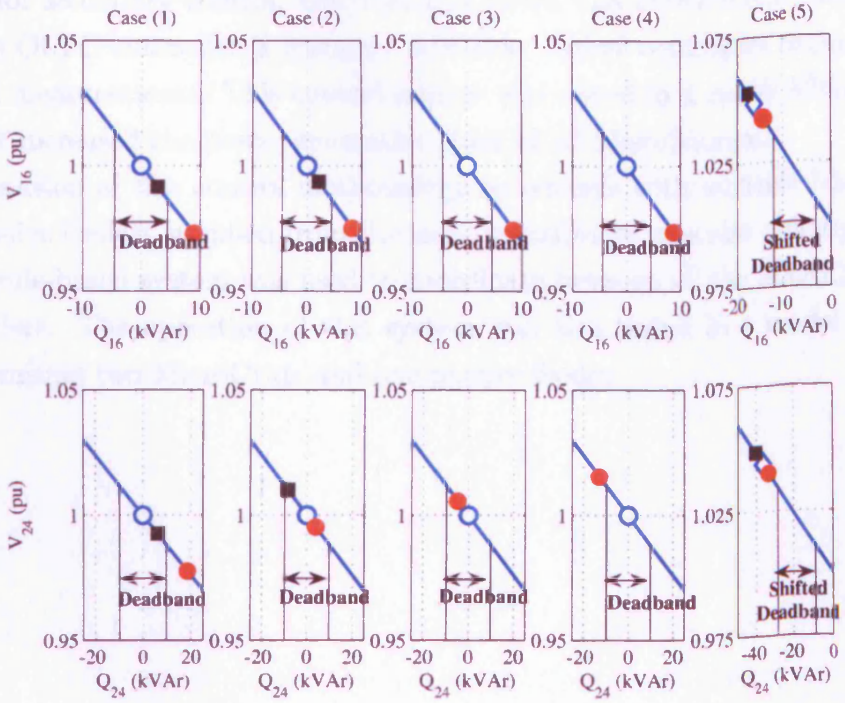

Figure 3.16: Voltage control with multiple MicroGrids/ passive feeders supplied from the same transformer: Snapshots showing the initial operating point, ○; the operating point after a change in generation or load, ●; and the operating point after a tap step, ■.

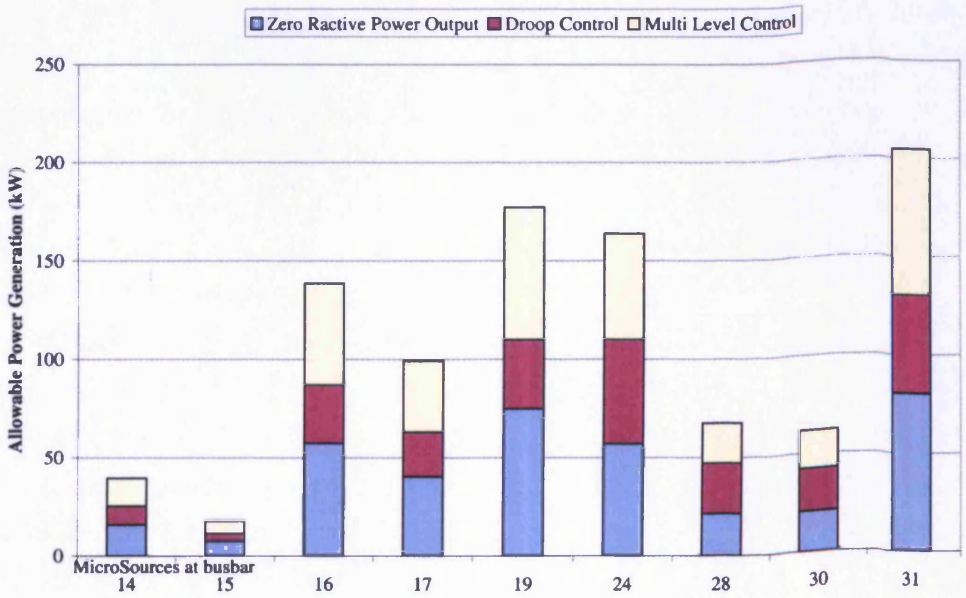

Figure 3.17: Maximum power generation of different MicroSources for the case of Multi-MicroGrid/Passive Feeders Operation

OLTC for secondary control. One communication link between one MicroSource and the OLTC controller is assumed available. Other controllers responds only to local measurements. This control scheme was tested in a model MicroGrid in which it increased the power generation limit of all MicroSources.

Expansion of this control methodology to systems with multiple MicroGrids and passive feeders supplied from the same transformer was also investigated. A simple rule-based system was used to coordinate between all the MicroGrids and the feeders. The operation of this system was also tested in a model network compromising two MicroGrids and one passive feeder.

Chapter 4

Frequency Control in MicroGrids

4.1 Introduction

A MicroGird should be able to operate as an electrical island. This is to increase the reliability of electricity supply and to allow consumers to benefit from their generators when the main grid connection is lost. In order to allow this, local frequency response is necessary to regulate the frequency during islanded operation.

Frequency excursions in an islanded MicroGrid are expected to be larger than those in a transmission network. This is due to fast changes in loads [82] and the limited frequency response capabilities of MicroSources. These excursions should be limited to the ranges that are considered in equipment product standards. These ranges are defined in the European Standard EN50160 [83].

The frequency response characteristic of the GB network was used as a guideline to define frequency targets in an islanded MicroGrid. These targets were chosen such that loads do not respond to frequency events during grid connected operation. These targets are outlined in this chapter.

A frequency control system for an islanded MicroGrid was simulated. This system employed MicroSources, storage, and non-critical loads to provide frequency response. Intelligent Load Management Controllers were used to shed and restore non-critical loads to supply the load frequency response required. MicroSource controllers, storage controllers and load controllers are described and their operation explained.

Four case studies were simulated to investigate the performance of this frequency control system. The simulation results are included.

4.2 Frequency Response Characteristic

4.2.1 Supply Standard - EN50160

The European standard EN50160 [83] defines frequency ranges that consumers could expect their supply to stay within. These ranges for LV networks are listed in Table 4.1. These values specify the operating ranges to be taken into account for equipment product standards [83].

Table 4.1: Frequency limits in LV networks according to the supply standard EN50160 [83]

Synchronous connection to an interconnected power system	Connection Available		Connection not Available	
Duration	99.5% of a year	100% of the time	95.0% of a week	100% of the time
Frequency range	50Hz±1% 49.5 to 50.5Hz	50Hz+4%/-6% 47.0 to 52.0Hz	50Hz±2% 49.0 to 51.0Hz	50Hz±15% 42.5 to 57.5Hz

4.2.2 Frequency Response in the GB Transmission Network

Frequency response for the GB transmission network is described in [84]. The typical frequency response characteristic is shown in Figure 4.1. This characteristic is achieved using frequency response provided by generating units. The transmission network operator should contract enough services to be able to achieve this characteristic for a sudden shortage in power of up to 1320MW which is the largest credible loss of generation risk.

Continues frequency response regulate the frequency during normal operating conditions. Their target is to maintain the frequency within a range of 50±0.2Hz.

Primary frequency response provides fast frequency support subsequent to any sudden shortage in power. It should contain the initial frequency dip within 7 to 15 seconds. It should not allow the frequency to drop below 49.2Hz.

Secondary frequency response service is responsible for restoring the frequency

to its nominal value. This service is slower than the primary response service. Its operating time ranges between 30 seconds to 30 minutes.

Further frequency response service is provided via load shedding. This service is only used during emergency conditions. This is when the contracted response fails to prevent the frequency from dropping to 48.8Hz.

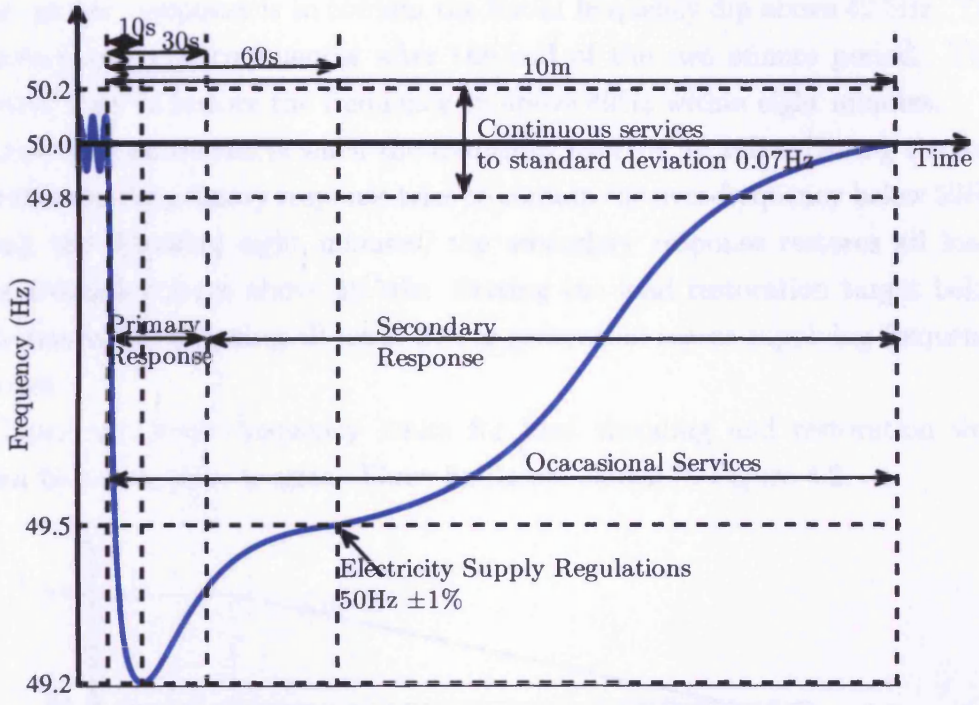

Figure 4.1: Frequency response characteristic of the GB transmission system, [84].

4.2.3 Frequency Targets for an Islanded MicroGrid

During grid connected operation, the MicroGrid frequency is set by the main network. Local frequency response is not required as they can not influence the network frequency due to the small size of the MicroGrid.

During islanded operation, frequency response must be provided locally within the MicroGrid. This service should utilise the available, and often limited, frequency response capabilities of MicroSources and storage. It also needs to use frequency response from loads. This is to account for the limited capabilities of MicroSources.

In case of power shortages, the primary load frequency response period commences when the frequency drops below 49.5Hz and lasts for two minutes. During these two minutes, no load is to be shed unless the frequency falls below 48Hz. This value allows a 0.8Hz margin below the frequency at which load shedding starts in the main network. This was to prevent the MicroGrid loads from responding to frequency events during grid-connected operation. The target of the primary response is to contain the initial frequency dip above 42.5Hz. The secondary response commences after the end of the two minute period. This response aims to restore the frequency to above 49Hz within eight minutes.

Load restoration starts when the frequency exceeds 49.25Hz. During the first two minutes, the primary response tries to contain the over-frequency below 52Hz. During the following eight minutes, the secondary response restores all loads if the frequency stays above 49.5Hz. Setting the load restoration target below 50Hz guarantees restoring all loads before generation ceases supplying frequency response.

Upper and lower frequency limits for load shedding and restoration were chosen based on these targets. These limits are shown in Figure 4.2.

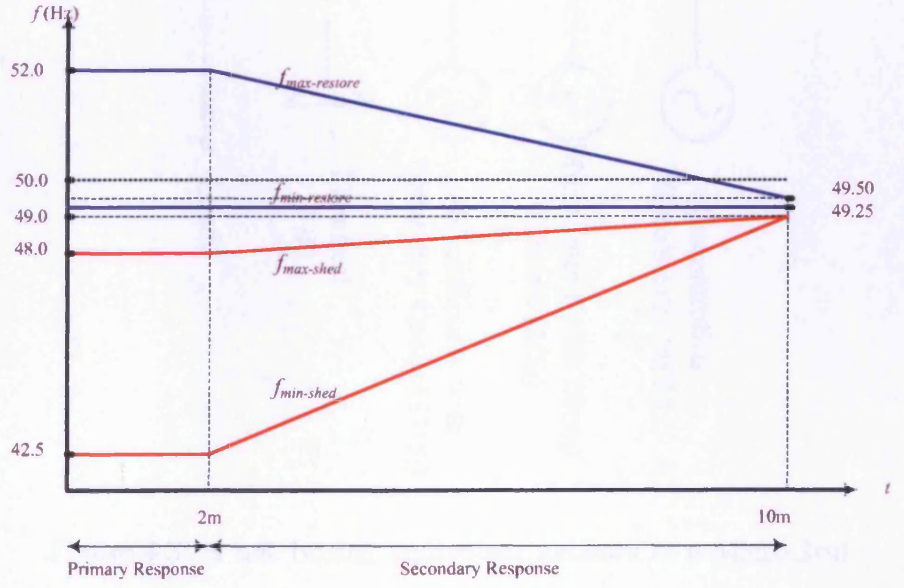

Figure 4.2: Upper and lower limits for shedding and restoration frequencies

4.3 The MicroGrid Model

At any time, the frequency has the same value at all locations in the MicroGrid. This allows using a one busbar equivalent of the MicroGrid network for frequency control studies. This equivalent network is shown in Figure 4.3. MicroSources that do not provide any frequency response service were lumped into one MicroSource, MS_1. MicroSources that are able to provide only primary response were lumped into MS_2. MicroSources that are able to provide both primary and secondary responses were lumped into MS_3.

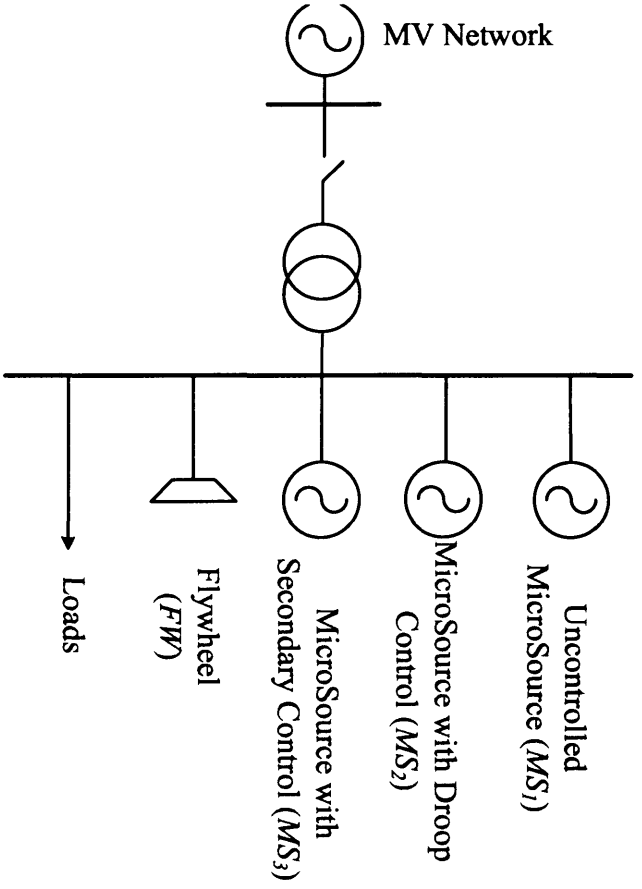

Figure 4.3: A one busbar equivalent network of a MicroGrid

Frequency in power networks is affected by power balance. Shortages in power cause frequency to drop. In a transmission network, this happens because any shortage in power is supplied from the kinetic energy stored in the inertia of rotating generators [41]. This causes the rotational speed of these generators to drop which cause the frequency to drop. In an islanded MicroGrid the inertia

that is connected to the MicroGrid directly is limited. A synthesised inertia response is supplied to the MicroGrid by the electric energy storage [43] and some MicroSources.

During islanded operation, the rate of change of the MicroGrid frequency, Δf_{MG}, is determined by the difference between power generation ΣP_{MS} and demand ΣP_D as well as the system inertia constant $2H_t$. This inertia is an aggregation of the inertia of any MicroSource that has a direct connection to the MicroGrid, the inertia of motor loads, and the inertia response provided by the power electronic converters of some MicroSources and energy storage. This model is shown in Figure 4.4.

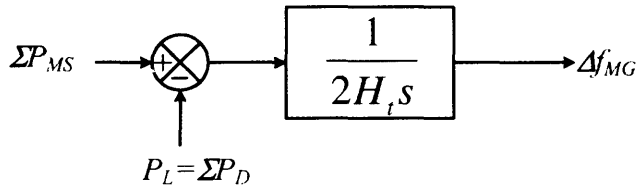

Figure 4.4: The Inertia Model of a MicroGrid

4.4 The MicroGrid Frequency Control System

4.4.1 MicroSource Controllers

It was assumed that MS_1 is not able to provide frequency response. Its MicroSource Controller was set not to respond to changes in the MicroGrid frequency.

Primary frequency response is provided by MS_2 via active power/frequency droop control [40, 42, 43]. The controller and the droop characteristics of MS_2 are shown in Figure 4.5.

MS_3 provides both primary and secondary frequency response. The primary response is provided via droop control. The secondary response aims to restore the frequency to 50Hz.

The secondary frequency response of MS_3 is provided by an integral control loop whose input is the frequency deviation. This loop shifts the droop characteristic such that the required power output is eventually supplied at

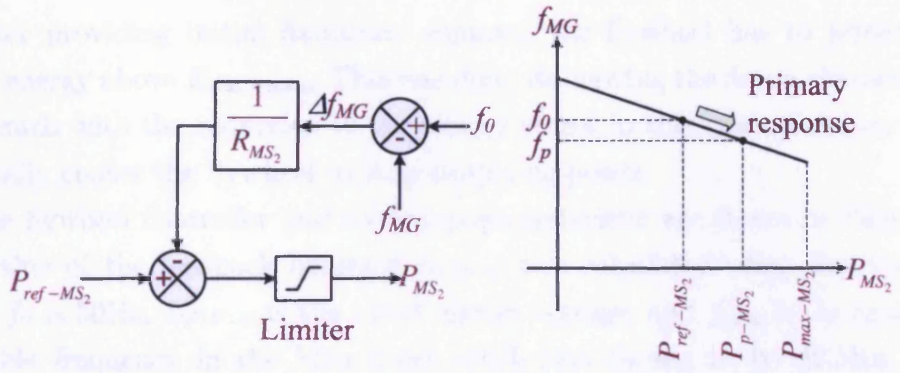

Figure 4.5: The controller and the droop characteristics of MS_2

50Hz [40, 43]. The value of the integral controller gain, k_{s-MS_3}, determines the speed of the secondary frequency response.

The controller and the droop characteristics of MS_3 are shown in Figure 4.6.

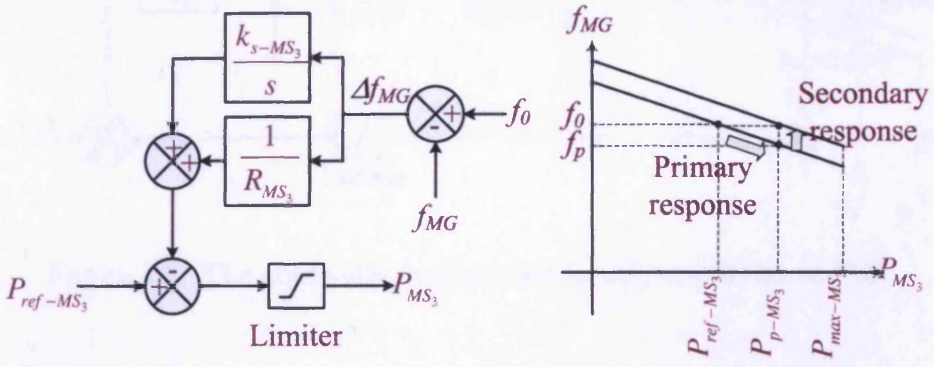

Figure 4.6: The controller and the droop characteristics of MS_3

4.4.2 Storage Controller

The energy stored in the flywheel, E_{FW}, has to be maintained above a certain level, E_{FW-Min}. This level is determined by the flywheel short circuit current and the operating time of the overcurrent relays in the MicroGrid. This energy has to be enough to sustain the required short circuit current for the maximum fault time.

The flywheel was set to provide an initial frequency support. This is done via droop control. When the flywheel is fully charged, $E_{FW} = E_{FW-0}$, the droop characteristic of the flywheel is such that the flywheel output power is zero at 50Hz.

After providing initial frequency support, the flywheel has to preserve its stored energy above E_{FW-min}. This was done via moving the droop characteristic downwards with the reduction in the energy stored in the flywheel,ΔE_{FW}. This eventually causes the flywheel to stop supplying power.

The flywheel controller and its droop characteristic are shown in Figure 4.7. The value of the feedback constant k_{s-FW} was calculated using Equation 4.1 where f_0 is 50Hz, E_{FW-0} is the rated energy storage, and f_{min} is the minimum allowable frequency in the MicroGrid which was chosen to be 42.5Hz. This choice of k_{s-FW} has the effect of moving the zero output power frequency, $f_0 + k_{s-FW}\Delta E_{FW}$, along the linear characteristic shown in Figure 4.8.

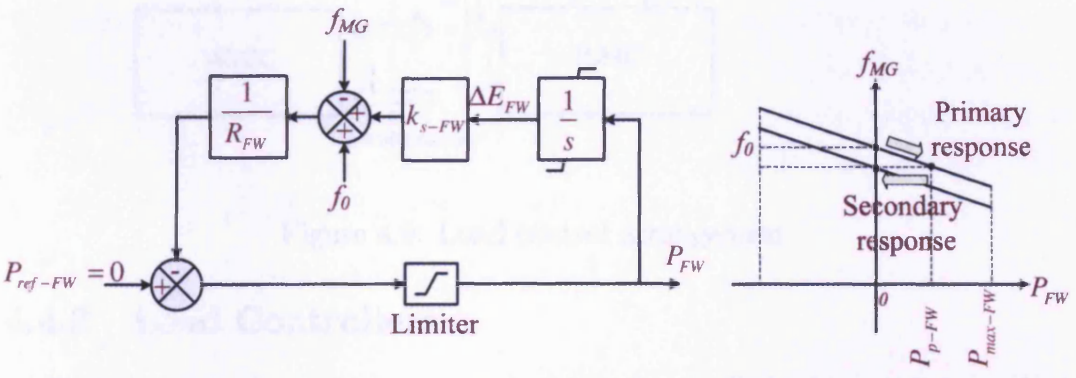

Figure 4.7: The controller and the droop characteristics of FW

$$k_{s-FW} = \frac{f_0 - f_{Min}}{E_{FW-0} - E_{FW-Min}} \tag{4.1}$$

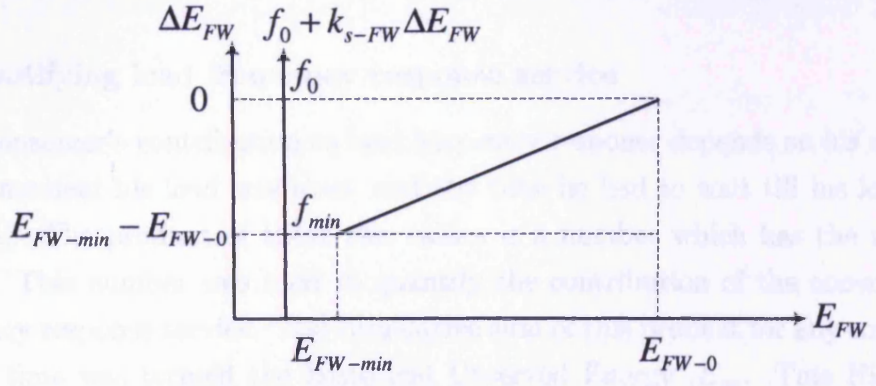

Figure 4.8: The relation between the energy stored in the flywheel and the frequency at which the its output power is zero

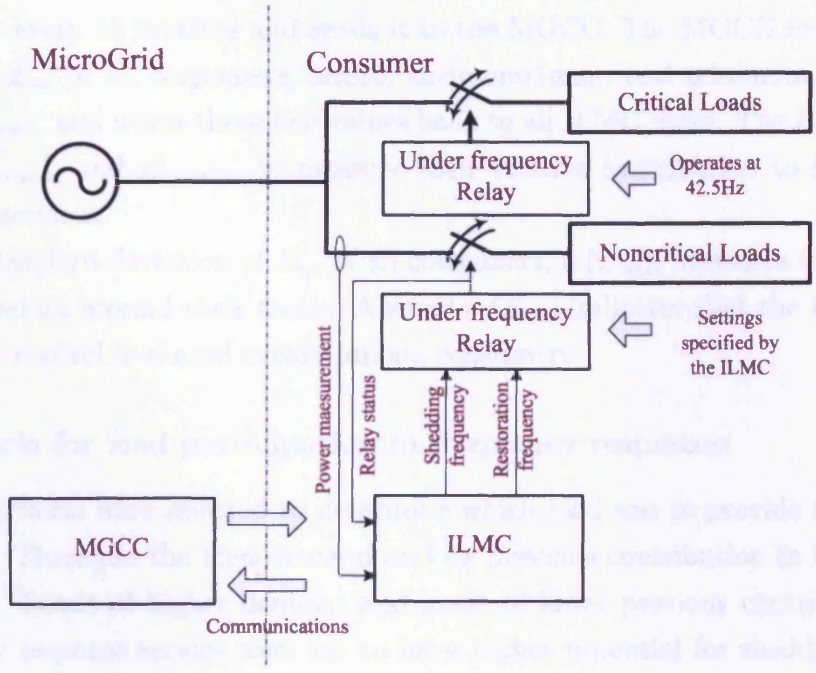

Figure 4.9: Load control arrangement

4.4.3 Load Controllers

It was assumed that a consumer's loads is supplied via two independent circuits. One circuit supplies the critical loads. This circuit is disconnected only if the frequency dropped below 42.5Hz. The other circuit, which supplies the non-critical loads, is controlled by an Intelligent Load Management Controller (ILMC) to provide frequency response. This ILMC sets the frequencies at which this load is shed and restored. This arrangement is shown in Figure 4.9.

i) Quantifying load frequency response service

A consumer's contribution to load frequency response depends on his demand at the moment his load was shed, and the time he had to wait till his load was restored. The product of these two values is a number which has the units of energy. This number was used to quantify the contribution of the consumer to frequency response service. The cumulative sum of this product for any consumer at any time was termed the Historical Unserved Energy ,E_{us}. This Historical Unserved Energy is a measure of the previous contribution of this consumer to the frequency response service.

The ILMC was set to keep track of the value of E_{us} of its consumer. It updates

this value every 15 minutes and sends it to the MGCC. The MGCC receives the values of E_{us} of all consumers, selects their maximum and minimum, E_{us-max} and E_{us-min}, and sends these two values back to all ILMC units. The ILMCs use these E_{us-max} and E_{us-min} to measure their relative contribution to frequency response services.

The standard deviation of E_{us} of all consumers, $\sigma(E_{us})$, measures the scatter of these values around their mean. A small $\sigma(E_{us})$ indicates that the burden of frequency control is shared evenly among consumers.

ii) Criteria for load participation in frequency responses

Two criteria were selected to determine which load was to provide frequency response. These are the load demand and its previous contribution to frequency response. Loads of higher demand and loads of lower previous contribution in frequency response service were set to have higher potential for shedding. This was to maintain equity among consumers and reduce the number of loads to be shed.

iii) Operation of the ILMC

The ILMC block diagram is shown in Figure 4.10. As long as the under frequency relay is on, the ILMC continuously monitors and stores the value of the non-critical load demand, P_{nc}. This value was used to specify the shedding and restoration frequencies of the load. During periods when the under frequency relay is tripped, no measurement of P_{nc} is available. In this case, the value that was stored prior to disconnection is to be used until the load is restored and a new measurement is available.

At any time, the shed load, P_{shed}, is given by Equation 4.2. This value was used to calculate the change in the historical unserved energy, ΔE_{us} using Equation 4.3 where T is 15 minutes.

$$P_{shed} = \begin{cases} P_{nc} & \text{Under frequency relay tripped} \\ 0 & \text{Under frequency relay not tripped} \end{cases} \tag{4.2}$$

$$\Delta E_{us} = \int_0^T P_{shed} dt \tag{4.3}$$

At the end of every 15 minute interval, the value of E_{us} is updated using

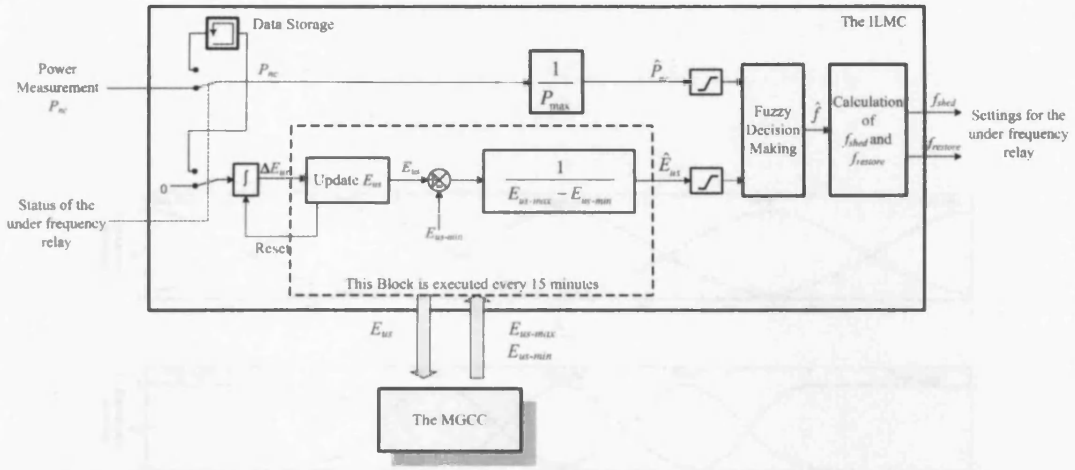

Figure 4.10: The block diagram of the ILMC

Equation 4.4 where the superscript i denotes the value before updating and the superscript $i+1$ denotes the updated value. The integrator is then reset. The updated value of E_{us} is sent to the MGCC. The MGCC compares the values of E_{us} for all consumers. It selects the maximum and minimum values and sends them to all ILMC units.

$$E_{us}^{i+1} = E_{us}^{i} + \Delta E_{us} \tag{4.4}$$

The values of P_{nc} and E_{us} were scaled into values ranging from 0 to 1 using Equation 4.5 and Equation 4.6. The value P_{max} in Equation 4.5 is an arbitrary value that the non-critical load demand will stay below most of the time. These scaled values, $\hat{P}_{nc}$ and $\hat{E}_{us}$, are used as inputs to a fuzzy logic controller.

$$\hat{P}_{nc} = \frac{P_{nc}}{P_{max}} \tag{4.5}$$

$$\hat{E}_{us} = \frac{E_{us} - E_{us-min}}{E_{us-max} - E_{us-min}} \tag{4.6}$$

The fuzzy logic controller used the membership functions shown in Figure 4.11 and the rules given in Table 4.2 to calculate its output $\hat{f}$. The value of $\hat{f}$ ranged from zero to one. The higher this value was, the higher the shedding and restoration frequencies for this load were.

The ILMC set the frequency values at which its load was shed, f_{shed}, or restored, $f_{restore}$ based on the value of $\hat{f}$. This was done using equations 4.7 and

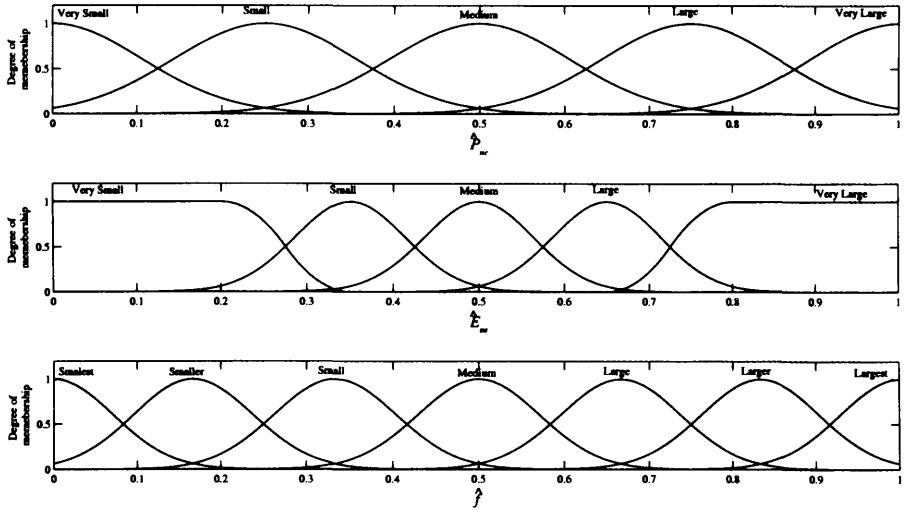

Figure 4.11: The membership functions of the fuzzy logic controller

Table 4.2: Fuzzy rules implemented in the ILMC units

		$\hat{P}_{nc}$				
		Very Small	**Small**	**Medium**	**Large**	**Very Large**
$\hat{E}_{us}$	**Very Small**	Small	Medium	Large	Larger	Largest
	Small	Smaller	Small	Medium	Large	Larger
	Medium	Smallest	Smaller	Small	Medium	Large
	Large	Smallest	Smallest	Smaller	Small	Medium
	Very Large	Smallest	Smallest	Smallest	Smaller	Small

4.8. In these equation; $f_{min-restore}$, $f_{max-restore}$, $f_{min-shed}$, and $f_{max-shed}$ are the upper and lower limits of shedding and restoration frequencies respectively. These values have already been defined in Figure 4.2.

$$f_{restore} = f_{min-restore} + (f_{max-restore} - f_{min-restore}) \times \hat{f} \quad (4.7)$$

$$f_{shed} = f_{min-shed} + (f_{max-shed} - f_{min-shed}) \times \hat{f} \quad (4.8)$$

4.5 Case Studies

This frequency control system was applied to the MicroGrid CIGRÉ benchmark model described in [21]. The MicroGrid network was simplified into the one busbar network shown in Figure 4.3. The ratings of the MicroSources and the flywheel and the parameters of their controllers are given in Appendix F, Table F.1.

4.5.1 Generation Frequency Response

This set of simulations were to investigate the frequency response of the flywheel and the MicroSources. Load control was not considered in any of these simulations. The total demand was assumed to be 45kW. This demand was initially supplied from the main grid. The grid connection was lost at t =2min.

The MicroGrid frequency, f_{MG}, the power output of the two MicroSources, P_{MS_2} and P_{MS_3}, and the power output of the flywheel, P_{FW}, were simulated for the three cases listed in Table 4.3. The results of these simulations are shown in Figure 4.12.

Table 4.3: Simulations used to investigate generation frequency response

Simulation case	**Elements providing frequency response**	
	Primary	**Secondary**
Case 4.5.1-a	MS_2, MS_3 and FW	
Case 4.5.1-b	MS_2, MS_3 and FW	MS_3
Case 4.5.1-c	MS_2, MS_3 and FW	MS_3 and FW

As the grid connection was lost, frequency dropped and the power outputs of MS_2, MS_3, and FW increased providing their primary frequency response. At

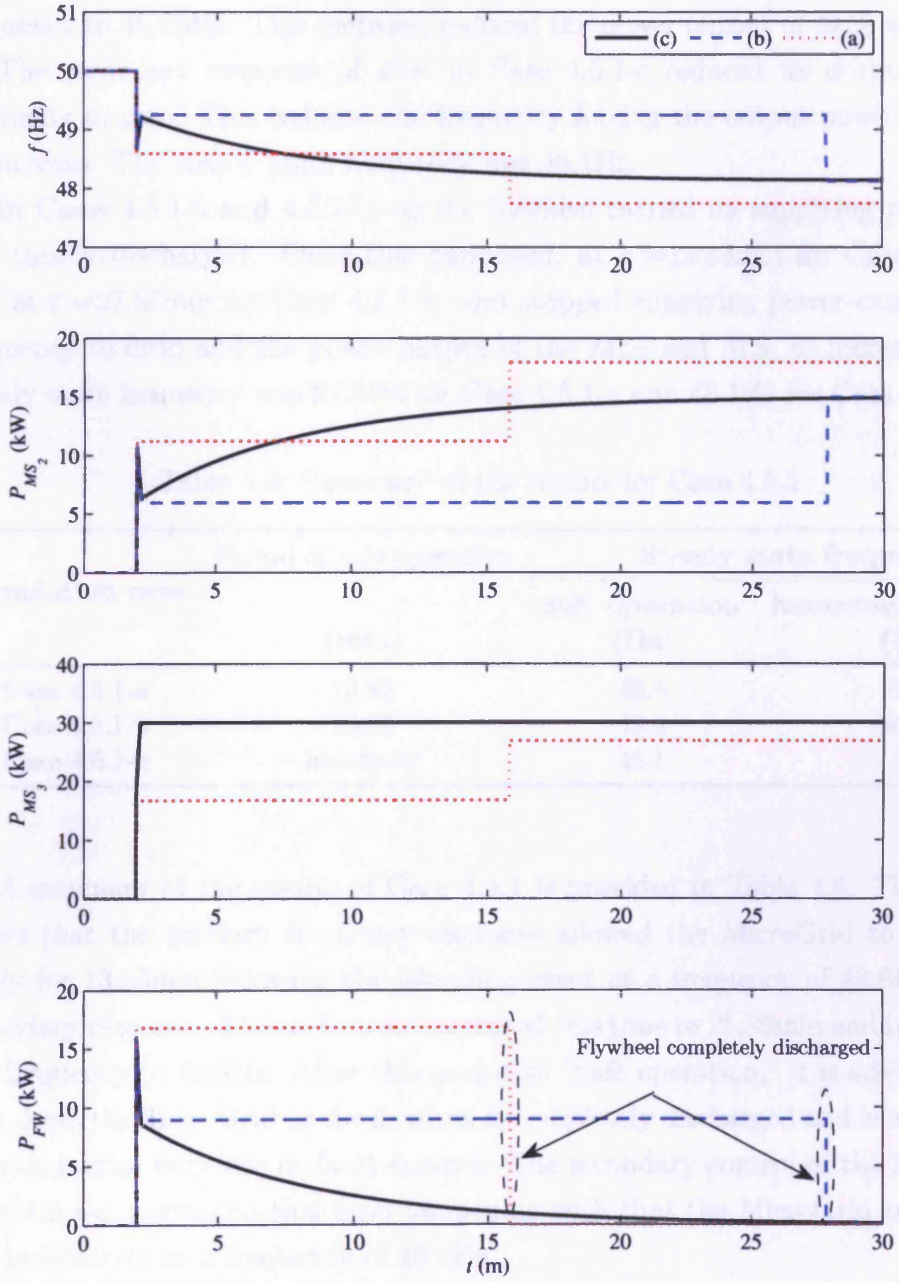

Figure 4.12: The MicroGrid frequency, the power output of MicroSources MS_2 and MS_3, and the power output of the Flywheel for Case 4.5.1. The connection to the main grid was lost at t=2m causing a shortage of 45kW of electric power

48.6Hz, this response was enough to supply the load and the frequency stopped dropping.

The secondary response of MS_3 in Cases 4.5.1-b and 4.5.1-c restored the frequency to 49.25Hz. This increase, reduced the power output of MS_2 and FW.

The secondary response of FW in Case 4.5.1-c reduced its output power gradually to zero. This reduced the frequency forcing the output power of MS_2 to increase. The steady state frequency was 48.1Hz.

In Cases 4.5.1-a and 4.5.1-b, as the flywheel carried on supplying power, it was totally discharged. Once this happened, at t =15.83min for Case 4.5.1-a and at t =27.85min for Case 4.5.1-b, and stopped supplying power causing the frequency to drop and the power output of the MS_2 and MS_3 to increase. The steady state frequency was 47.8Hz for Case 4.5.1-a and 48.1Hz for Case 4.5.1-b.

Table 4.4: Summary of the results for Case 4.5.1

Simulation case	Period of safe operation	**Steady state frequency**	
	(min)	**safe operation (Hz)**	**hazardous operation (Hz)**
Case 4.5.1-a	13.83	48.6	47.8
Case 4.5.1-b	25.85	49.3	48.1
Case 4.5.1-c	indefinite	48.1	

A summary of the results of Case 4.5.1 is provided in Table 4.4. This table shows that the primary frequency response allowed the MicroGrid to operate safely for 13.83min following the islanding event at a frequency of 48.6Hz. The secondary response of MicroSources increased this time to 25.85min and improved the frequency to 49.3Hz. After this period of "Safe operation," it is advisable to shut down the MicroGrid as the flywheel is completely discharged and is unable to provide inertia response or fault current. The secondary control of the flywheel, Case 4.5.1-c, prevented this from happening such that the MicroGrid is able to run indefinitely at a frequency of 48.1Hz.

The results shown in Table 4.4 illustrate that there is a trade-off between running the system at a 49.3Hz for 25min or at 48.1Hz for much longer time. In order to guarantee that energy supply to critical loads will be last till the grid connection is restored, the second option was considered suitable. In this frequency response from non-critical loads is essential to restore the frequency to

above 49Hz.

4.5.2 Load Frequency Response - Constant Load Operation

This set of simulations investigated the effect of load frequency response on the MicroGrid frequency during islanded operation. The demand of each consumer was assumed to be constant. The data for this case is given in Appendix F. The demand of different consumers is listed in Table F.2. The initial output of the MicroSources is listed in Table F.3. The initial value of the Historical Unserved Energy were assumed to be zero for all consumers.

The MicroGrid was disconnected from the main grid at t=2min causing unbalance between local generation and loads. Frequency variations and the response of different controllers in the MicroGrid were simulated for the four different cases listed in Table 4.5.

Table 4.5: Simulations used to investigate load frequency response

Case	Elements providing frequency response service	
	Primary	**Secondary**
Case 4.5.2-a	MS_2, MS_3, FW and ILMC	
Case 4.5.2-b	MS_2, MS_3, FW and ILMC	MS_3 and FW
Case 4.5.2-c	MS_2, MS_3, FW and ILMC	ILMC
Case 4.5.2-d	MS_2, MS_3, FW and ILMC	MS_3, FW and ILMC

Figure 4.13 shows the time variations in f_{MG}, P_{FW}, E_{FW}, and the total load in the MicroGrid, P_L. Figure 4.14 shows only f_{MG}, P_{FW} and , P_L at the instants when the grid connection was lost, t=2min, and when the flywheel was totally discharged, t=9.95min.

In all cases, the primary response restricted the frequency drop to 47Hz in the first 12 seconds after islanding. It then restored it to 47.6Hz. This was done by shedding four loads and increasing the outputs of MS_2, MS_3, and FW to their rated values.

In Cases 4.5.2-a and 4.5.2-c, the flywheel continued supplying power until it was totally discharged. As this happened, it suddenly stopped supplying power. This resulted in a sudden frequency drop. MicroSources, already working near

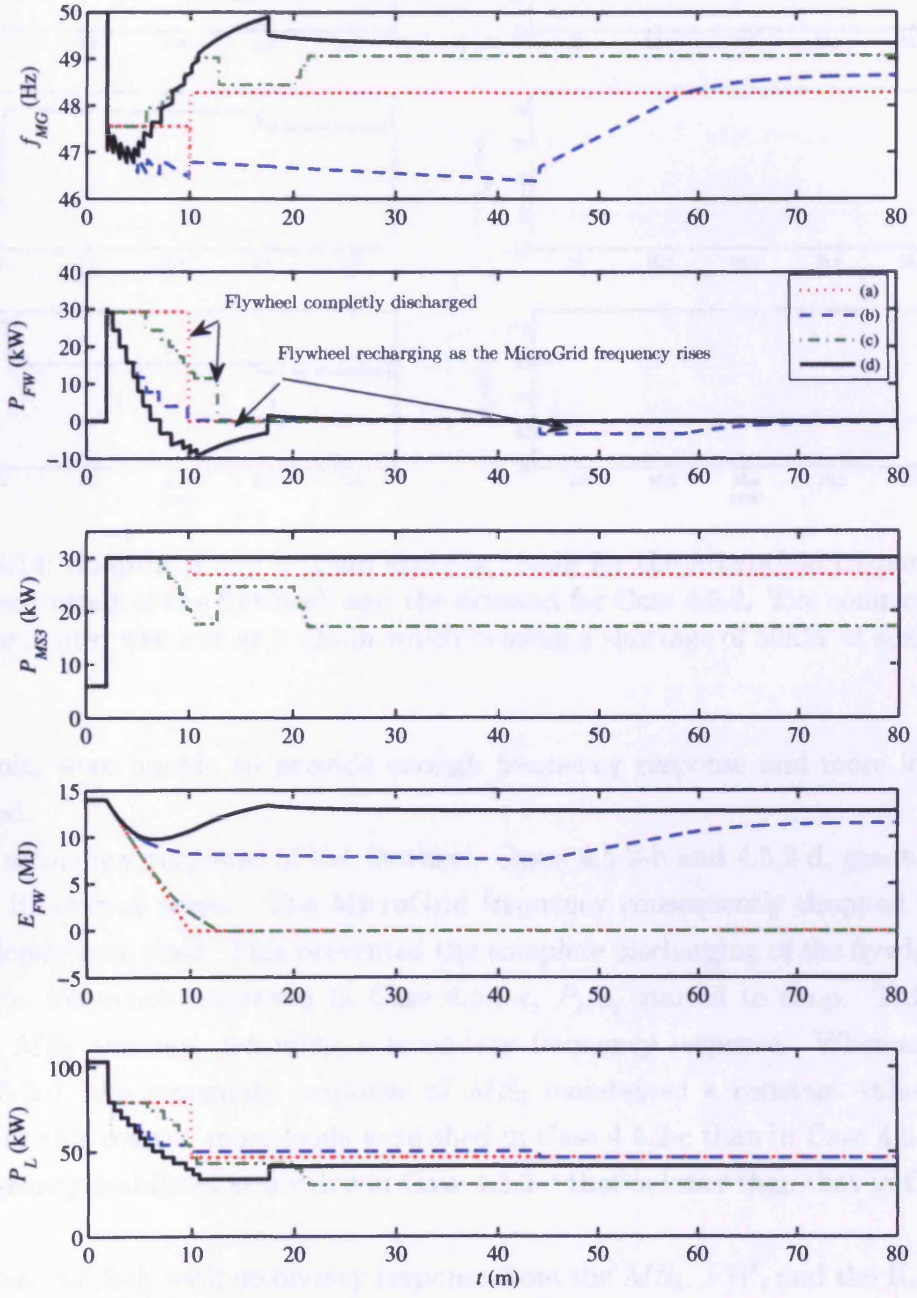

Figure 4.13: The MicroGrid frequency, the power output of the flywheel and the MicroSource MS_3, the energy stored in the flywheel, and the demand for Case 4.5.2. The connection to the main grid was lost at t=2min causing a shortage of 90kW of electric power.

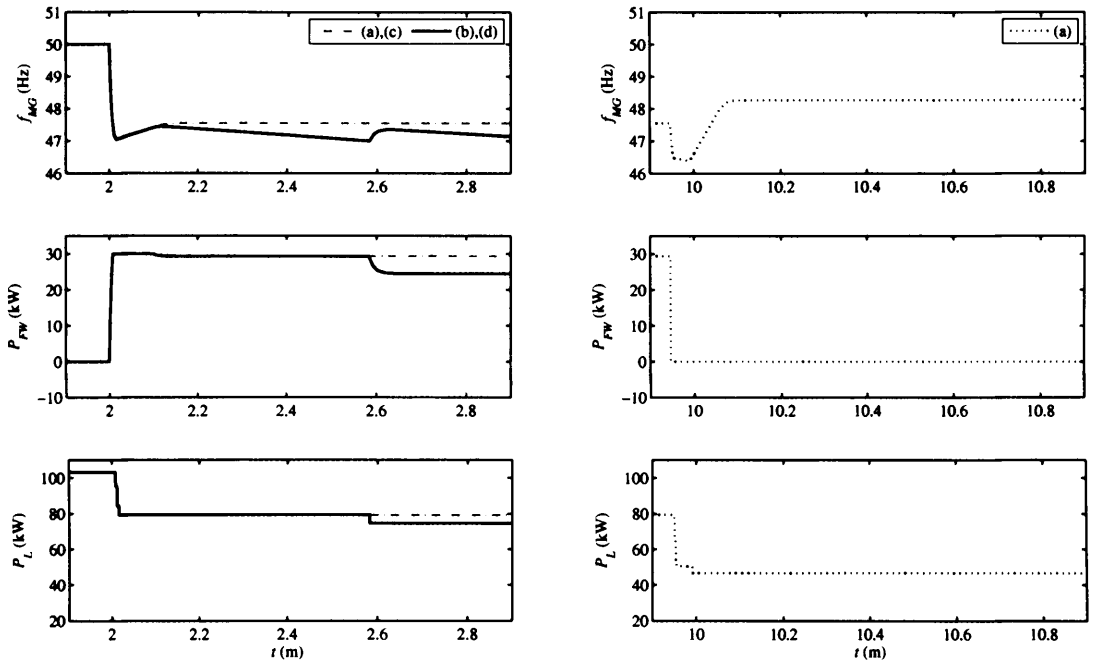

Figure 4.14: Snapshots at t = 2min and t = 10min for the MicroGrid frequency, the power output of the flywheel, and the demand for Case 4.5.2. The connection to the main grid was lost at t=2min which causing a shortage of 90kW of electric power.

their limit, were unable to provide enough frequency response and more loads were shed.

The secondary response of the flywheel, Cases 4.5.2-b and 4.5.2-d, gradually reduced its output power. The MicroGrid frequency consequently dropped and further loads were shed. This prevented the complete discharging of the flywheel.

As the frequency improved in Case 4.5.2-c, P_{MS_3} started to drop. This is because MS_3 was not providing a secondary frequency response. Whereas in Case 4.5.2-d, the secondary response of MS_3 maintained a constant value of P_{MS_3}. For this reason, more loads were shed in Case 4.5.2-c than in Case 4.5.2-d and frequency stabilised at a value in Case 4.5.2-c that is lower than that in Case 4.5.2-d.

In Case 4.5.2-d, with secondary response from the MS_3, FW, and the ILMC units, the frequency was restored to above 49Hz at t=10.8min. Moreover, the flywheel was not discharged.

4.5.3 Load Frequency Response - Time Varying Loads

This case was simulated to test the performance of the frequency control system when loads vary due to daily activities of consumers. An 80-min period was simulated. The total demand of the MicroGrid was assumed to be 100% during the first 30 minutes, 50% during the following 30 minutes, and 20% during the last 10 minutes. This choice was made to illustrate the operation of the ILMC for the cases when demand is greater than generation and loads have to be shed and when demand drops and loads are able to be restored. Demand patterns for individual consumers were generated using the steps included in Appendix E. The ILMC units, the MicroSources, and the flywheel were assumed to provide primary and secondary frequency responses.

The data for this simulation is in Appendix F. Initial values of the power output of the MicroSources are given in Table F.3. The initial values of E_{us} for consumers are in Table F.4.

The grid connection was lost at t =2min. Variations in f_{MG}, P_{FW}, P_{MS_2}, and P_{MS_3} were simulated. The simulation results are shown in Figure 4.15. The same figure shows the two curves of the MicroGrid total demand, P_L. One of these curves is the total demand if loads were not shed. The other curve is the total demand after load shedding. Load switching patterns and the standard deviation of the values of the Historical Unserved Energy of different consumers, $\sigma(E_{us})$ are shown in the same figure as well.

Each horizontal line in the load switching patterns corresponds to one load in the MicroGrid where white area represents the period of disconnection and shaded area represents the period of connection. For example, the non-critical load of the first consumer, represented by the lowest horizontal line, was disconnected at t =8min and then restored again at t =34min. Similarly, the second consumer, represented by the next line, was disconnected at t =2min and restored at t =38min.

The primary response prevented the frequency from dropping below 46Hz and then restored it to 47.5Hz. Four loads were shed and the power outputs of MS_2, MS_3, and FW increased to their rated values.

The secondary response of the flywheel slowly reduced its output. This resulted in further frequency drop and caused two more loads to be shed.

The secondary response of MS_3 maintained a constant output most of the time. This reduced the need of further load shedding. P_{MS_3} did not drop below

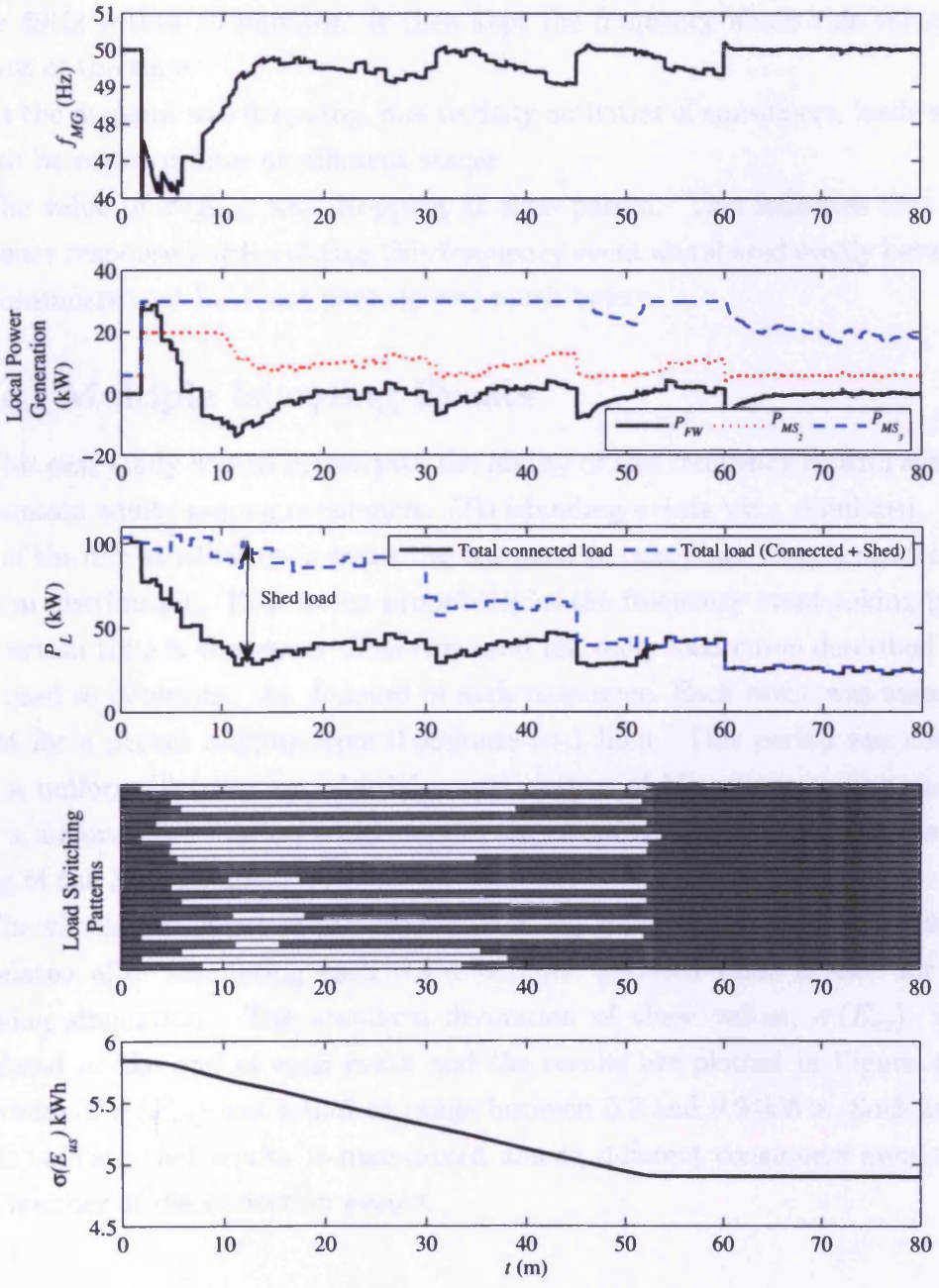

Figure 4.15: The MicroGrid frequency, local generation, demand variation, load switching patterns, and standard deviation of unserved energy of all consumers for Case 4.5.3. An islanding event at t=2min causing a 90kW shortage in electric power. Demand drops gradually due to normal day activities.

its rating until loads were all restored. when loads were shed. reduced its output. This resulted in further frequency drop and caused two more loads to be shed.

The secondary frequency response of the ILMC restored the frequency to above 49Hz within 10 minutes. It then kept the frequency above this value for the rest of the time.

As the demand was dropping, due to daily activities of consumers, loads were able to be restored later at different stages.

The value of $\sigma(E_{us})$ was dropping as time passed. This indicates that the frequency response burden during this frequency event was shared evenly between the consumers that have not participated much before.

4.5.4 Multiple Islanding Events

This case study was to investigate the ability of this frequency control system to maintain equity among consumers. 500 islanding events were simulated. The time of the day at which each event was assumed to take place was chosen from a uniform distribution. That is the probability of the frequency event taking place at a certain time is the same. This time and the daily load curve described [21] were used to determine the demand of each consumer. Each event was assumed to last for a period ranging from 0.5minute to 1 hour. This period was chosen from a uniform distribution. Initial power output of MicroSources was chosen from a uniform distribution which minimum was of zero and maximum was the rating of the MicroSource.

The simulation starts with zero value of E_{us} for all consumers. This value is updated after simulating each event and the updated value is used for the following simulation. The standard divination of these values, $\sigma(E_{us})$, were calculated at the end of each event and the results are plotted in Figure 4.16. The value of $\sigma(E_{us})$ was found to range between 0.2 and 0.94kWh. Such small values indicate that equity is maintained among different consumers even after large number of disconnection events.

4.6 Conclusion

A frequency control system for an islanded MicroGrids was simulated. This system uses MicroSources, storage, and non-critical loads to provide frequency response service.

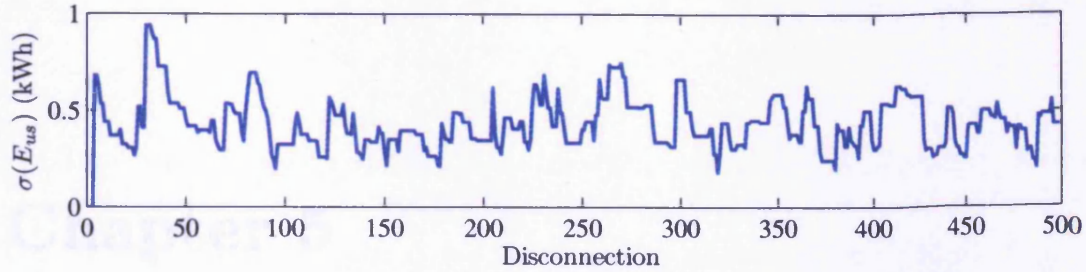

Figure 4.16: Variation in $\sigma\left(E_{us}\right)$ due to 500 islanding events chosen randomly

Some MicroSources were used to provide primary frequency response services. Some other MicroSources were used to provide primary frequency response followed by a secondary service that tries to restore the frequency to 50Hz.

The energy storage was used to provide initial frequency support. Afterwards, it starts dropping its power output such that it reserves its energy.

Non-critical loads were controlled by Intelligent Load Management Controllers to provide both primary and secondary frequency response services. These ILMC manage load shedding and restoration such that the number of affected consumer is low and equity is maintained among them.

This frequency control system was applied to the CIGRÉ benchmark MicroGrid system. Several study cases were simulated to investigate the performance of this system.

Chapter 5

Integrated Operation of an Energy MicroGrid

5.1 Introduction

In the Energy MicroGrid, CHP units, Electric Water Heaters (EWH), and pumps link the District Heat System (DHS) to the electric power network. This coupling allows both networks to be controlled to support each other rather than independent of each other. It also provides an opportunity to use cheap thermal storage rather than expensive electric storage.

An Integrated Optimal Power Flow (IOPF) for heat and electric power was formulated. The objective of this IOPF is to determine optimal operating schedules for heat and power generation in an energy system. Heat and power networks were modelled independently in this IOPF. These two models were then coupled through models of the energy conversion equipment that links them.

Integrated Operation of the Energy MicroGrid is described. It defines an approach where the storage and the equipment that couples the heat and the power networks in the Energy MicroGrid are controlled to provide support for both networks. The advantages of this approach when used in the model Energy MicroGrid were investigated using the IOPF. Four cases were considered to account for normal operation and three possible contingencies.

5.2 Modelling of a Multi-Carrier Energy System

An energy hub [20,85] is a multi-input/multi-output unit. Its inputs are power supplied from the different energy networks constituting a Multi-Carrier Energy System. Its outputs are power supplied back to these networks or to loads. Inputs are linked to outputs through an array of energy conversion systems and energy storage. An example of an energy hub is shown in Figure 5.1.

A Multi-Carrier Energy System may be modelled as a set of interconnected energy hubs [85]. This allows the interactions between the different energy networks to be represented.

Energy hub models have been used in several studies. These studies include load flow studies [85], optimsation of hub layout [86, 87], optimisation of hub coupling parameters [88], optimal dispatch [89], and optimal power flow [90].

Other studies used independent models for different networks in the Multi-Carrier Energy System. These models were then linked together via models of the energy conversion equipment [33, 91, 92]. These integrated models were used for optimal scheduling of gas and electricity systems [33,91,92], for assessing system behavior during significant outages in gas networks [33], and for asset planing of gas and electricity infrastructure [34].

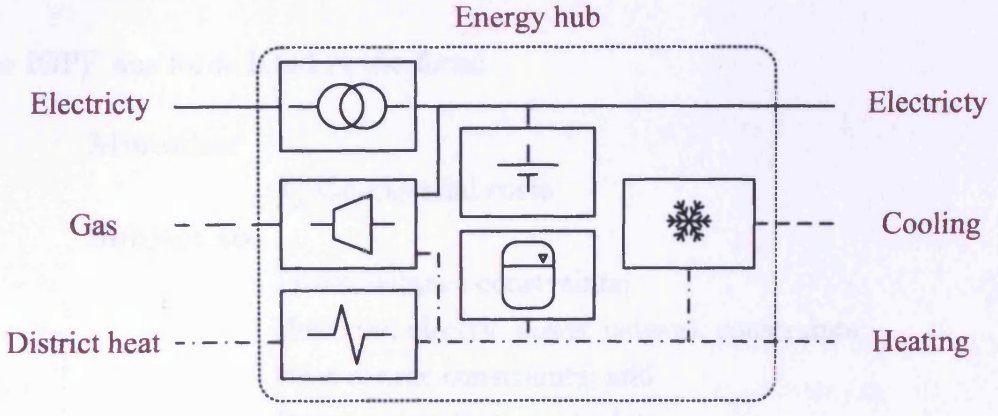

Figure 5.1: Example of an energy hub

5.3 The Integrated Optimal Power Flow (IOPF)

An Optimal Power Flow (OPF) was defined in [5] as a tool for transmission system analysis. It has also been used for studies of integrated gas and electric power networks [33, 34, 91, 92]. In these studies, the OPF was formulated as a constrained optimisation problem that determines a feasible operating point where an objective function exhibits a minimum value. The outputs of these OPFs include the optimal settings for all generators, reactive power compensators, and transformer tap changers in an electric power system [5, 33]. They also include the optimal dispatch for different supply terminals and storage facilities in a gas network [33, 34].

Different constraints have been used in OPFs. These constraints include load flow constraints, generation capability constraints, line flow constraints, busbar voltage limits, and security constraints [5, 33]. Several objective functions; such as operational costs [5, 33], the total system costs [34], or energy losses; have been used. This makes an OPF a strong and flexible tool for power system studies [5].

In this research, an IOPF was defined as an OPF that optimises the operation of a Multi-Carrier Energy System. The Multi-Carrier Energy System that was considered comprises a DHS and an electric power system.

5.4 Formulation of the IOPF

The IOPF was formulated in the form:

Minimise:

$\sum$ Operational costs

Subject to:

Power balance constraints;
Heat and electric power network constraints;
Heat source constraints; and
Power generation constraints.

The inputs to this IOPF are:

1. heat and electric power demand;

2. available electric power generation for all renewables-based generation;
3. available fuel supply for non-renewable generation;
4. available fuel supply for boilers/CHP units of district heat stations;
5. electric power prices for each generator;
6. fuel prices;
7. costs and charges associated with load shedding; and
8. technical constraints of both heat and electric power networks.

The outputs of the IOPF are:

1. schedules of active and reactive power output of all generators;
2. schedules of electric load shedding when necessary;
3. schedules of heat generation of different CHP units and EWHs in the district heat network;
4. schedule of the settings of reactive power compensators and transformer tap changers, if available; and
5. schedule of the control settings of district heat stations including supply temperature and pressure.

The mathematical formulation of this IOPF uses the equations described in Chapter 2 for the DHS and the models described in [5] for the electricity network.

5.4.1 Objective Function

The objective of the IOPF was chosen in order to minimise the cost of energy, C_{Total}, required to serve heat and electric power demand. Linear operating cost functions were assumed. Fixed costs, such as capital and maintenance costs, were not modelled.

The cost of electric power generation at a specific time step, t_i, is given by Equation 5.1. In this equation, $\mathbb{G}$ is the set of all generators in the network, c_{G_j}

is the price of electricity supplied by the generator G_j, P_{G_j} is the power output of this source, $t_{i+1} - t_i$ is the length of the time step t_i.

$$C_P(t_i) = \sum_{G_j \in \mathbb{G}} c_{G_j}(t_i) P_{G_j}(t_i) (t_{i+1} - t_i) \tag{5.1}$$

The cost of heat production is given by Equation 5.2. In this equation, $\mathbb{S}$ is the set of all heat sources in the Energy MicroGrid, c_{S_j} is the fuel price, F_{G_j} is the fuel supplied to the heat source S_j.

$$C_\Phi(t_i) = \sum_{S_j \in \mathbb{S}} c_{S_j}(t_i) F_{S_j}(t_i) (t_{i+1} - t_i) \tag{5.2}$$

The total cost, C_{Total}, is the sum of these two costs, $C_P(t_i)$ and $C_\Phi(t_i)$, over the entire period of study. This is given by Equation 5.3 where $\mathbb{T}$ is the set of time steps constituting the time period of study.

$$C_{Total} = \sum_{t_i \in \mathbb{T}} C_P(t_i) + C_\Phi(t_i) \tag{5.3}$$

5.4.2 District Heat Station Constraints

A district heat station S_i connected at node N_j is shown on Figure 5.2. In this figure, T is temperature, p is pressures, $\dot{m}$ is mass flow rate, and Φ is heat output. The subscript denotes whether the variable is defined for the source S_i or for the N_j. This is followed by S if the variable is defined at the supply line or R if it is defined at the return line.

i) Network interface constraints

The constraints describing the interface of the district heat station to the DHS are:

$$T_{S_iR} = T_{N_jR} \tag{5.4}$$

$$\Phi_{S_i} = c_p \dot{m}_{S_i} (T_{S_iS} - T_{S_iR}) \tag{5.5}$$

$$p_{S_i} = p_{N_jS} - p_{N_jR} \tag{5.6}$$

The supply temperature of the district heat station has to be above a minimum level, T_{Min}, so that heat loads can be served. On the other hand, it should not

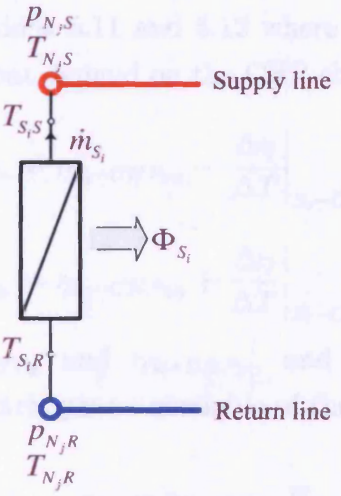

Figure 5.2: Heat Source

increase above a maximum level, T_{Max}, so that no steam is formed in the pipe network.

$$T_{Min} \leq T_{S_iS} \leq T_{Max} \tag{5.7}$$

ii) The reference pressure constraints

One heat source in the DHS sets its supply pressure to a reference value of p_{S-Ref} and its return pressure to a reference value p_{R-Ref}.

$$p_{N_jS} = p_{S-Ref} \tag{5.8}$$

$$p_{N_jR} = p_{R-Ref} \tag{5.9}$$

iii) Heat production constraints

The heat output of the district heat station, Φ_{S_i}, is produced by a CHP unit, Φ_{S_i-CHP}, and by an Electric Water Heater (EWH), Φ_{S_i-EWH}.

$$\Phi_{S_i} = \Phi_{S_i-CHP} + \Phi_{S_i-EWH} \tag{5.10}$$

iv) CHP constraints

The heat efficiency, $\eta_{S_i-CHP_\Phi}$, and the electric power efficiency $\eta_{S_i-CHP_P}$, of the CHP were assumed to vary linearly with the supply temperature, T_{S_iS}.

This is expressed by Equations 5.11 and 5.12 where $\eta_{S_i-CHP_{P0}}$, $\eta_{S_i-CHP_{\Phi 0}}$, and $\frac{\Delta\eta}{\Delta T}\Big|_{S_i-CHP}$ are constants that depend on the CHP characteristics.

$$\eta_{S_i-CHP_P} = \eta_{S_i-CHP_{P0}} - \frac{\Delta\eta}{\Delta T}\Big|_{S_i-CHP} T_{S_iS} \tag{5.11}$$

$$\eta_{S_i-CHP_\Phi} = \eta_{S_i-CHP_{\Phi 0}} + \frac{\Delta\eta}{\Delta T}\Big|_{S_i-CHP} T_{S_iS} \tag{5.12}$$

The efficiencies, $\eta_{S_i-CHP_\Phi}$ and $\eta_{S_i-CHP_P}$, and the fuel input, F_{S_i-CHP}, determine the heat and electric power available of the CHP unit.

$$\Phi_{S_i-CHP-Max} = \eta_{S_i-CHP_\Phi} F_{S_i-CHP} \tag{5.13}$$

$$P_{S_i-CHP-Max} = \eta_{S_i-CHP_P} F_{S_i-CHP} \tag{5.14}$$

These values were used as the upper limits of the actual CHP output. This is to allow curtailing both heat and electricity.

$$\Phi_{S_i-CHP} \leq \Phi_{S_i-CHP-Max} \tag{5.15}$$

$$P_{S_i-CHP} \leq P_{S_i-CHP-Max} \tag{5.16}$$

v) Electric water heater constraints

The heat supplied by the EWH is determined by its power input and its efficiency. The heat output of the EWH was not allowed to be curtailed.

$$\Phi_{S_i-EWH} = \eta_{S_i-EWH} P_{S_i-EWH} \tag{5.17}$$

The power input to the heater is limited by its rating, $P_{S_i-EWH-Rated}$. This was modelled by an inequality constraint.

$$0 \leq P_{S_i-EWH} \leq P_{S_i-EWH-Rated} \tag{5.18}$$

The EWH was assumed to be purely resistive. Its reactive power input at all cases was set to zero.

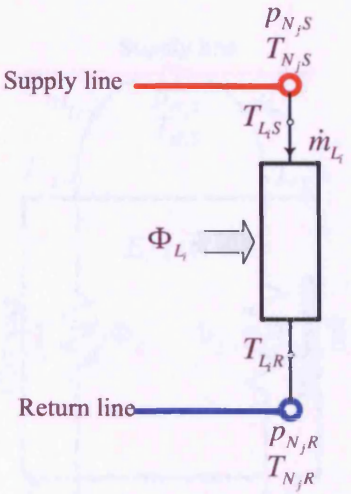

Figure 5.3: Heat Load

$$Q_{S_i-EWH} = 0 \tag{5.19}$$

vi) Water pump constraints

The power required by the water pump, P_{S_i-Pump}, is a function of the pressure difference and the mass flow rate of the district heat station. This is shown by Equation 5.20 where ρ is the water density.

$$P_{S_i-Pump} = \frac{\dot{m}_{S_i} p_{S_i}}{\rho} \tag{5.20}$$

This pump was assumed to work at a constant power factor of $\cos\phi_{S_i-Pump}$.

$$Q_{S_i-Pump} = P_{S_i-Pump} \frac{\sqrt{1-\cos^2\phi_{S_i-Pump}}}{\cos\phi_{S_i-Pump}} \tag{5.21}$$

5.4.3 Heat Load Constraints

Figure 5.3 shows a heat load L_i connected at node N_j. The constraints associated with this load are:

$$T_{L_iS} = T_{N_iS} \tag{5.22}$$

$$\Phi_{L_i} = c_p \dot{m}_{L_i} (T_{L_iS} - T_{L_iR}) \tag{5.23}$$

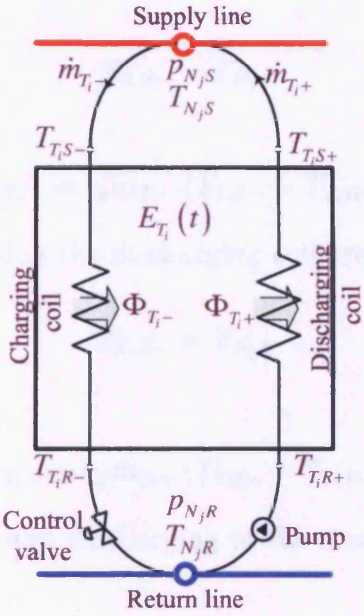

Figure 5.4: Hot water tank

$$p_{L_i} = p_{N_jS} - p_{N_jR} \tag{5.24}$$

The load pressure has to be maintained above a certain level, p_{L_iMin}. This is to guarantee that the water flow required to meet the demand can be sustained.

$$p_{L_i} \geq p_{L_iMin} \tag{5.25}$$

5.4.4 Storage Constraints

Figure 5.4 shows a hot water storage tank, T_i, connected at the node N_j. This tank is charged via a heat exchanger coil and discharged via another heat exchanger coil. Variables associated with the node, the tank, and the heat exchanger coils are marked on the figure. The positive sign in the subscripts are used with variables related to the discharging coil whereas the negative sign is used with these related to the charging coil.

i) Network interface constraints

The constraints describing the charging coil are:

$$T_{T_iS-} = T_{N_jS} \tag{5.26}$$

$$\Phi_{T_i-} = c_p \dot{m}_{T_i-} \left(T_{T_iS-} - T_{T_iR-}\right) \tag{5.27}$$

The constraints describing the discharging coil are:

$$T_{T_iR+} = T_{N_jR} \tag{5.28}$$

$$\Phi_{T_i+} = c_p \dot{m}_{T_i+} \left(T_{T_iS+} - T_{T_iR+}\right) \tag{5.29}$$

Simultaneous charging and discharging of the storage was not allowed. This constraint is given by:

$$\dot{m}_{T_i+} \times \dot{m}_{T_i-} = 0 \tag{5.30}$$

The pressure constraints are:

$$p_{T_i} = p_{N_jS} - p_{N_jR} \tag{5.31}$$

$$p_{T_i} \geq p_{T_iMin} \tag{5.32}$$

ii) Energy constraint

The energy stored in the tank at the next time step, $E_{T_i}(t_{k+1})$ is determined by the energy stored at present, $E_{T_i}(t_k)$; the charging rate, $\Phi_{T_i-}(t_k)$; and the discharging rate, $\Phi_{T_i+}(t_k)$. This constraint is given by:

$$E_{T_i}(t_{k+1}) = E_{T_i}(t_k) + \left(\Phi_{T_i-}(t_k) - \Phi_{T_i+}(t_k)\right)(t_{k+1} - t_k) \tag{5.33}$$

$t_{k+1} - t_k$ in this constraint is the length of the time step.

iii) Pump constraints

The pump constraints are:

$$P_{T_i-Pump} = \frac{\dot{m}_{T_i+} p_{T_i}}{\rho} \tag{5.34}$$

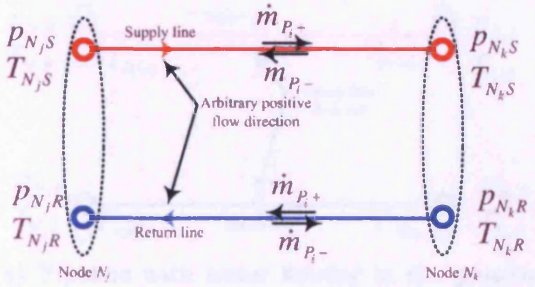

Figure 5.5: A double pipeline

$$Q_{T_i-Pump} = P_{T_iPump} \frac{\sqrt{1-\cos^2 \phi_{T_iPump}}}{\cos \phi_{T_iPump}} \tag{5.35}$$

5.4.5 Pipeline Constraints

Figure 5.5 shows a double pipeline P_i connecting node N_j to node N_k. An arbitrary positive flow direction was assumed to be from N_j to N_k in the supply line and from N_k to N_j in the return line.

Two independent mass flow rates variables were defined for this pipeline. The first variable, $\dot{m}_{P_i+}$, is in the positive direction whereas the second variable, $\dot{m}_{P_i-}$, is in the negative direction. One of these two variables has to be zero at any time.

$$\dot{m}_{P_i+} \times \dot{m}_{P_i-} = 0 \tag{5.36}$$

The sum of these variables is the mass flow rate in the pipe.

$$\dot{m}_{P_i} = \dot{m}_{P_i+} + \dot{m}_{P_i-} \tag{5.37}$$

The difference in static pressure between the two nodes connected by the pipeline depends on the flow rate as shown by Equations 5.38 and 5.39. In these equations, r_{P_i} is a constant whose value is determined by the dimensions and the roughness of the internal surface of the pipe.

$$p_{N_jS} - p_{N_kS} = r_{P_i}\left(\dot{m}^2_{P_j+} - \dot{m}^2_{P_j-}\right) \tag{5.38}$$

$$p_{N_jR} - p_{N_kR} = r_{P_i}\left(\dot{m}^2_{P_j-} - \dot{m}^2_{P_j+}\right) \tag{5.39}$$

The inlets and outlets of the pipe line and the temperatures at these points

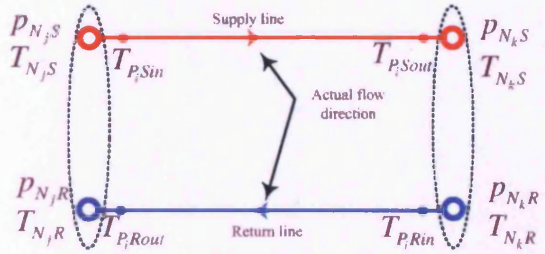

(a) Pipeline with water flowing in the positive direction

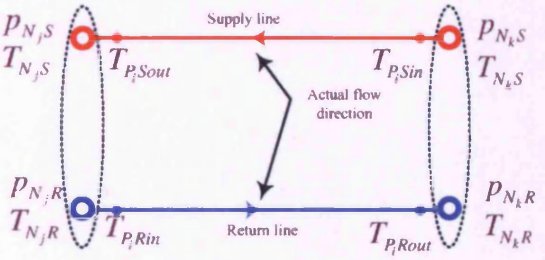

(b) Pipeline with water flowing in the negative direction

Figure 5.6: The inlet and the outlet temperatures for a double pipeline

were defined based on the actual flow direction. Figure 5.6 shows the pipeline of Figure 5.5 with the inlet and outlet temperatures marked on it for the case of positive flow, Figure 5.6(a), and negative flow, Figure 5.6(b).

The pipe inlet temperature constraints are:

$$\left(T_{P_iSin} - T_{N_jS}\right) \dot{m}_{P_i+} = 0 \tag{5.40}$$

$$\left(T_{P_iSin} - T_{N_kS}\right) \dot{m}_{P_i-} = 0 \tag{5.41}$$

$$\left(T_{P_iRin} - T_{N_jR}\right) \dot{m}_{P_i-} = 0 \tag{5.42}$$

$$\left(T_{P_iRin} - T_{N_kS}\right) \dot{m}_{P_i+} = 0 \tag{5.43}$$

The flow rates were multiplied by these constraints such that only the constraints associated with non-zero flow components are enforced.

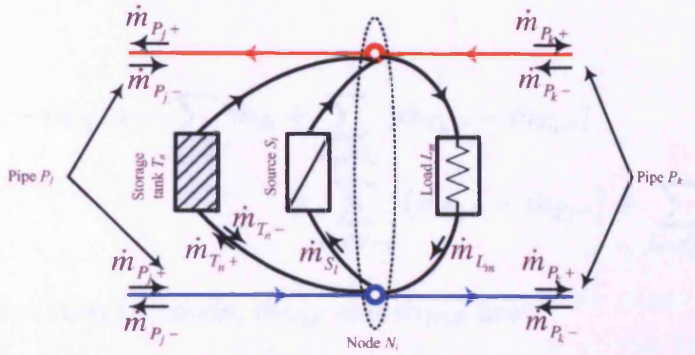

Figure 5.7: General node configuration

The temperature of the water leaving the pipe is given by:

$$T_{P_i Sout} = \begin{cases} (T_{P_i Sin} - T_a)\left(1 - \frac{\lambda_{P_j} L_{P_j}}{c_p \dot{m}_{P_j}}\right) + T_a & \text{if } \frac{\lambda_{P_j} L_{P_j}}{c_p \dot{m}_{P_j}} \leq 1 \\ T_a & \text{if } \frac{\lambda_{P_j} L_{P_j}}{c_p \dot{m}_{P_j}} \geq 1 \end{cases} \tag{5.44}$$

$$T_{P_i Rout} = \begin{cases} (T_{P_i Rin} - T_a)\left(1 - \frac{\lambda_{P_j} L_{P_j}}{c_p \dot{m}_{P_j}}\right) + T_a & \text{if } \frac{\lambda_{P_j} L_{P_j}}{c_p \dot{m}_{P_j}} \leq 1 \\ T_a & \text{if } \frac{\lambda_{P_j} L_{P_j}}{c_p \dot{m}_{P_j}} \geq 1 \end{cases} \tag{5.45}$$

5.4.6 Node Constraints

Elements connected to a node N_i were subdivided into five different sets. These are the set of sources, $\mathbb{S}_{N_i}$; loads, $\mathbb{L}_{N_i}$; storage tanks, $\mathbb{T}_{N_i}$; and two sets of pipelines, $\mathbb{P}+_{N_i}$ and $\mathbb{P}-_{N_i}$.

A Pipeline that is in $\mathbb{P}+_{N_i}$ has its positive flow direction directed towards the node N_i. On the other hand, a Pipelines the is in $\mathbb{P}-_{N_i}$ has its positive direction directed away from this node.

Figure 5.7 shows a node N_i in a district heat network to which one element of each set is connected. The flow directions marked on the elements in Figure 5.7 are the arbitrary positive flow directions associated with these elements. Flow variables used and their directions are marked next to the elements.

The continuity constraint applied at node i is given by:

$$\sum_{P_k \in \mathbb{P}+_i} (\dot{m}_{P_k+} - \dot{m}_{P_k-}) + \sum_{S_l \in \mathbb{S}_i} \dot{m}_{S_l} + \sum_{T_n \in \mathbb{T}_i} (\dot{m}_{T_n+} - \dot{m}_{T_n-}) = \sum_{P_j \in \mathbb{P}-_i} (\dot{m}_{P_j+} - \dot{m}_{P_j-}) + \sum_{L_m \in \mathbb{L}_i} \dot{m}_{L_m} \quad (5.46)$$

The flow rates into the node, $\dot{m}_{NiS}$ and $\dot{m}_{NiR}$ are:

$$\dot{m}_{NiS} = \sum_{S_l \in \mathbb{S}_i} \dot{m}_{S_l} + \sum_{T_n \in \mathbb{T}_i} \dot{m}_{T_n+} + \sum_{P_k \in \mathbb{P}+_i} \dot{m}_{P_k+} + \sum_{P_j \in \mathbb{P}-_i} \dot{m}_{P_j-} \quad (5.47)$$

$$\dot{m}_{NiR} = \sum_{L_m \in \mathbb{L}_i} \dot{m}_{L_m} + \sum_{T_n \in \mathbb{T}_i} \dot{m}_{T_n-} + \sum_{P_k \in \mathbb{P}+_i} \dot{m}_{P_k-} + \sum_{P_j \in \mathbb{P}-_i} \dot{m}_{P_j+} \quad (5.48)$$

The sum of the temperatures of the water flowing into the node weighted by the associated flow rates, $\hat{T}_{NiS}$ and $\hat{T}_{NiR}$, are:

$$\hat{T}_{NiS} = \sum_{S_l \in \mathbb{S}_i} T_{S_l S} \dot{m}_{S_l} + \sum_{T_n \in \mathbb{T}_i} T_{T_n out+} \dot{m}_{T_n+} + \sum_{P_k \in \mathbb{P}+_i} T_{P_k Sout} \dot{m}_{P_k+} + \sum_{P_j \in \mathbb{P}-_i} T_{P_j Sout} \dot{m}_{P_j-} \quad (5.49)$$

$$\hat{T}_{NiR} = \sum_{L_m \in \mathbb{L}_i} T_{L_m R} \dot{m}_{L_m} + \sum_{T_n \in \mathbb{T}_i} T_{T_n out-} \dot{m}_{T_n-} + \sum_{P_k \in \mathbb{P}+_i} T_{P_k Rout} \dot{m}_{P_k-} + \sum_{P_j \in \mathbb{P}-_i} T_{P_j Rout} \dot{m}_{Pj+} \quad (5.50)$$

The temperatures at the node, T_{NiS} and T_{NiR}, are given by equations 5.51 and 5.52.

$$\hat{T}_{NiS} = \dot{m}_{NiS} T_{NiS} \quad (5.51)$$

$$\hat{T}_{NiS} = \dot{m}_{NiS} T_{NiS} \quad (5.52)$$

5.4.7 Generator Constraints

Figure 5.8 shows an electric power generator G_i. The rating of this generator is $P_{G_i-rated}$; its active power output is P_{G_i}; and its reactive power output is Q_{G_i}.

The output constraints of this generator are:

$$P_{G_i-min} \leq P_{G_i} \leq P_{G_i-max} \tag{5.53}$$

$$Q_{G_i-min} \leq Q_{G_i} \leq Q_{G_i-max} \tag{5.54}$$

The value of P_{G_i-max} for MicroSources that use renewables is determined by the available renewable resource and the rated power. For other MicroSources, P_{G_i-max} is equal to $P_{G_i-rated}$ unless there is a limitation on the fuel supply. For the grid connection, P_{G_i-max} is equal to the connection capacity.

The active and reactive power capabilities of a generator are determined by its interface to the network as well as its rating. The operating ranges for MicroSources with power electronic interfaces and for the grid connection is defined by the shaded half circle in Figure 5.9. If reverse power flow is allowed, the grid connection will be able to operate within the entire circle.

Based on Figure 5.9, the reactive power limits, Q_{G_i-max} and Q_{G_i-min}, are:

$$Q_{G_i-max} = \sqrt{P_{G_i-rated}^2 - P_{G_i}^2} \tag{5.55}$$

$$Q_{G_i-min} = -\sqrt{P_{G_i-rated}^2 - P_{G_i}^2} \tag{5.56}$$

5.4.8 Electric Load and Electric Load Shedding Constraints

Figure 5.10 shows an electric load L_i connected to the MicroGrid. The active and reactive power demand of this load are P_{L_i} and Q_{L_i}. To account for load shedding, a virtual generator V_i is assumed to be connected in parallel with the load. A high energy price was used for this generator in order to limit load shedding to emergency conditions.

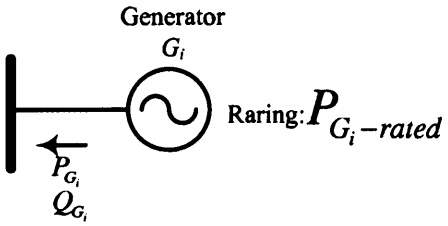

Figure 5.8: Electric power generator

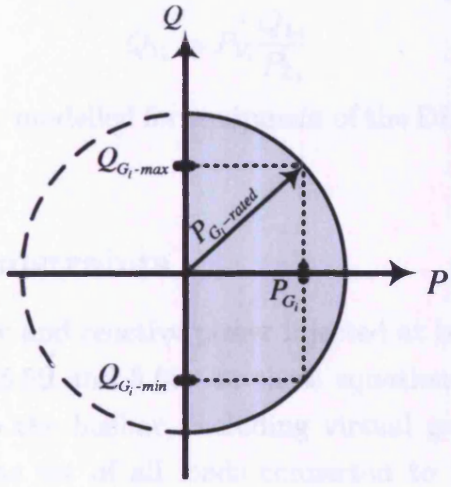

Figure 5.9: Active and reactive power capabilities of MicroSources

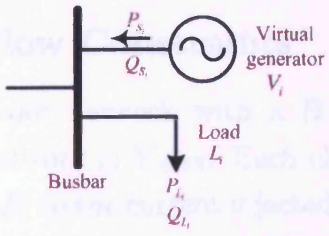

Figure 5.10: Electric Load

The constraints for the load shedding generator are:

$$P_{V_i} \leq P_{L_i} \tag{5.57}$$

$$Q_{V_i} = P_{V_i} \frac{Q_{L_i}}{P_{L_i}} \tag{5.58}$$

No load shedding was modelled for equipment of the DHS such as water pumps and electric heaters.

5.4.9 Busbur Constraints

Constraints for active and reactive power injected at busbar B_i, P_{B_i} and Q_{B_i}, are given by equations 5.59 and 5.60. In these equations, $\mathbb{G}_{B_i}$ is the set of all generators connected to the busbar, including virtual generators used for load shedding; and $\mathbb{L}_{B_i}$ is the set of all loads connected to it, including any DHS equipment that consume electric power.

$$P_{B_i} = \sum_{G_j \in \mathbb{G}_{B_i}} P_{G_j} - \sum_{L_l \in \mathbb{L}_{B_i}} P_{L_l} \tag{5.59}$$

$$Q_{B_i} = \sum_{G_j \in \mathbb{G}_{B_i}} Q_{G_j} - \sum_{L_l \in \mathbb{L}_{B_i}} Q_{L_l} \tag{5.60}$$

The busbar voltage magnitude has to be kept within adequate limits.

$$V_{min}^2 \leq V_{rB_i}^2 + V_{iB_i}^2 \leq V_{max}^2 \tag{5.61}$$

5.4.10 AC Power Flow Constraints

Figure 5.11 shows a power network with a $\mathbb{B}$ set of busbars. The bus admittance matrix of this network is $\mathbf{Y}_{BUS}$. Each element of this matrix, $Y_{B_iB_j}$ relates the voltage of busbar B_i to the current injected at busbar B_j. This element may be expressed in the form $Y_{B_iB_j} = G_{B_iB_j} - \mathbf{j}B_{B_iB_j}$.

The AC power flow constraints for this network are:

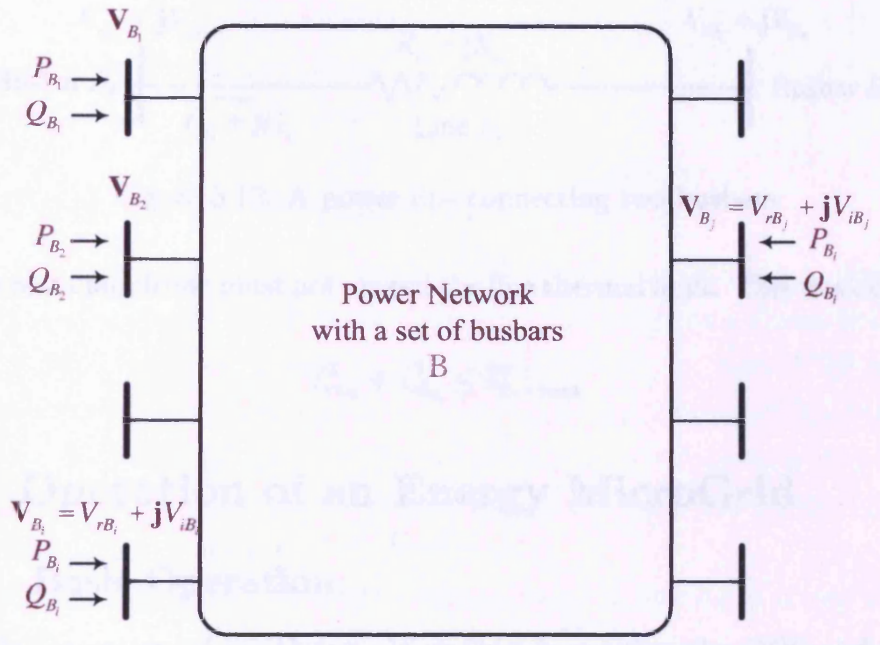

Figure 5.11: A power network

$$P_{B_i} = \sum_{B_j \in \mathbb{B}} \left[V_{rB_i} \left(V_{rB_j} G_{B_i B_j} + V_{iB_j} B_{B_i B_j} \right) + V_{iB_i} \left(V_{iB_j} G_{B_i B_j} - V_{rB_j} B_{B_i B_j} \right) \right] \tag{5.62}$$

$$Q_{B_i} = \sum_{B_j \in \mathbb{B}} \left[V_{iB_i} \left(V_{rB_j} G_{B_i B_j} + V_{iB_j} B_{B_i B_j} \right) - V_{rB_i} \left(V_{iB_j} G_{B_i B_j} - V_{rB_j} B_{B_i B_j} \right) \right] \tag{5.63}$$

5.4.11 Line Constraints

Figure 5.12 shows a power line L_i connecting busbar B_j to busbar B_k. The line parameters are marked on the figure. The real and imaginary components of the current flow in the line L_i are given by:

$$I_{rL_i} = \frac{\left(V_{rB_j} - V_{rB_k} \right) R_{L_i} + \left(V_{iB_j} - V_{iB_k} \right) X_{L_i}}{R_{L_i}^2 + X_{L_i}^2} \tag{5.64}$$

$$I_{iL_i} = \frac{-\left(V_{rB_j} - V_{rB_k} \right) X_{L_i} - \left(V_{iB_j} + V_{iB_k} \right) R_{L_i}}{R_{L_i}^2 + X_{L_i}^2} \tag{5.65}$$

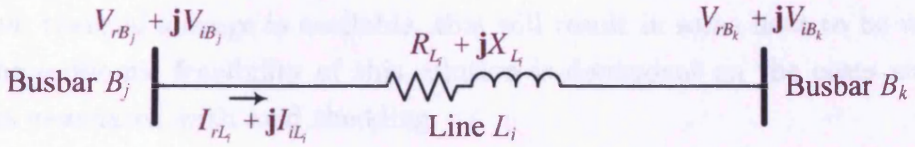

Figure 5.12: A power line connecting two busbars

The current magnitude must not exceed the line thermal limit. This was expressed by:

$$I_{rL_i}^2 + I_{iL_i}^2 \leq I_{L_i-max}^2 \tag{5.66}$$

5.5 Operation of an Energy MicroGrid

5.5.1 Basic Operation

Basic Operation of an Energy MicroGrid is running the DHS and the LV network independent of each other. Heat is produced only by the CHP which responds solely to variations in the heat demand. The electric power output of this CHP is determined by its heat output. In the LV network, the generation available is used to supply the electrical demand. If local generation available exceeds demand, generation will be curtailed; and if demand exceeds local generation, this demand will be either supplied from the main electricity grid or, in case of islanded operation, shed.

5.5.2 Integrated Operation

Integrated Operation of the Energy MicroGrid is running the DHS and the LV network as one system. In this case, the district heat station, which is the point that links both networks, and a thermal store are controlled to provide services for both of them. These services are provided via several control functions such as heat and electric load following, control of the supply temperature, and control of EWHs.

i) Load following - Heat and electricity

CHP units were allowed to generate more heat than required. This was to reduce load shedding during an emergency condition such as islanded operation.

If no thermal storage is available, this will result in some heat to be wasted and the economic feasibility of this solution is dependent on the costs and the charges associated with load shedding.

ii) Supply temperature settings

In some CHP units, an increase in the supply temperature increases the heat-to-power ratio, Φ/P ratio, of this unit. In Integrated Operation of the Energy MicroGrid, this is used to vary the Φ/P ratio of these CHP units in response to variations in energy prices. That is, at high electricity prices and low fuel prices, the CHP will operate at a low supply temperature such that it has a low Φ/P ratio, whereas at low electricity prices and high fuel prices it operates at high supply temperature and high Φ/P ratio.

Heat losses and power required to pump water in the pipes of the DHS are dependent on the heat demand, the mass flow rate, and the supply temperature. The interactions between these variables are illustrated in Figure 5.13 which shows that increasing T_S, causes heat losses to increase and the power consumed by pumps to decrease.

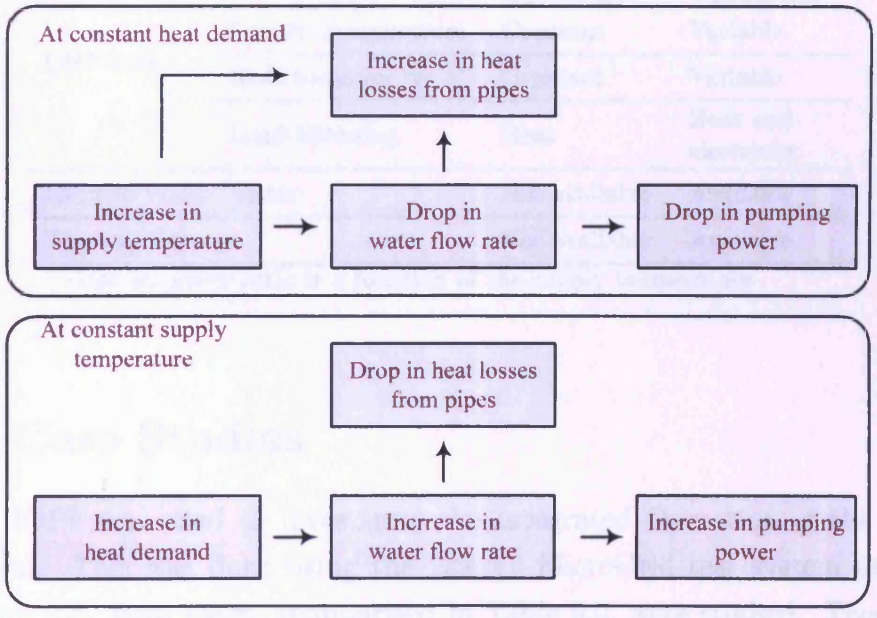

Figure 5.13: Effect of heat demand and supply temperature on thermal and hydraulic losses in a DHS

The optimal supply temperature is determined by the trade-off between heat losses and pumping power.During periods of low heat demand, the flow rate is

low. This causes heat losses to be more significant than pumping power. In this case, a low supply temperature is desirable in order to reduce the losses. During periods of high heat demand, the mass flow rate and the pumping power is high. In this case, it is better to operate at a high supply temperature.

iii) The Electric Water Heater (EWH)

An EWH was assumed to be available in the district heat station. This EWH is used to convert electric power into heat when power prices are very low.

iv) Thermal Storage

Thermal storage was used to decouple heat production from heat demand. That is to allow optimising the schedules of both the CHP and the EWH.

The differences between the Basic and the Integrated Operation of the Energy MicroGrid are summarised in Table 5.1.

Table 5.1: Basic Operation and Integrated Operation of the Energy MicroGrid

		Basic Operation	**Integrated Operation**
CHP unit	Supply Temperature	Constant	Variable
	Heat-to-power ratio*	Constant	Variable
	Load following	Heat	Heat and electricity
Electric Water Heater		Not available	Available
Thermal Storage		Not available	Available

* Heat-to-power ratio is a function of the supply temperature

5.6 Case Studies

The IOPF was used to investigate the Integrated Operation of the Energy MicroGrid. This was done using the Energy MicroGrid test system described in Section 2.8. Four cases, summarised in Table 5.2, were studied. These cases account for normal operation, a contingency in the power network that cause the grid connection to be lost, a contingency in the fuel supply system that limits the capacity of the CHP and Non-renewable MicroSources, and the two contingency taking place together.

Table 5.2: Cases used to assess the Integrated Operation

	Grid Connection	Maximum output of the		
		CHP (Total Output) kW	MicroTurbine kW	Fuel Cell kW
Case study 5.6.1: Grid Connected Operation with No Restrictions on Fuel	Available	315.0kW	30kW	10kW
Case study 5.6.2: Islanded Operation with No Restrictions on Fuel	Not available	315.0kW	30kW	10kW
Case study 5.6.3: Grid Connected Operation with Limited Fuel Supply	Available	157.5kW	15kW	5kW
Case study 5.6.4: Islanded Operation with Limited Fuel Supply	Not available	157.5kW	15kW	5kW

In all simulations, no power was allowed to be exported to the main electricity grid. This was to examine the possibility of balancing demand and generation locally.

Energy prices used are shown in Figure 5.14. The gas and electricity prices in this figure are market prices corresponding to the period from 23/12/2008 to 26/12/2008 [93, 94]. The prices associated by Non-renewable MicroSources were chosen arbitrarily such that in the first 24 hours, Non-renewable MicroSources are "must-run"; in the following 24 hours, they are cheaper to use than grid imports; in the third 24 hours, their prices are comparable to grid imports; and in the last 24 hours, they are expensive to use.

The total domestic demand for heat and electricity, shown in Figure 5.15, was considered. This demand was assumed based on the daily electric load curve described in the CIGRÉ benchmark MicroGrid model [21] and on the average domestic CHP output profiles described in [95].

Typical data for wind and PV generation, Figure 5.16, were assumed. The PV output was based on the winter-day average found in [95].

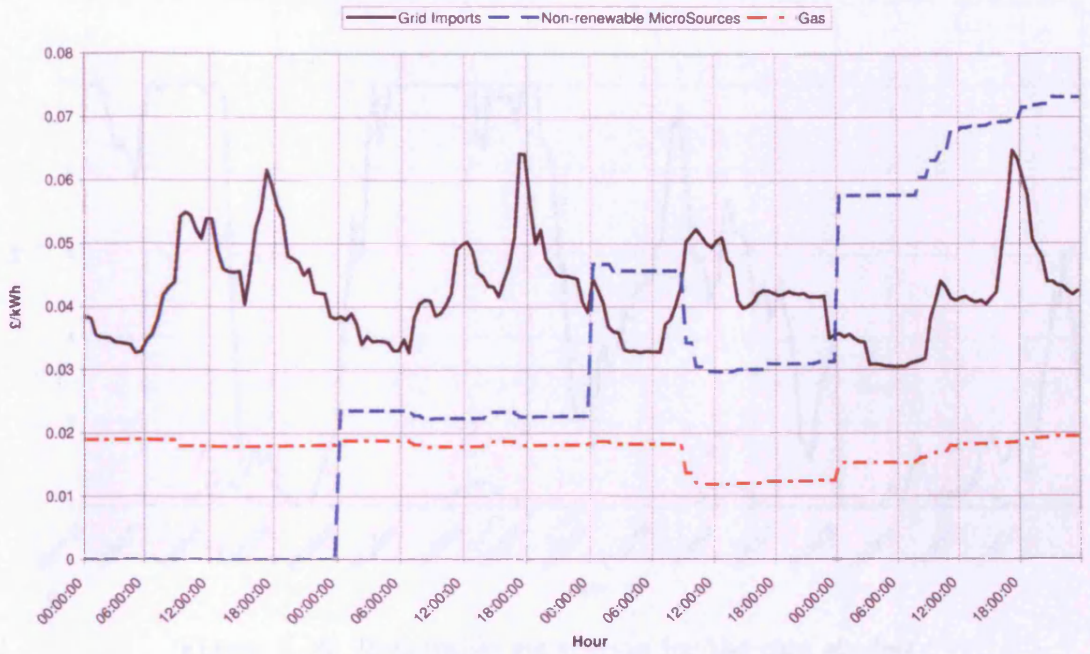

Figure 5.14: Energy prices used in the case studies

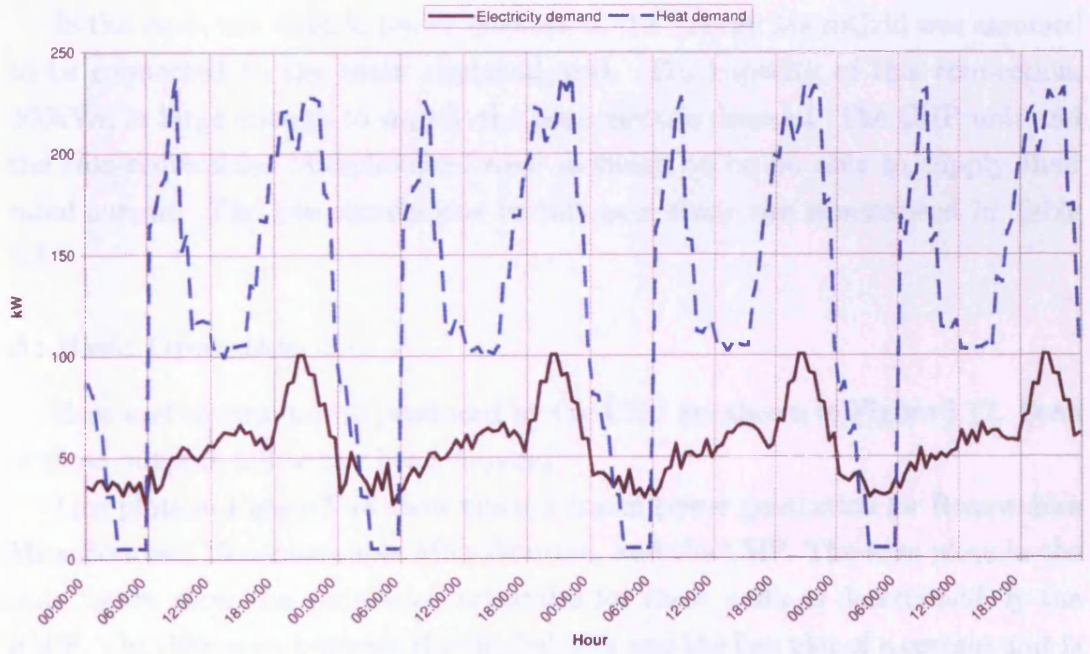

Figure 5.15: Domestic demand for the case studies

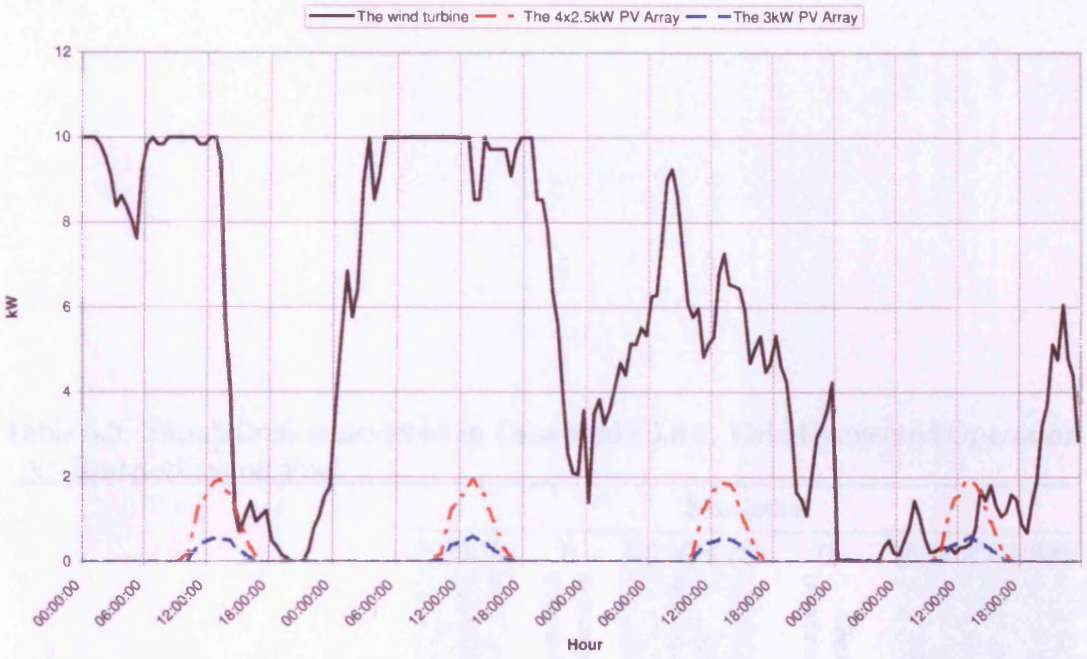

Figure 5.16: Renewable generation for the case studies

5.6.1 Grid Connected Operation with No Restrictions on Fuel

In this case, the electric power network of the Energy MicroGrid was assumed to be connected to the main electrical grid. The capacity of this connection, 400kVA, is large enough to supply the peak electric demand. The CHP unit and the Non-renewables MicroSources were assumed to be be able to supply their rated output. The five simulations in this case study are summarised in Table 5.3.

A: Basic Operation

Heat and electric power produced by the CHP are shown in Figure 5.17. Both of these outputs follow the heat demand.

Line plots in Figure 5.18 show the maximum power generation for Renewables MicroSources, Non-renewable MicroSources, and the CHP. The area plots in the same figure show the generation schedules for these units as determined by the IOPF. The difference between the shaded area and the line plot of a certain unit is the generation curtailed. The arrows in the figure highlight some of the occasions when power was curtailed. The pie-chart shows the percentage contribution of

Table 5.3: Simulations considered in Case study 5.6.1: Grid Connected Operation - No Restrictions on Fuel

		Simulation				
		A Basic Operation	B Basic Operation with T_S Control	C Basic Operation with EWH	D Basic Operation with Storage	E Integrated Operation
Hot water supply temperature	Min	85°C	70°C	85°C	85°C	70°C
	Max	85°C	100°C	85°C	85°C	100°C
Heat efficiency of the CHP	Min*	77.5%	65.0%	77.5%	77.5%	65.0%
	Max**	77.5%	90.0%	77.5%	77.5%	90.0%
Power efficiency of the CHP	Max*	12.5%	25.0%	12.5%	12.5%	25.0%
	Min**	12.5%	0.0%	12.5%	12.5%	0.0%
Load following of the CHP		Heat	Heat	Heat	Heat	Heat and electricity
The EWH				Available		Available
Thermal storage					Available	Available

* Corresponding to minimum supply temperature
** Corresponding to maximum supply temperature

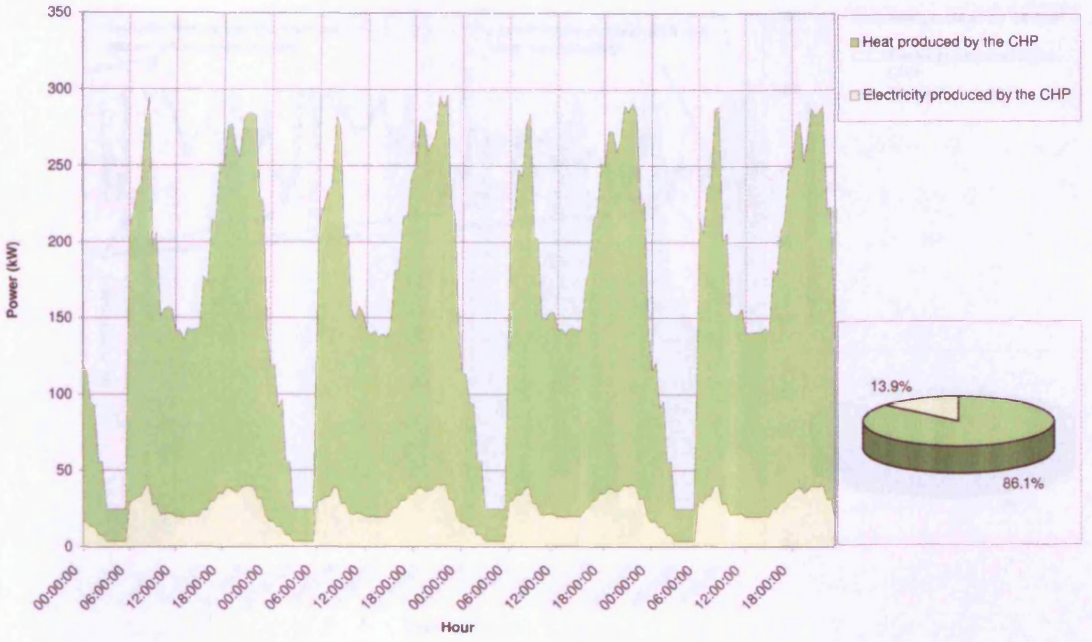

Figure 5.17: CHP output for Case study 5.6.1-A: Grid Connected - No Restrictions on Fuel - Basic Operation

different sources into the total electric power generation.

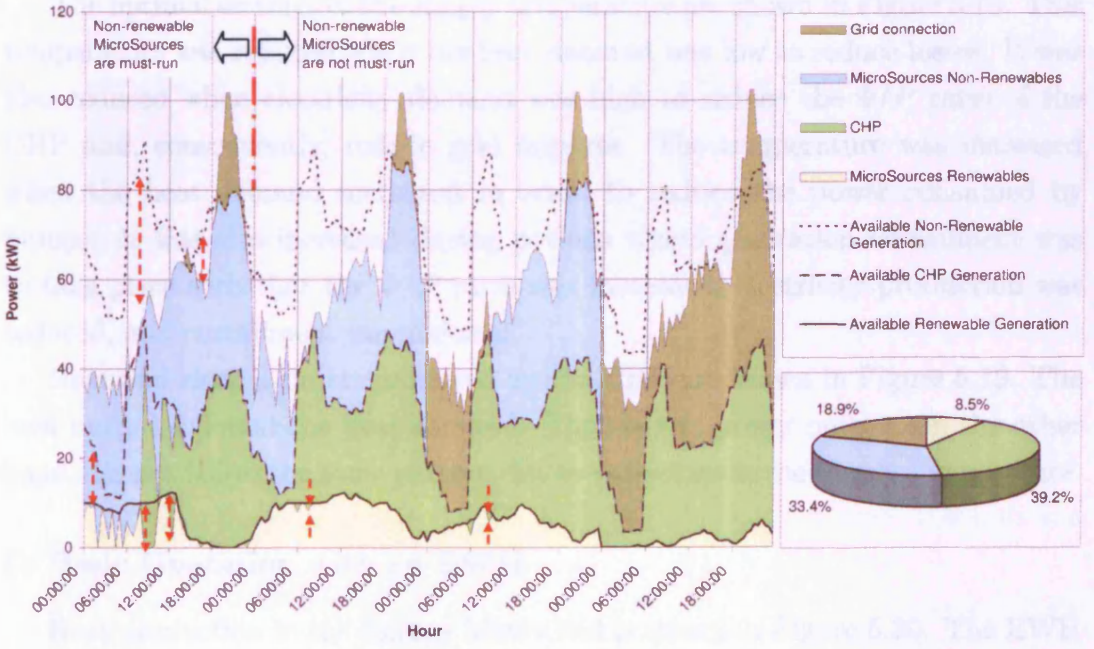

Figure 5.18: Electric power generation for Case study 5.6.1-A: Grid Connected - No Restrictions on Fuel - Basic Operation

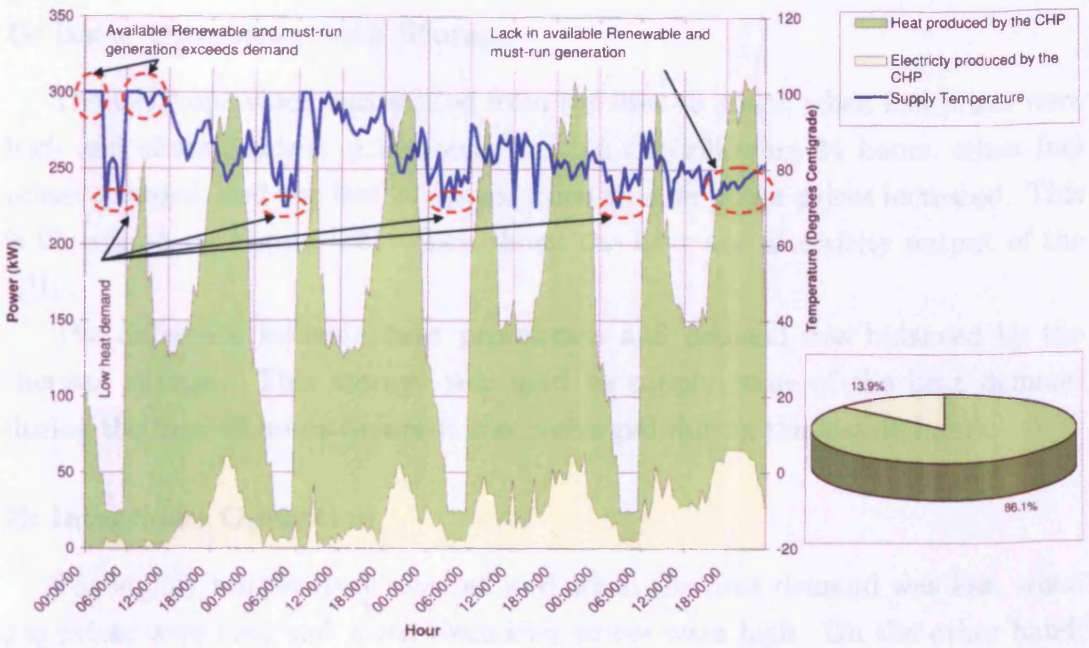

Figure 5.19: CHP output for Case study 5.6.1-B: Grid Connected - No Restrictions on Fuel - Basic Operation with T_S Control

B: Basic Operation with T_S Control

The optimal settings of the supply temperature are shown in Figure 5.19. This temperature was reduced when the heat demand was low to reduce losses. It was also reduced when electricity demand was high to reduce the Φ/P ratio of the CHP and, consequently, reduce grid imports. The temperature was increased when the heat demand increased in order to reduce the power consumed by pumps. It was also increased during periods where generation curtailment was to take place such that the Φ/P ratio was increased, electricity production was reduced, and curtailment was reduced.

Heat and electric power produced by the CHP are shown in Figure 5.19. The heat output followed the heat demand. The electric power output, on the other hand, did not follow the same pattern due to variations in the supply temperature.

C: Basic Operation with an EWH

Heat production in the Energy MicroGrid is shown in Figure 5.20. The EWH was used to convert surplus electricity into heat. This took place during periods when local generation exceeded demand. This minimised generation curtailment and reduced the load on the CHP unit.

D: Basic Operation with Storage

The CHP operation was shifted from the first 48 hours, when fuel prices were high and electric power prices were low, to the following 24 hours, when fuel prices dropped, and the last 24 hours, when electric power prices increased. This is illustrated by Figure 5.21 which shows the heat and electricity output of the CHP.

The difference between heat production and demand was balanced by the thermal storage. This storage was used to supply some of the heat demand during the first 48 hours before it was recharged during the last 48 hours.

E: Integrated Operation

The supply temperature was reduced when the heat demand was low, when gas prices were low, and when electricity prices were high. On the other hand, this temperature was increased when the heat demand increased, when gas prices were high, and when electricity prices were low.

The CHP usage was shifted from periods of high gas prices and low electricity prices towards periods of high electricity prices and low gas prices.

Finally, the EWH was used to convert surplus electric power into heat.

The supply temperature and the outputs of the CHP unit are shown in Figure 5.22. The electric power generation is shown in Figure 5.23.

Discussion

Table 5.4 shows a summary of the energy utilisation, energy costs and average energy prices for all simulations in Case 5.6.1. Table 5.5 shows the percentage changes in the results of simulations 5.6.1-B, -C, -D, and -E compared to the base simulation of Case 5.6.1-A.

The fuel consumed by the CHP was reduced in Case 5.6.1-B by 0.8% and in Case 5.6.1-D by 0.2%. This was due to the reduction in the CHP output curtailed. A 2.2% reduction was achieved in Case 5.6.1-C as some of the heat demand was supplied by the EWH.

The percentage of electricity demand served by the CHP unit increased from 39.2% in Case 5.6.1-A to 48.6% in Case 5.6.1-E. This was accompanied by only a slight increase of 0.7% in fuel consumption. This increase was very low because thermal losses were reduced, less heat demand was served by the CHP, and none

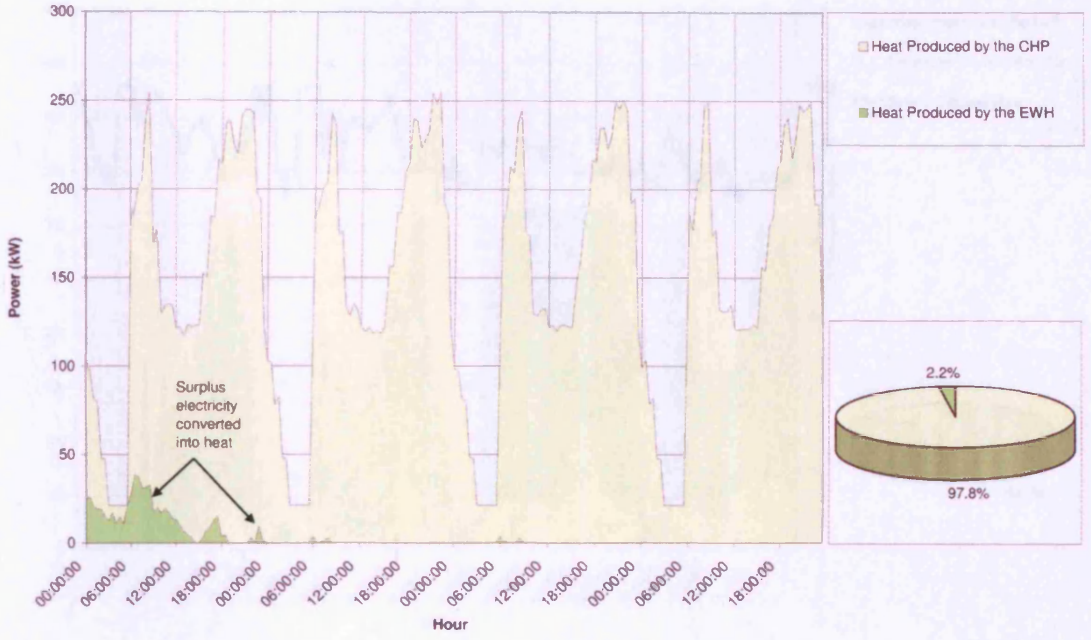

Figure 5.20: Heat production for Case study 5.6.1-C: Grid Connected - No Restrictions on Fuel - Basic Operation with an EWH

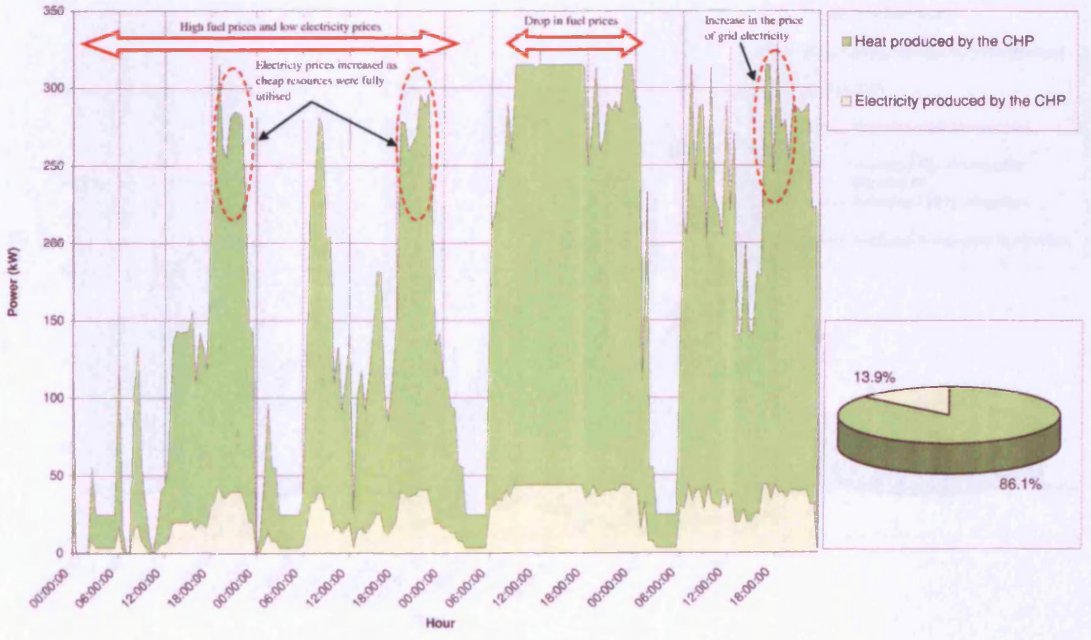

Figure 5.21: CHP output for Case study 5.6.1-D: Grid Connected - No Restrictions on Fuel - Basic Operation with thermal storage

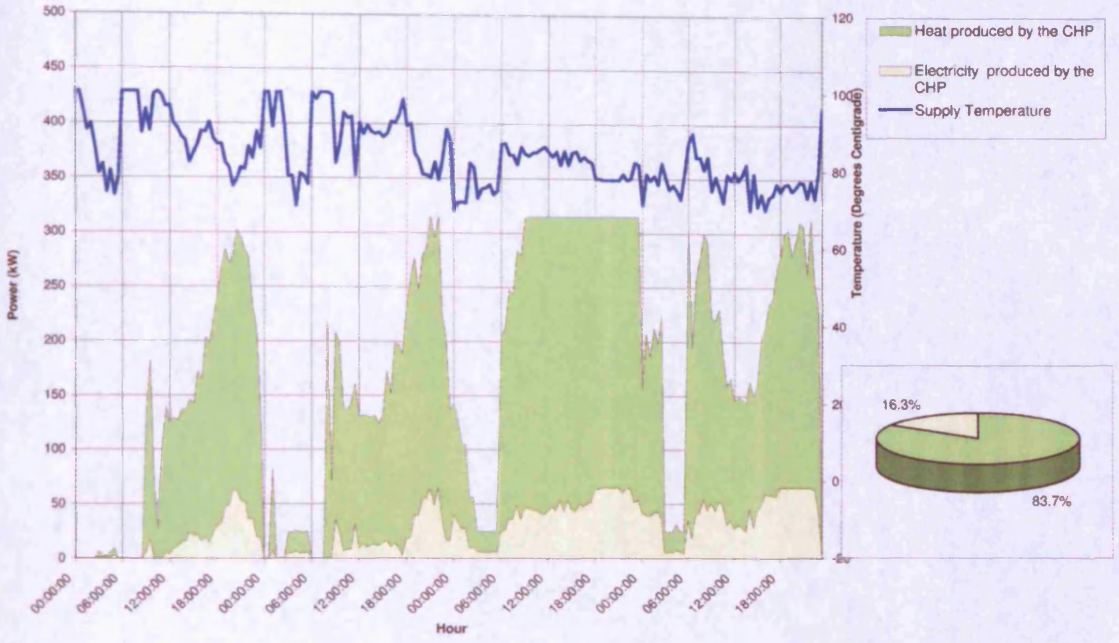

Figure 5.22: CHP output for Case study 5.6.1-E: Grid Connected Operation - No Restrictions on Fuel - Integrated Operation

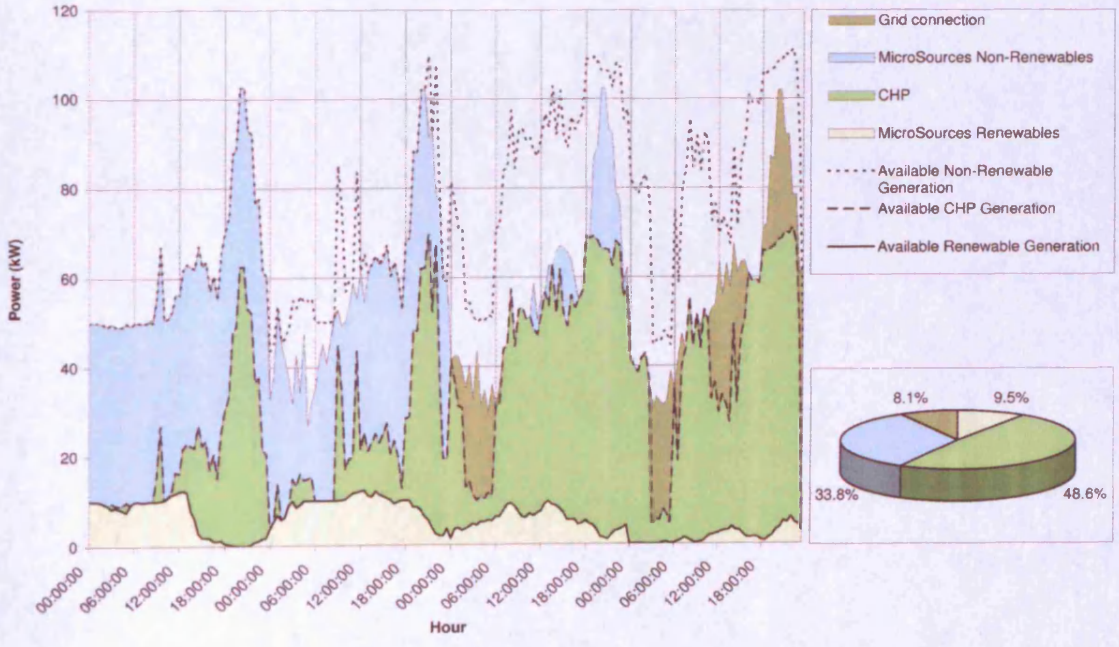

Figure 5.23: Electric power generation for Case study 5.6.1-E: Grid Connected Operation - No Restrictions on Fuel - Integrated Operation

Table 5.4: Summary of the results of Case study 5.6.1: Grid Connected Operation - No Restrictions on Fuel

		Amount kWh	Cost £	Average price £/kWh
A: Basic Operation	Grid Imports	1035.3	43.0	0.04150
	Non-Renewable MicroSources	1834.5	27.4	0.01492
	Renewables MicroSources	465.3	0.0	0.0
	Gas	18334.1	312.8	0.01706
	Total energy consumption	21669.2	383.2	
	Energy curtailed	367.9		
B: Basic Operation with T_S-Control	Grid Imports	610.5	23.3	0.03820
	Non-Renewables MicroSources	2091.3	30.8	0.01475
	Renewables MicroSources	519.3		
	Gas	18179.2	309.6	0.01703
	Total energy consumption	21400.2	363.8	
	Energy curtailed	89.0		
C: Basic Operation with EWH	Grid Imports	1035.1	43.0	0.04150
	Non-Renewable MicroSources	1996.3	27.4	0.01370
	Renewables MicroSources	531.5		
	Gas	17925.0	305.2	0.01702
	Total energy consumption	21487.8	375.5	
	Energy curtailed	0.0		
D: Basic Operation with Storage	Grid Imports	944.3	39.1	0.04138
	Non-Renewable MicroSources	1788.7	22.9	0.01274
	Renewables MicroSources	491.5		
	Gas	18300.3	300.4	0.01642
	Total energy consumption	21524.8	362.3	
	Energy curtailed	117.4		
E: Integrated Operation	Grid Imports	455.2	17.5	0.03845
	Non-Renewable MicroSources	1887.7	22.4	0.01184
	Renewables MicroSources	531.6		
	Gas	18457.3	301.5	0.01633
	Total energy consumption	21332.1	341.4	
	Energy curtailed	0.0		

Table 5.5: Percentage changes in the results for different simulations in Case study 5.6.1: Grid Connected Operation - No Restrictions on Fuel. Simulation 5.6.1-A was used as a reference

	Percentage change in	Amount %	Cost %	Average price %
B: Basic Operation with T_S-Control	Grid Imports	-41.0	-45.8	-8.0
	Non-Renewables MicroSources	+14.0	+12.4	-1.1
	Renewables MicroSources	+11.6		
	Gas	-0.8	-1.0	-0.2
	Total	-1.2	-5.1	
	Energy curtailed	-75.8		
C: Basic Operation with EWH	Grid Imports	0.0	0.0	0.0
	Non-Renewable MicroSources	+8.8	0.0	-8.2
	Renewables MicroSources	+14.2		
	Gas	-2.2	-2.4	-0.2
	Total	-0.8	-2.0	
	Energy curtailed	-100.0		
D: Basic Operation with Storage	Grid Imports	-8.8	-9.1	-0.3
	Non-Renewable MicroSources	-2.5	-16.4	-14.6
	Renewables MicroSources	+5.6		
	Gas	-0.2	-4.0	-3.8
	Total	-0.7	-5.5	
	Energy curtailed	-68.1		
E: Integrated Operation	Grid Imports	-56.0	-59.3	-7.3
	Non-Renewable MicroSources	+2.9	-18.2	-20.6
	Renewables MicroSources	+14.2		
	Gas	+0.7	-3.6	-4.3
	Total	-1.6	-10.9	
	Energy curtailed	-100.0		

of the CHP output was curtailed..

Power imported from the grid was reduced in Case 5.6.1-B by 45.8% due to the change of the Φ/P ratio during periods of high power prices and low fuel prices. It was also reduced in Case 5.6.1-D due to the shift that took place in the pattern of CHP utilisation. These two effects combined together resulted in a 59.3% reduction in Case 5.6.1-E.

Compared to the Basic Operation, all other simulations included an improvement in the utilisation of the energy resources as less curtailment took place. There was also an improvement in the average energy prices as the usage of each resource was increased when it was cheap and reduced when it was expensive. As a result, there was always a reduction in the total energy cost.

5.6.2 Islanded Operation with No Restrictions on Fuel

This case was to investigate the system performance when the connection to the main electricity grid is not available. Electricity demand, both active and reactive, has to be either supplied locally or shed. No restrictions were imposed on the fuel supply for the CHP unit and the Non-renewables MicroSources. This allows them to supply their rated output. The three simulations in this case study are summarised in Table 5.6.

A: Basic Operation

Electric power generation and electric load shedding are shown in Figure 5.24. Loads had to be shed during periods of high electricity demand. This caused 158.6kWh of this demand not to be served. On the other hand, generation was curtailed during periods of low demand. This caused 365.9kWh of free electric energy to be wasted.

B: Basic Operation with electricity driven CHP

As the CHP was not restricted to follow heat demand, its output was increased at periods of high electricity demand. This is shown in Figure 5.25. This increased electric energy available during these periods and reduced load shedding.

Table 5.6: Simulations considered in Case study 5.6.2: Islanded Operation - No Restrictions on Fuel

		Simulation		
		A Basic Operation	B Basic Operation with electricity driven CHP	C Integrated Operation
Load following of the CHP		Heat	Heat and electricity	Heat and electricity
Hot water supply temperature	Min	85°C	85°C	70°C
	Max	85°C	85°C	100°C
Heat efficiency of the CHP	Min*	77.5%	77.5%	65.0%
	Max**	77.5%	77.5%	90.0%
Power efficiency of the CHP	Max*	12.5%	12.5%	25.0%
	Min**	12.5%	12.5%	0.0%
The EWH				Available
Thermal storage				Available

* Corresponding to minimum supply temperature
** Corresponding to maximum supply temperature

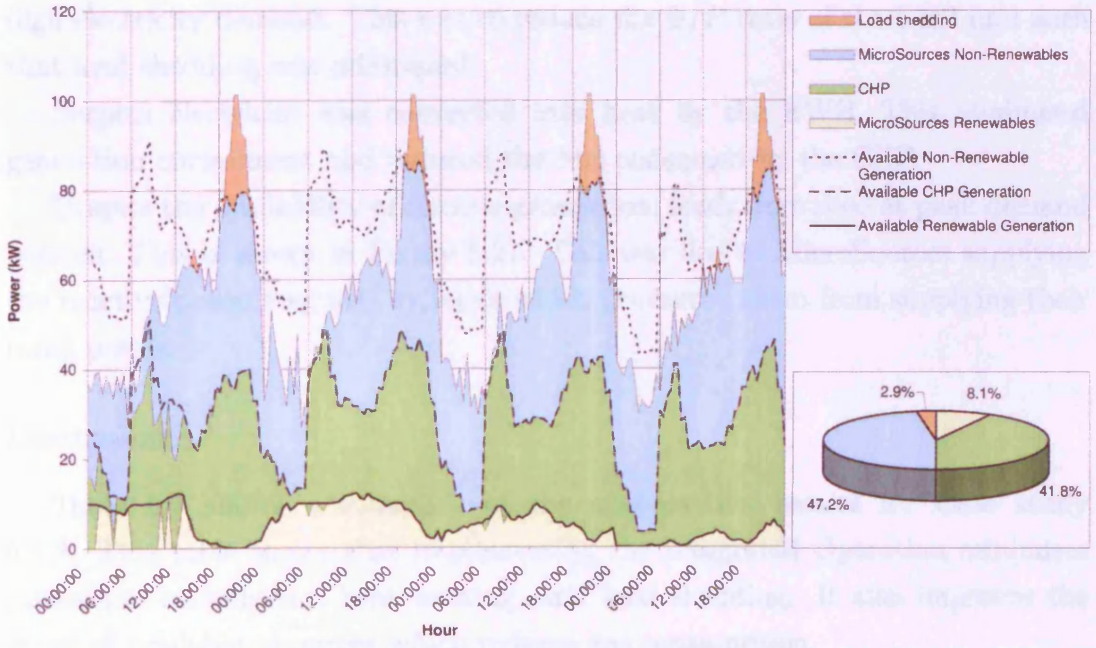

Figure 5.24: Electric power generation for Case study 5.6.2- A:Islanded Operation - No Restrictions on Fuel - Basic Operation

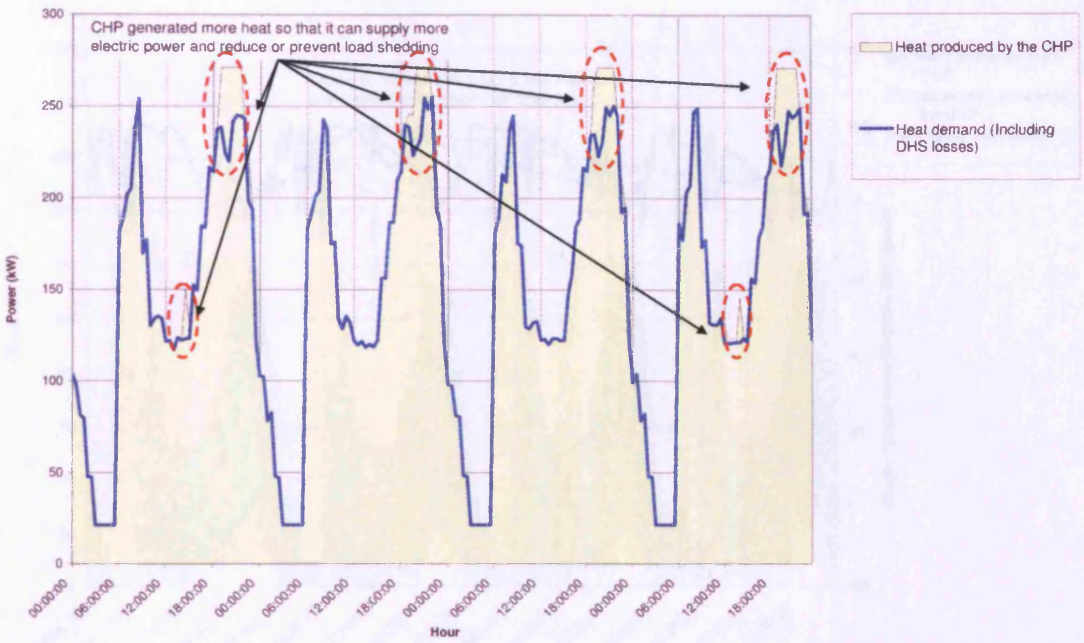

Figure 5.25: Heat supply and demand for Case study 5.6.2- B:Basic Operation with electricity driven CHP

C: Integrated Operation

The supply temperature, shown in Figure 5.26, was reduced during periods of high electricity demand. This was to reduce the Φ/P ratio of the CHP unit such that load shedding was minimised.

Surplus electricity was converted into heat by the EWH. This minimised generation curtailment and reduced the fuel consumed by the CHP.

Despite the availability of electric generation, loads were shed at peak demand periods. This is shown in Figure 5.27. This was due to MicroSources supplying the reactive power required by loads which prevented them from supplying their rated power.

Discussion

Table 5.7 shows a summary of the optimisation results for Case study 5.6.2. This table shows that implementing the Integrated Operation minimises generation curtailment, heat wasting, and load shedding. It also improves the usage of available resources which reduces gas consumption.

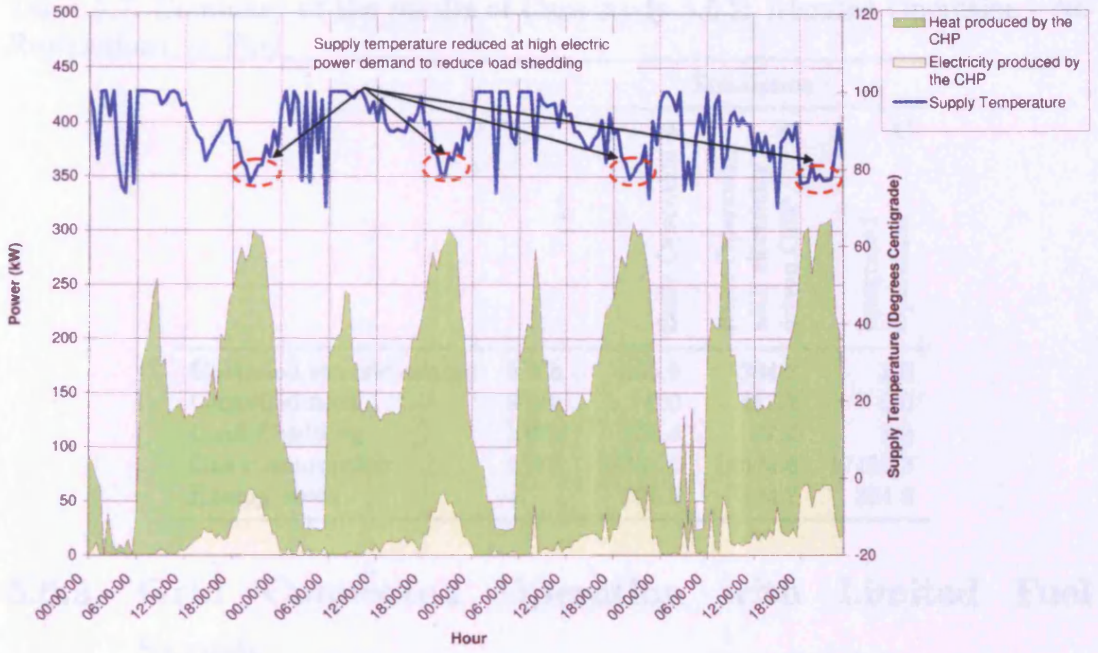

Figure 5.26: CHP output for Case study 5.6.2-C:Islanded Operation - No Restrictions on Fuel- Integrated Operation

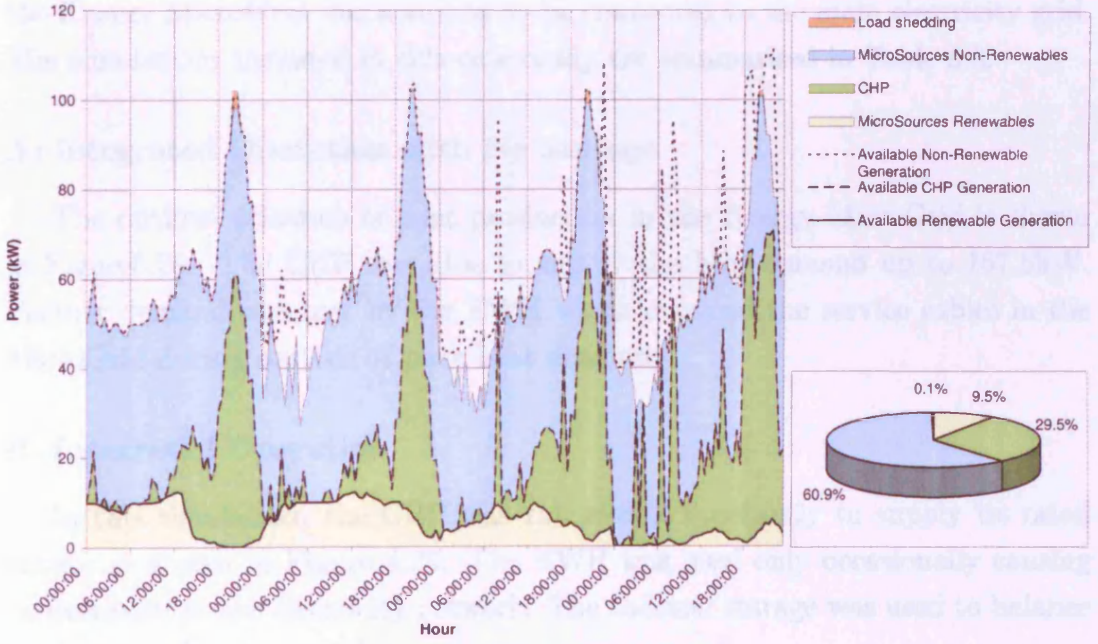

Figure 5.27: Electric power generation for Case study 5.6.2-C:Islanded Operation - No Restrictions on Fuel- Integrated Operation

Table 5.7: Summary of the results of Case study 5.6.2: Islanded Operation - No Restrictions on Fuel

		Simulation		
		A	B	C
		Basic Operation	Basic Operation with electricity driven CHP	Integrated Operation
Curtailed electric energy	kWh	365.9	364.3	3.5
Curtailed heat	kWh	0.0	457.7	0.0
Load Shedding	kWh	158.6	87.4	8.0
Gas consumption	kWh	18334.1	18924.6	17450.3
Energy costs	£	394.6	404.7	394.8

5.6.3 Grid Connected Operation with Limited Fuel Supply

This case was to investigate the system performance with limited fuel supply. A shortage in fuel that limits the output of Non-renewable MicroSources and the CHP unit to 50% of their rating was assumed to take place. The LV network of the Energy MicroGrid was assumed to be connected to the main electricity grid. The simulations included in this case study are summarised in Table 5.8.

A: Integrated Operation with No Storage

The optimal schedule of heat production in the Energy MicroGrid is shown in Figure5.28. The CHP was able to supply the heat demand up to 157.5kW. Further demand was met by the EWH which overload the service cables in the MicroGrid during periods of peak heat demand.

B: Integrated Operation

In this simulation, the CHP was run almost constantly to supply its rated output as shown in Figure 5.29. The EWH was used only occasionally causing no overloads in the electricity network. The thermal storage was used to balance the heat production and demand.

The schedule of electric power generation in the Energy MicroGrid is shown in Figure 5.30.

Table 5.8: Simulations considered in Case study 5.6.3: Grid Connected Operation - Limited Fuel Supply

		Simulation	
		A	B
		Integrated Operation with no storage	Integrated Operation
Load following of the CHP		Heat and electricity	
Hot water supply temperature	Min	70°C	
	Max	100°C	
Heat efficiency of the CHP	Min*	65%	
	Max**	90%	
Heat efficiency of the CHP	Min*	0%	
	Max**	25%	
The EWH		Available	
Thermal storage		Not available	Available

* Corresponding to minimum supply temperature
** Corresponding to maximum supply temperature

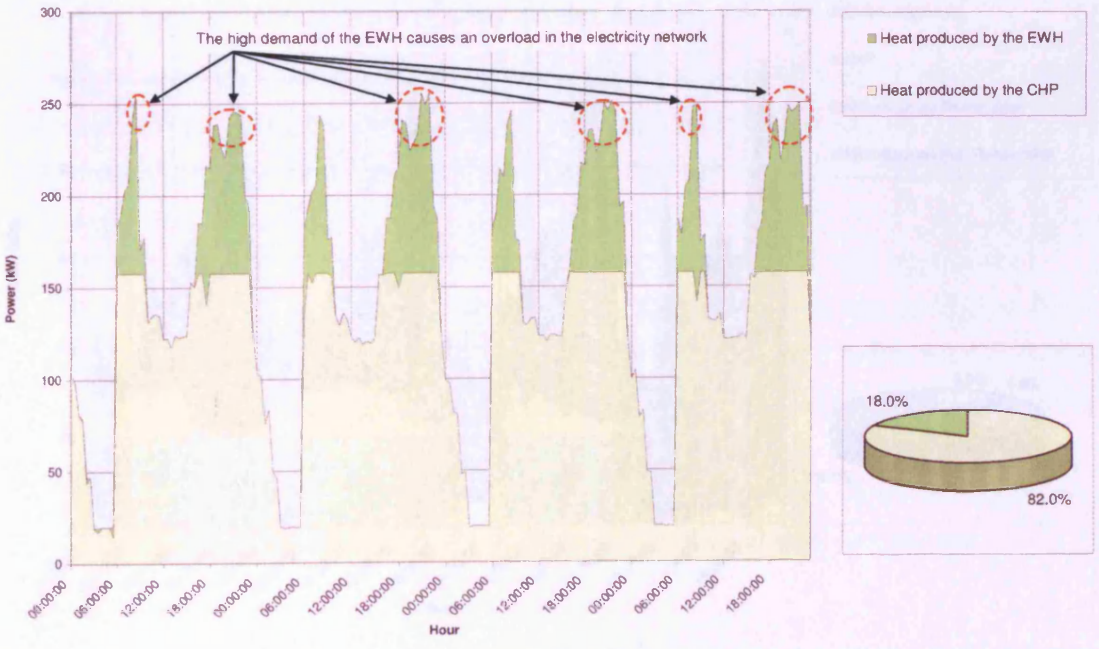

Figure 5.28: Heat production for Case study 5.6.3-A:Grid Connected Operation-Limited Fuel Supply - Integrated Operation with no Storage

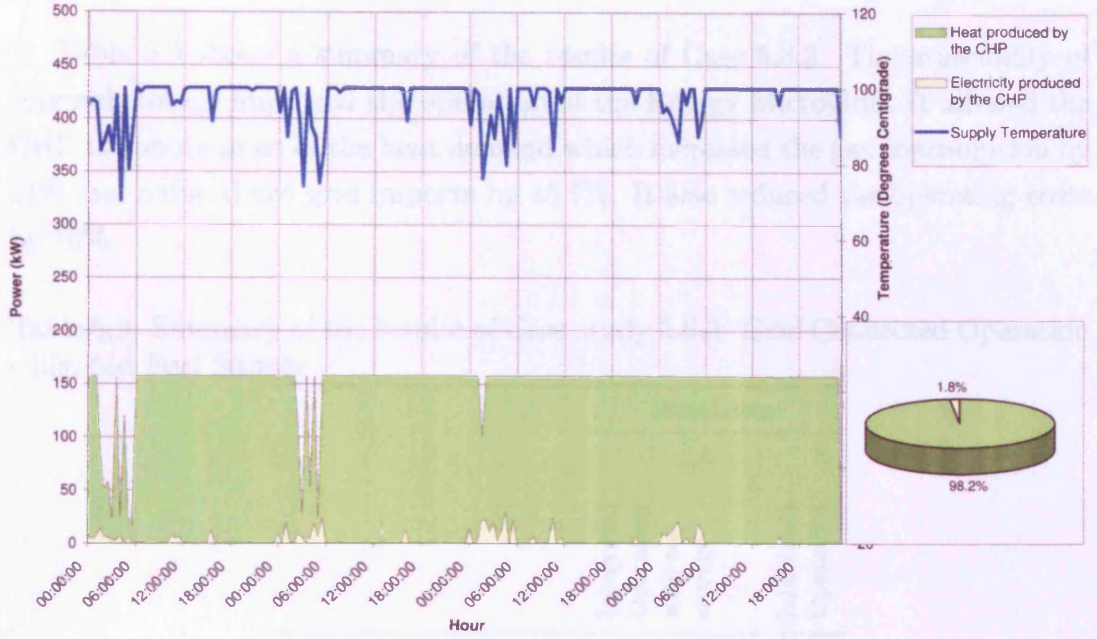

Figure 5.29: CHP Output for Case study 5.6.3-B:Grid Connected Operation - Limited Fuel Supply - Integrated Operation with Storage

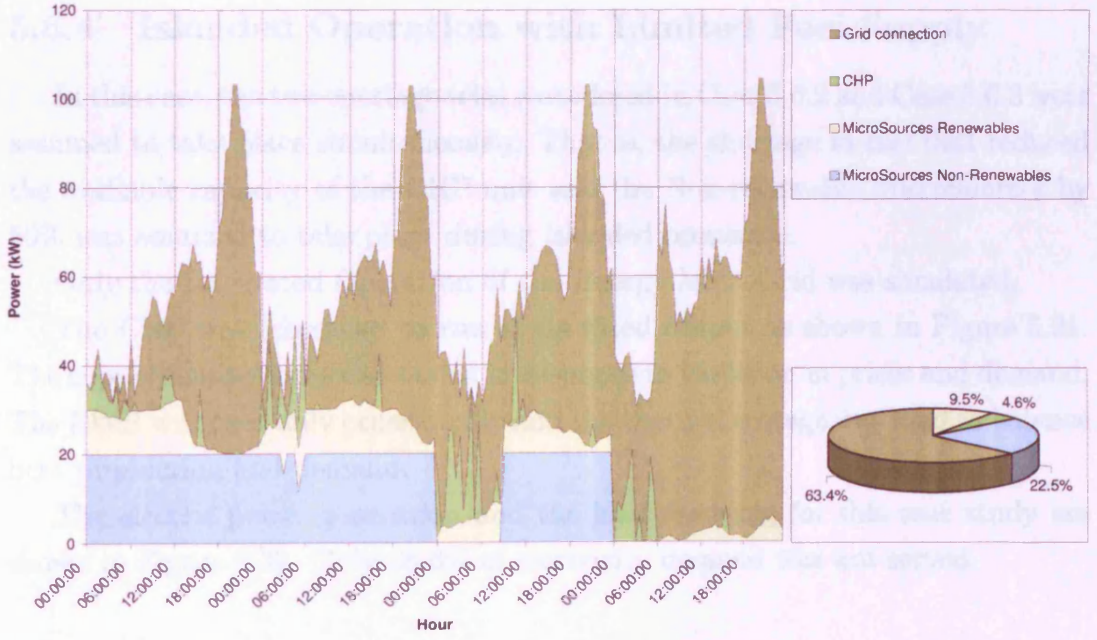

Figure 5.30: Electric power generation for Case study 5.6.3- B:Grid Connected Operation - Limited Fuel Supply - Integrated Operation with Storage

Discussion

Table 5.9 shows a summary of the results of Case 5.6.3. The availability of thermal storage improved the operation of the Energy MicroGrid. It allowed the CHP to supply most of the heat demand which increased the gas consumption by 21% and reduced the grid imports by 45.7%. It also reduced the operating costs by 16%.

Table 5.9: Summary of the results of Case study 5.6.3: Grid Connected Operation - Limited Fuel Supply

		Simulation	
		A	B
		Integrated Operation with no storage	Integrated Operation
Grid Imports	kWh	6505.8	3531.3
Gas consumption	kWh	13128.6	15969.4
Energy Costs	£	532.1	446.9

5.6.4 Islanded Operation with Limited Fuel Supply

In this case, the two contingencies considered in Case 5.6.2 and Case 5.6.3 were assumed to take place simultaneously. That is, the shortage in fuel that reduced the available capacity of the CHP unit and the Non-renewable MicroSources by 50% was assumed to take place during islanded operation.

Only the Integrated Operation of the Energy MicroGrid was simulated.

The CHP was scheduled to run at its rated output as shown in Figure 5.31. The supply temperature was varied in response to variation in prices and demand. The EWH was used only occasionally and the thermal storage was used to balance heat production and demand.

The electric power generation and the load shedding for this case study are shown in Figure 5.32. Only 38.6% of electricity demand was not served.

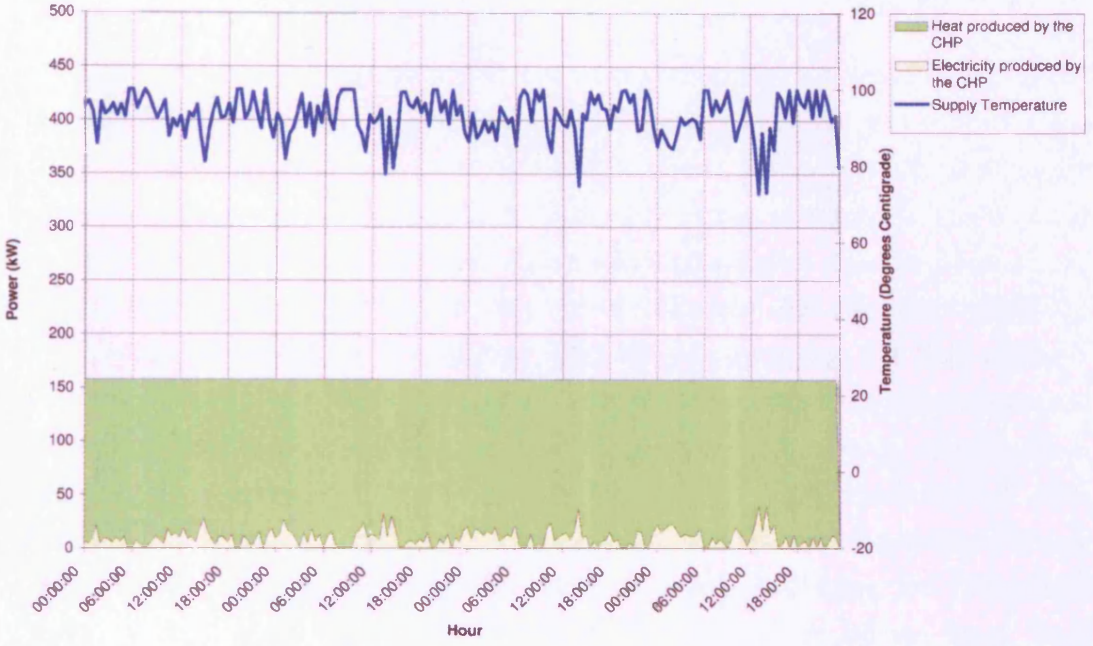

Figure 5.31: CHP output for Case study 5.6.4:Islanded Operation - Limited Fuel Supply- Integrated Operation

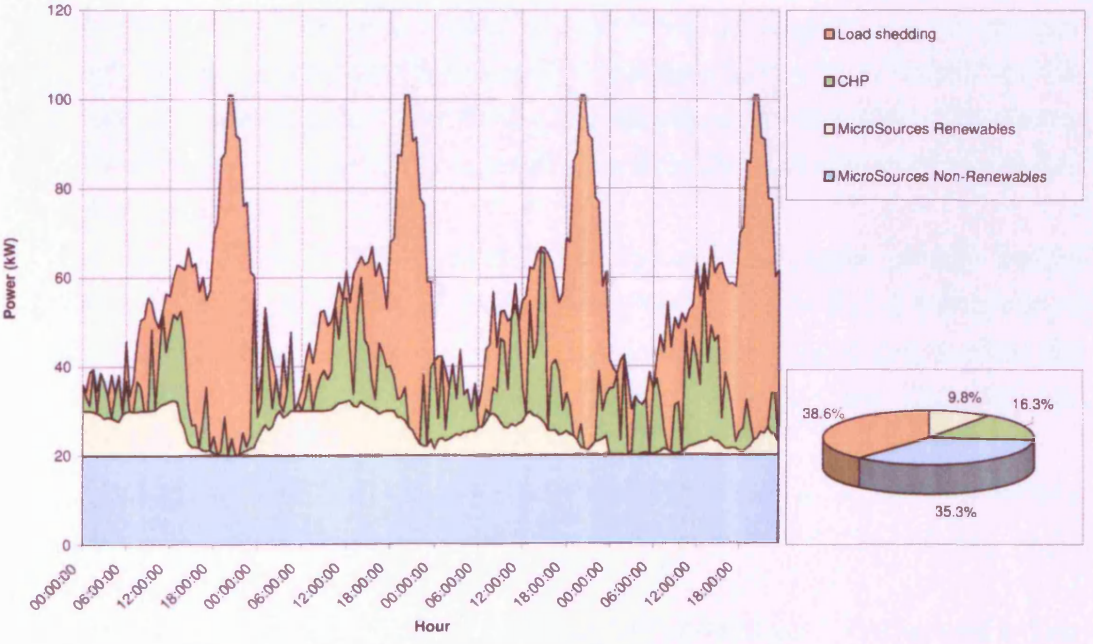

Figure 5.32: Electric power generation for Case study 5.6.4:Islanded Operation - Limited Fuel Supply- Integrated Operation

5.7 Conclusion

An Integrated Optimal Power Flow for heat and electric power was formulated. This IOPF included a model for an electric power network and a model for a district heat system that were coupled together via models of the energy conversion equipment. The objective of this IOPF was to minimise the costs of operation of the Energy MicroGrid while maintaining power balance constraints, physical constraints, and technical constraints of the heat and electricity networks.

Integrated Operation of the Energy MicroGrid is operating the heat network and the electricity network of the Energy MicroGrid as a single integrated system. The district heat station and the thermal storage were controlled to support both networks. This support was provided via the control of the heat-to-power ratio of the CHP, the use of an Electric Water Heater, and the use of a thermal store.

The IOPF was used to investigate the advantages of using the Integrated Operation in the Energy MicroGrid test system. Four study cases were considered. These cases included normal operation, islanded operation of the LV network, operation with a shortage in the fuel supply, and islanded operation of the LV network with a shortage in fuel supply.

The heat-to-power ratio of some CHP unit is a function of its supply temperature. This ratio was varied by the IOPF in response to the changes in energy prices. This was found to reduce the electric energy curtailed and the heat wasted. This, in turn, reduced the fuel consumed by the CHP. The control of the heat-to-power ratio was also found to reduce the load shed during islanded operation.

The use of Electric Water Heater was found to minimise electric energy curtailed. This was accompanied with a reduction in the the fuel consumption of the CHP. Having this EWH as an auxiliary source of heat was found to allow the district heat network to meet its demand if the CHP output was limited due to a shortage in its fuel supply.

Allowing the CHP to provide electric-load-following during emergency conditions, e.g. during islanded operation, reduces load shedding but may cause surplus heat to be wasted.

Thermal storage was found to have several advantages. It decoupled heat production from heat demand which allowed the CHP to run when electricity prices are high and fuel prices are low. It also prevented excess heat from being wasted when the CHP unit was providing electric load following. Finally, it

allowed the district heat system to meet its demand when the capacity of the CHP was reduced. This was not accompanied by any overload on the electric power network.

In summary, heat and electricity networks in an Energy MicroGrid should be operated as one integrated system rather than two independent systems. To achieve this:

- an electric water heater should be available to convert any surplus electricity into heat;
- the CHP unit should be used to provide electric load following, as well as heat load following, when there is a shortage in electric power generation;
- the supply temperature setting of the CHP unit should vary with thermal demand in order to optimise thermal and hydraulic losses;
- for CHP units whose heat-to-power ratio is a function of the supply temperature, the temperature setting should be varied in response to the availability and the prices of fuel and electricity; and
- thermal storage should be available in order to decouple heat production from heat demand such that no energy is utilisation and energy costs are optimised.

Chapter 6

Conclusions

6.1 Energy MicroGrids

Energy supply systems are expected to undergo major change. This change will be influenced by legislation and financial incentives as well as increasing environmental awareness. In order to address the technical challenges of this change, concepts such as MicroGrids and Multi-Carrier Energy Systems were formulated. These two concepts were combined together in this research to define an Energy MicroGrid.

An Energy MicroGrid is a Multi-Carrier Energy System that serves the energy needs of a small area. These needs are served via a district heat system, an LV network, and a gas network. Connected to the LV network is a set of MicroSources, these are electric power generators of low rating, and an electric energy storage unit. Heat, gas, and electricity networks of the Energy MicroGrid are coupled together at a district heat station whose main function is to produce the heat required to meet the heat demand.

Due to the technologies used by MicroSources and the interests of their owners to maximise their usage, it is difficult to match electric power generation and demand. This imbalance causes voltage excursions and, if the power network is operated as an island, frequency excursions.

Voltage regulation during grid connected operation was investigated. A voltage control system where an On-Load-Tap-Changer was coordinated with reactive power control of MicroSources was described. A simple rule-based system was used in cases where several MicroGrids and passive feeders are connected to the same transformer. The performance of this voltage control system when

applied to the CIGRÉ MicroGrid benchmark model was simulated.

A frequency control system for the islanded MicroGrid was investigated. This control system used MicroSources, electrical storage, and non-critical loads to provide frequency response. This response was provided via droop operation, in the case of MicroSources and storage, and by Intelligent Load Management Controllers, in the case of non-critical loads. Fuzzy logic was used by Intelligent Load Management Controllers to set the shedding and restoration frequencies of their loads based on the demand and the previous contribution of these loads to frequency response. The performance of this control system when applied to the CIGRÉ MicroGrid benchmark model was simulated.

Finally, this research addressed the balancing of generation and demand in the Energy MicroGrid. This was by operating the electric power network and the district heat network as an integrated system. The control options associated with this integrated operation were defined. An integrated optimisation tool, the Integrated Optimal Power Flow, was used to assess the benefits of using this approach.

6.2 Voltage and Frequency Control in the Energy MicroGrid

The MicroGrid should operate within acceptable voltage limits. These limits should be within those of the standard electric power supply regulations. In this research, these limits were chosen to be ±6% of the nominal voltage.

The frequency of a MicroGrid during grid connected operation is set by the main network. This is due to the small size of the MicroGrid compared to the large power system. For this condition, there was no need to define frequency limits for the MicroGrid as the frequency defined by the main grid will apply.

During islanded operation, the frequency of the MicroGrid is determined by power balance and local frequency response. For this condition, the primary frequency response target was to maintain the frequency between 42.5Hz and 52Hz. This is for the first two minutes following a sudden loss of power balance. In the subsequent eight minutes, the secondary frequency response is to restore the frequency to between 49Hz and 50Hz.

6.2.1 Control of MicroSources

MicroSource Controllers determine the response of a MicroSource to changes in its terminal voltage and frequency. MicroSource Controllers operate either on PQ control, where they do not respond to voltage and frequency excursions, or on droop control, where they provide voltage and frequency support.

Voltage/reactive power droop control was used for all MicroSources. This was found to reduces voltage excursions in the MicroGrid. This approach is fast and requires no communications. Also, despite having limited effect, it allows MicroSources to increase their output without exceeding the maximum voltage.

Operation at constant reactive power output was found to be suitable for MicroSources that are located near the transformer. This is due to the high X/R ratio of the transformer and the low X/R ratio of the distribution feeders which would cause unnecessary circulation of reactive power if these MicroSources were operated on voltage/reactive power droops.

During grid connected operation of the MicroGrid, MicroSources can not influence the network frequency. If they were operated on frequency/active power droops, they would change their active power output as the network frequency changed.

Once the connection of the MicroGrid to the main electricity grid is lost, MicroSource were found able to influence the power balance in the MicroGrid, and hence the MicroGrid frequency. In this case, frequency/active power droop operation was used to provide frequency support.

An integral frequency control loop was used for some MicroSources. This loop was able to provide secondary frequency response. This response improved the MicroGrid frequency and reduced the need to shed loads.

6.2.2 Control of Electric Storage

The electric storage unit provides several services to the MicroGrid. This includes providing reference voltage and frequency, inertia response, fault current, and primary frequency response. It was necessary to maintain an adequate level of energy stored such that these services were available at all times.

Reactive power control of the electric storage was treated in the same way as that of MicroSources. Voltage/reactive power droop control was used to provide voltage support during grid connected operation as well as during islanded

operation. Storage would have been operated at constant reactive power output during grid connected operation only if it were located near the transformer.

In this research, as well as in the literature studied, frequency/active power droops were used with the electric storage unit. This was to provide primary frequency response. In this research, the frequency at which the storage supplied zero output power was set to vary with the energy stored. This was to prevent the complete discharging of the storage.

6.2.3 Load Control

Each consumer was assumed to have two independent circuits with loads connected to them according to their importance. Both circuits were controlled by under-frequency relays. Critical loads were shed only when the frequency fell below 42.5Hz. Non-critical loads were controlled to provide frequency response when necessary.

"Historical Unserved Energy" was used to quantify the contribution of consumers to frequency response. This is cumulative sum of the product of the demand, in Watts, and the period of disconnection, in seconds.

Load shedding was set to start when the frequency dropped below 48Hz so that it was not initiated by frequency events taking place during grid connected operation. The target of this response was preventing the frequency from dropping below 42.5Hz in the first two minutes then restoring this frequency to above 49Hz within the next eight minutes.

Load restoration was set to start at 49.25Hz. Its target was to restore all loads in the first two minutes before the frequency reached 52Hz. In the following eight minutes, it restored gradually the frequency to between 49.25Hz and 49.5Hz. The latter values was chosen to be less than 50Hz, which is the target frequency of the secondary frequency response of MicroSources. This guaranteed that all loads were restored before the MicroSources ceased to supply frequency response.

Intelligent Load Management Controllers (ILMCs) were used to determine the shedding and restoration frequencies for non-critical loads based on their demand and their previous contribution to frequency response. This ILMCs used fuzzy logic to calculate a number that specified the load's potential to contribute to frequency response. Based on this number and the frequency targets, the ILMC set the shedding and restoration frequencies for the non-critical loads.

The fuzzy rules were chosen such that loads of higher demand and low value

of Historical Unserved Energy had more potential to provide frequency response service. This reduced the number of consumers disconnected during a frequency event while maintaining equity among consumers.

6.2.4 Control of On-Load-Tap Changers

A vacuum-switch OLTC has been developed at Areva T&D for 11/0.4kV transformers. This OLTC was assumed to be installed in the MicroGrid to provide secondary voltage control. The controller of this OLTC was coordinated with MicroSource Controllers.

The OLTC was controlled to keep the reactive power output of a specific MicroSource, the Control MicroSource, within a deadband. While doing this, it brings the reactive power output of all other MicroSources closer to zero and their voltage closer to 1.0 p.u. This allows MicroSources to increase their output power without violating voltage limits.

The deadband was set to move in response to the active power output of the Control MicroSource. This was to account for the voltage drop across the cables connecting the Control MicroSource to the main feeder.

The steps followed to select the Control MicroSource, and the equation used to calculate the deadband and its response to active power output were included in Chapter 3.

A simple rule based system was used to determine the OLTC responses for cases where multiple MicroGrids and passive distribution feeders are supplied from the same transformer.

6.2.5 Communication Requirements

A communication link is required from the control MicroSource to the OLTC controller. The speed of this link is determined by the minimum time between any two tapping operations. If this link is lost, the MicroGrid will be able to carry on supplying power but it might cause generation to be curtailed or voltage to drop below 0.94p.u.

Two way communications are required between the MGCC and each ILMC unit. This is to allow ILMC units to send the Historical Unserved Energy of their consumers to the MGCC and to allow the MGCC to send the maximum and the minimum of these values back to all ILMC units. This was scheduled to take

place once every 15 minutes. If these communication links fail, the MicroGrid is able to run but equity among consumers is compromised.

6.3 The IOPF

An Integrated Optimal Power Flow for heat and electric power was formulated. This IOPF performed a multi-time-period optimisation of a district heat system and an electric power system that were linked together via district heat stations. The objective of the optimisation was to minimise the cost of energy required to supply the total heat and electricity demand.

Steady state models were used for both heat and electric power networks. The electric power network was modelled by the AC load flow equations. The district heat system was modelled by hydraulic flow equations, thermal energy balance equations, and heat transfer equations.

The inputs to the IOPF were demand, generation available, and energy prices. The outputs of the IOPF were schedules for the outputs of all electric power generators, district heat stations, and thermal storage; any electric load shedding required; and settings for the supply temperature of the district heat station.

The IOPF was applied to an Energy MicroGrid model where it was used to produce optimal schedules for the district heat station and the MicroSources.

6.4 Integrated Operation of an Energy MicroGrid

The Energy MicroGrid is a small Multi-Carrier Energy System where heat and electric power networks are coupled. The Integrated Operation of this system was defined as controlling both networks to support the other while supplying its loads. This is in contrast to Basic Operation of the Energy MicroGrid which was used to denote operating both networks to supply their loads without considering the interactions between them.

This Integrated Operation was achieved via controlling both the district heat station and the thermal storage.

6.4.1 Control of the District Heat Station

The district heat station is the main source of heat in the Energy MicroGrid. It is also the point of coupling between the district heat system and the electric power network. This allows the district heat station to support both of them when required.

The district heat station was used to reduce any shortage of electric power in the Energy MicroGrid by:

Producing more heat: The CHP was allowed to produce more heat than required. This, at constant heat-to-power ratio, is accompanied by an increase in its electric power output. This, in turn, reduce the shortage of electric power in the Energy MicroGrid. This was found to reduce load shedding when the Energy MicroGrid was operated as an electric island. On the other hand, when no thermal storage was available, the excess heat produced was wasted.

Reducing the heat-to-power ratio: The heat-to-power (Φ/P) ratio of some CHP units is controllable. Reducing this ratio means that the CHP increases its electric power output without having to generate more heat than required. This was found to improve the operation of the Energy MicroGrid during periods when electricity was expensive or not available.

The district heat station was controlled to reduce the curtailment of electric power generation in the Energy MicroGrid by:

Increasing the heat-to-power ratio: When possible, increasing the Φ/P ratio of the CHP reduces the electric power available. This was found to reduce the need to curtail the electric power generation of the CHP as well as other MicroSources. This, in return, reduced the fuel consumed by the CHP. It was also found to reduce the need to curtail the generation of other MicroSources which improves the overall utilisation of energy.

Electric water heating: The use of an electric water heater to convert any surplus electricity to heat was found to prevent generation curtailment. It was also found to reduce the fuel consumption of the CHP unit.

Electric water heating was identified as an alternative for the control of the Φ/P ratio of CHP units. Converting some of the CHP electricity output into

heat had an effect that was similar to increasing the Φ/P ratio of the CHP. This is suitable for use with all CHP units.

6.4.2 Thermal storage

The availability of thermal storage in the energy MicroGrid was found to have several advantages. These advantages are:

Reduction in energy waste: In some cases, the CHP unit had to produce more heat than required. This was to increase its electric power output and reduce load shedding. Without thermal storage, this excess heat would be wasted.

Reduction in operating costs: With no thermal storage, the heat output of the district heat station was found to be dictated by the heat demand. With thermal storage, these two quantities are decoupled. This was found to shift heat production towards periods with cheap fuel or electricity.

Increase in the security of heat supply: When a contingency limited the fuel supply to the CHP unit, electric power was used to produce heat. If the shortage in fuel was high, the increase in the demand of electric power was found to overload the network. Moreover, if the electric power network of the Energy MicroGrid was operated as an island, the Energy MicroGrid may fail to meet its heat demand. Having thermal storage was found to solve this problem. This was by allowing the CHP unit to run at its available capacity for the entire period of shortage.

Possible reduction in capital costs: The results showed that, with thermal storage, the Energy MicroGrid was able to meet its heat demand when the CHP output was reduced due to a shortage in fuel. This meant that a combination of a hot water tank and a CHP unit of a reduced rating were able to meet the heat demand.

6.5 Future work

6.5.1 Effect of the Rating of MicroSources

The rating of a MicroSource determines the slope of its droop line. The increase in the rating will cause more reactive power to be injected in response to the voltage rise caused by the increase in active power injection. This will cause the voltage at the transformer busbar to drop. If there is any loads that are connected to this busbar they will suffer voltage drop. This effect in the Benchmark MicroGrid network is not severe due to the low penetration level of MicroSources. The operation at much higher penetration levels should be investigated.

6.5.2 Effect of the Location of the Control MicroSource

The location of the Control MicroSource affects the operation of the voltage control system. In this research, a centrally located MicroSource was chosen to be the Control MicroSource. This was feasible because of the size of the MicroGrid and the distribution of the MicroSources in the Benchmark MicroGrid network. In some cases, this centrally located MicroSource may not be available. In this case, another MicroSource will have to be used as a Control MicroSource. This case should be investigated.

6.5.3 Reactive Power Balance

The reactive power capability of a MicroSource is limited by the kVA rating of its converter and its active power output. When the MicroSource supplied its rated active power output, it was not able to deliver or absorb any VArs. This caused a shortage in reactive power during islanded operation of the MicroGrid. In this case, loads had to be shed in order to maintain reactive power balance. An example of this scenario is the Case 5.6.2 where loads were shed and generation was curtailed simultaneously.

Implications related to shortage in reactive power need to be investigated. This include effects on both voltage and dynamic stability of the islanded MicroGrid. A load shedding scheme that mitigates these problems will have to be developed.

6.5.4 The Integrated Optimal Power Flow

The IOPF model was used in this research to investigate the operation of an Energy MicroGrid. This model may be expanded and used to investigate more research questions. This include the following:

1. The addition of more energy conversion equipment such as:

   a- heat pumps; and

   b- different technologies of CHP units.

2. Increasing the details of the equipment that are already modelled such as:

   a- CHP behavior at partial loading;

   b- Detailed models for heat loads; and

   c- Detailed models for district heat station.

3. Modelling different objectives such as:

   a- minimising emissions; or

   b- minimising energy or exergy losses.

4. Applying the IOPF to larger systems such as energy systems of a medium sized community or a large city. In such case, models of gas network may have to be included.

5. Modelling uncertainties in generation, demand, and energy prices. This is to allow the IOPF to be used for:

   a- short and long term operational planning; and

   b- pricing of services such as voltage support, reactive power balancing, and storage.

6.5.5 Sizing of Equipment

The IOPF model was used in this research to investigate the operation of an Energy MicroGrid. The network that was used is a benchmark network where ratings of equipment were chosen to allow several research studies to be conducted. The sizing of equipment; for example the rating of the CHP and the electric

heater, the size of the thermal store, and the installed capacity of MicroSources of different technologies; would influence the viability using an Energy MicroGrid solution to serve small housing estates and local communities. This sizing need to be made based on life cycle analysis, load duration curves, generation availability, reliability of energy supply required, and contingencies expected.

References

[1] "Directive 2001/80/EC of the European Parliament and of the council of 23 October 2001 on the limitation of emissions of certain pollutants into the air from large combustion plants." Official Journal of the European Communities, November 2001. http://eur-lex.europa.eu/LexUriServ/LexUriServ.do?uri=OJ:L:2001:309:0001:0001:EN:PDF Last accessed, March 2010.

[2] European Commission, "The EU emissions trading scheme." http://ec.europa.eu/environment/climat/pdf/brochures/ets_en.pdf, Last accessed, March 2010, 2009.

[3] HM Government, "The UK renewable energy strategy." http://www.decc.gov.uk/en/content/cms/what_we_do/uk_supply/energy_mix/renewable/res/res.aspx, Last accessed, February 2010, July 2009.

[4] HM Government, "The UK low carbon transition plan." http://www.decc.gov.uk/en/content/cms/publications/lc_trans_plan/lc_trans_plan.aspx, Last accessed, February 2010, July 2009.

[5] A. Wood and B. Wollenberg, *Power Generation Operation and Control.* New York, United States: John Wiley & Sons, Inc., second ed., 1996.

[6] C. Foote, A. Roscoe, R. Currie, G. Ault, and J. McDonald, "Ubiquitous energy storage," in *International Conference on Future Power Systems*, (Amsterdam, Netherlands), November 2005.

[7] D. Pudjianto, C. Ramsay, and G. Strbac, "Virtual power plant and system integration of distributed energy resources," *Renewable Power Generation, IET*, vol. 1, pp. 10 –16, march 2007.

[8] P. Lund, "The Danish Cell project - Part 1: Background and general approach," in *IEEE Power Engineering Society General Meeting*, pp. 1–6, June 2007.

[9] "Interim report, system disturbance on 4 November 2006," tech. rep., Union for the Co-ordination of Transmission of Electricity, 2006. `http://www.entsoe.eu/index.php?id=59` Last accessed, February 2010.

[10] B. Skagestad and P. Mildensteib, *District Heating and Cooling Connection Handbook.* International Energy Agency.

[11] The European Commission, "Biomass plant and district heating system rehabilitation project in Lithuania." Official Journal of the European Communities. `http://www.energie-cites.org/db/ignalina_140_en.pdf` Last accessed, January 2009.

[12] R. McDougall and B. Jensen, "District heating systems for small scale development areas," in *The 11^{th} International Symposium on District Heating and Cooling*, 2008.

[13] M. Chaudry, J. Ekanayake, and N. Jenkins, "Optimum control strategy for a μCHP unit," *International Journal of Distributed Energy Resources*, vol. 4, no. 4, pp. 265–280, 2008.

[14] N. Hatziargyriou, N. Jenkins, G. Strbac, J. Lopes, J. Ruela, A. Engler, J. Oyarzabal, G. Kariniotakis, and A. A., "MicroGrids- large scale integration of microgeneration to low voltage grids," in *CIGRÉ Sessions*, (Paris, France), 2006.

[15] N. Hatziargyriou, H. Asano, R. Iravani, and C. Marnay, "MicroGrids," *IEEE Power and Energy Magazine*, vol. 5, no. 4, pp. 78 – 94, 2007.

[16] R. Lasseter, "MicroGrids," in *Proceedings of the IEEE Power Engineering Society Transmission and Distribution Conference*, (New York, United states), pp. 305–308, January 2002.

[17] R. Lasseter and P. Piagi, "Control and design of MicroGrid components," tech. rep., Power Systems Engineering Research Center, January 2006. `http://www.pserc.org/cgi-pserc/getbig/publicatio/reports/2006report/lasseter_microgridcontrol_final_project_report.pdf`.

[18] New Energy and Industrial Technology Development Organisation (NEDO). Web page. `http://www.nedo.go.jp/english/archives/171129/171129.html`, Last accessed, August 2009.

[19] Y. Fujioka, H. Maejima, S. Nakamura, Y. Kojima, M. Okudera, and S. Uesaka, "Regional power grid with renewable energy resources: A demonstrative project in Hachinohe," in *CIGRÉ Sessions*, (Paris, France), August 2006.

[20] M. Geidl and G. Andersson, "A modeling and optimization approach for multiple energy carrier power flow," in *IEEE Power Engineering Society PowerTech*, (St. Petersburg, Russia), 2005.

[21] S. Papathanassiou, N. Hatziargyriou, and K. Strunz, "A benchmark low voltage MicroGrid network," in *Proceedings of the CIGRÉ Symposium: Power Systems with Dispersed Generation*, (Athens, Greece), 2005.

[22] G. W. Stagg and A. H. El-Abiad, *Computer methods in power system analysis.* McGraw-Hill series in electronic systems, New York, United States: McGraw-Hill, Inc., second ed., 1968.

[23] K. Warwick, A. Ekwue, and A. R., *Artificial intelligence techniques in power systems.* IEE Power Engineering Series, London: Institution of Electrical Engineers, 1997.

[24] M. S. and K. Bollinger, "Applications of artificial intelligence in power systems," *Electric Power Systems Research*, vol. 41, no. 2, pp. 117–131, 1997.

[25] W. Anis-Ibrahim and M. Morcos, "Artificial intelligence and advanced mathematical tools for power quality applications: A survey," *IEEE Transactions on Power Delivery*, vol. 17, no. 2, pp. 668–673, 2002.

[26] Z. Zhang, G. Hope, and M. O.P., "Expert systems in electric power systems - A bibliographical survey," *IEEE Transactions on Power Systems*, vol. 4, no. 4, pp. 1355–1362, 1989.

[27] A. Germond and D. Niebur, "Survey of knowledge-based systems in power systems: Europe," *Proceedings of the IEEE*, vol. 80, no. 5, pp. 732–744, 1992.

[28] D. Srinivasan, A. Liew, and C. Chang, "Applications of fuzzy systems in power systems," *Electric Power Systems Research*, vol. 35, no. 1, pp. 39–43, 1995.

[29] R. Bansal, "Bibliography on the fuzzy set theory applications in power systems (1994-2001)," *IEEE Transactions on Power Systems*, vol. 18, no. 4, pp. 1291–1299, 2003.

[30] D. Luenberger, *Linear and nonlinear programming.* Addison-Wesley, second ed., 1989.

[31] Fair Isaac Corporation, *Xpress-Optimizer, Reference manual, Release 20.0*, 2009.

[32] Fair Isaac Corporation, *XPress-SLP Program Reference Manual, Release 1.41*, 2008.

[33] M. Chaudry, N. Jenkins, and G. Strbac, "Multi-time period combined gas and electricity network optimisation," *Electric power systems Research*, vol. 78, no. 7, pp. 1265–1279, 2008.

[34] M. Chaudry, *Interactions between gas and electricity networks.* PhD thesis, University of Manchester, June 2010.

[35] The Consortium for Electric Reliability Technology Solutions (CERTS). Web page. `http://certs.lbl.gov/certs-der.html`, Last accessed, August 2009.

[36] N. Hatziargyriou, A. Dimeas, A. Tsikalakis, J. Pecas Lopes, G. Kariniotakis, and J. Oyarzabal, "Management of MicroGrids in market environment," in *International Conference on Future Power Systems*, (Amsterdam, Netherlands), 2005.

[37] S. Chatzivasiliadis, N. Hatziargyriou, and A. Dimeas, "Development of an agent based intelligent control system for MicroGrids," in *IEEE Power and Energy Society General Meeting: Conversion and Delivery of Electrical Energy in the 21st Century*, (Pittsburgh, United states), August 2008.

[38] J. Oyarzabal, J. Jimeno, J. Ruela, A. Engler, and C. Hardt, "Agent based micro grid management system," in *International Conference on Future Power Systems*, (Amsterdam, Netherlands), November 2005.

[39] N. Jayawarna, X. Wu, V. Zhang, N. Jenkins, and M. Barnes, "Stability of a MicroGrid," in *The 3rd IET International Conference on Power Electronics, Machines and Drives*, (Dublin, Ireland), pp. 316 – 320, 2006.

[40] J. P. Lopes, C. Moreira, and A. Madureira, "Defining control strategies for MicroGrids islanded operation," *IEEE Transactions on Power Systems*, vol. 21, no. 2, pp. 916 – 924, 2006.

[41] P. Kundur, *Power System Stability and Control.* The EPRI Power System Engineering Series, New York, United States: McGraw-Hill, Inc., 1994.

[42] A. Engler and N. Soultanis, "Droop control in LV-grids," in *International Conference on Future Power Systems*, (Amsterdam, Netherlands), 2005.

[43] A. Arulampalam, M. Barnes, A. Engler, A. Goodwin, and N. Jenkins, "Control of power electronic interfaces in distributed generation MicroGrids," *International Journal of Electronics*, vol. 91, no. 9, pp. 503 – 523, 2004.

[44] J. Pecas Lopes, C. Moreira, A. Madureira, F. Resende, X. Wu, N. Jayawarna, Y. Zhang, N. Jenkins, F. Kanellos, and N. Hatziargyriou, "Control strategies for MicroGrids emergency operation," in *International Conference on Future Power Systems*, (Amsterdam, Netherlands), 2005.

[45] M. Chandorkar, D. Divan, and R. Adapa, "Control of parallel connected inverters in standalone AC supply systems," *IEEE Transactions on Industry Applications*, vol. 29, pp. 136–143, Jan/Feb 1993.

[46] N. Jayawarna, N. Jenkins, M. Barnes, M. Lorentzou, S. Papthanassiou, and N. Hatziagyriou, "Safety analysis of a MicroGrid," in *International Conference on Future Power Systems*, (Amsterdam, Netherlands), 2005.

[47] J. A. Baroudi, V. Dinavahi, and A. M. Knight, "A review of power converter topologies for wind generators," *Renewable Energy*, vol. 32, no. 14, pp. 2369 – 2385, 2007.

[48] C. Moreira, F. Resende, and J. Pecas-Lopes, "Using low voltage MicroGrids for service restoration," *IEEE Transactions on Power Systems*, vol. 22, no. 1, pp. 395 – 403, 2007.

[59] J. Winberg, "On hot water storage in district heating subscriber stations," tech. rep., Lund Institute of Technology, Lund, Sweden, June 1998.

[60] V. Stevanovic, S. Prica, B. Maslovarica, B. Zivkovica, and S. Nikodijevic, "Efficient numerical method for district heating system hydraulics," *Energy Conversion and Management*, vol. 48, no. 8, 2007.

[61] A. Benonysson, *Dynamic modelling and operational optimization of district heating systems,*. PhD thesis, Laboratory of Heating and Air Conditioning, Technical University of Denmark, September 1991.

[62] B. Bøhm, S. Ha, W. Kim, B. Kim, T. Koljonen, H. Larsen, M. Lucht, Y. Oark, K. Sipilä, M. Wigbels, and M. Wistvacka, "Simple models for operational optimisation," tech. rep., IEA District heating and cooling, Annex VI, April 2002.

[63] S. Liew and G. Strbac, "Maximising penetration of wind generation in existing distribution networks," *IEE Proceedings: Generation, Transmission and Distribution*, vol. 149, pp. 256–262, May 2002.

[64] A. Shafiu, T. Bopp, I. Chilvers, G. Strbac, N. Jenkins, and H. Li, "Active management and protection of distribution networks with distributed generation," in *IEEE Power Engineering Society General Meeting*, vol. 1, (Denver, CO, United states), pp. 1098 - 1103, 2004.

[65] C. Oats, A. Barlow, and V. Levi, "Tap changer for distributed power," in *19th International Conference on Electricity Distribution*, (Vienna, Austria), CIRED, May 2007.

[66] N. Jenkins, R. Allan, P. Crossly, D. Kirschen, and G. Strbac, *Embedded Generation.* IEE Power and Energy Series, London, UK: Institution of Electrical Engineers, 2000.

[67] B. Weedy and B. Cory, *Electric Power Systems.* Chichester, UK: John Wiley & Sons, fourth ed., 1998.

[68] E. Mogos and X. Guillaud, "A voltage regulation system for distributed generation," in *IEEE PES Power Systems Conference and Exposition*, (New York, United states), pp. 787 - 794, 2004.

[69] L. Kojovic, "Impact of DG on voltage regulation," in *Proceedings of the IEEE Power Engineering Society Transmission and Distribution Conference*, vol. 1, (Chicago, United States), pp. 97 – 102, 2002.

[70] T. Kim and J. Kim, "Voltage regulation coordination of distributed generation system in distribution system," in *Proceedings of the IEEE Power Engineering Society Transmission and Distribution Conference*, (Vancouver, Canada), pp. 480 – 484, 2001.

[71] D. Gaonkar, P. Rao, and R. Patel, "Hybrid method for voltage regulation of distribution system with maximum utilization of connected distributed generation source," in *IEEE Power India Conference*, (New Delhi, India), pp. 261 – 265, 2005.

[72] R. Shuttleworth, X. Tian, C. Fan, and A. Power, "New tap changing scheme," *IEE Proceedings: Electric Power Applications*, vol. 143, no. 1, pp. 108 – 112, 1996.

[73] M. Roberts and W. Ashman, "A thyristor assisted mechanical on-load tap changer," in *Proceedings of IEE conference on Power thyristors and their applications*, pp. 185 – 192, 1969.

[74] G. Cooke and K. Williams, "New thyristor assisted diverter switch for on load transformer tap changers changers," *IEE Proceedings: Electric Power Applications*, vol. 139, no. 6, pp. 507 – 511, 1992.

[75] C. Dai and Y. Baghzouz, "Impact of distributed generation on voltage regulation by LTC transformer," in *11th International Conference on Harmonics and Quality of Power*, (Lake Placid, United states), pp. 770 – 773, 2004.

[76] C. Dai and Y. Baghzouz, "On the voltage profile of distribution feeders with distributed generation," in *IEEE Power Engineering Society General Meeting*, vol. 2, (Toronto, Ont., Canada), pp. 1136 – 1140, 2003.

[77] R. Dugan, S. Santoso, M. McGranaghan, and H. Beaty, *Electric power system quality.* McGraw-Hill, second ed., November 2002.

[78] M. Fila, G. Taylor, J. Hiscock, M. Irving, and P. Lang, "Flexible voltage control to support distributed generation in distribution networks," in *Universities Power Engineering Conference, UPEC*, September 2008.

[79] J.-H. Choi and J.-C. Kim, "Advanced voltage regulation method of power distribution systems interconnected with dispersed storage and generation systems (revised)," *IEEE Transactions on Power Delivery*, vol. 16, no. 2, pp. 329 – 334, 2001.

[80] V. Thornly, N. Jenkins, P. Reay, J. Hill, and C. Barbier, "Field experience of active network management of distribution networks with distributed generation," in *19th International Conference on Electricity Distribution*, (Vienna, Austria), CIRED, May 2007.

[81] P. Piagi and R. H. Lasseter, "Autonomous control of MicroGrids," in *IEEE Power Engineering Society General Meeting*, (Montreal, Canada), 2006.

[82] A. Wright and S. Firth, "The nature of domestic electricity-loads and effects of time averaging on statistics and on-site generation calculations," *Applied Energy*, vol. 84, no. 4, pp. 389 – 403, 2007.

[83] "Voltage characteristics of electricity supplied by public distribution systems, EN50160," European Committee for Electrotechnical Standardisation, 2000.

[84] I. Erinmez, D. Bickers, G. Wood, and W. Hung, "NGC experience with frequency control in England and Wales - provision of frequency response by generators," in *IEEE Engineering Society Winter Meeting*, vol. 1, (New York, NY, USA), pp. 590 – 596, 1999.

[85] M. Geidl, *Integrated Modeling and Optimization of Multi-Carrier Energy Systems.* PhD thesis, Power Systems Laboratory, ETH Zurich, 2007.

[86] M. Geidl and G. Andersson, "Optimal coupling of energy infrastructures," in *IEEE Power Engineering Society PowerTech*, (Lausanne, Switzerland), 2007.

[87] M. Geidl and G. Andersson, "Operational and structural optimization of multi-carrier energy systems," *European Transactions on Electrical Power*, vol. 16, no. 5, pp. 463–477, 2006.

[88] M. Geidl and G. Andersson, "Operational and topological optimization of multi-carrier energy systems," in *International Conference on Future Power Systems*, (Amsterdam, Netherlands), 2005.

[89] M. Geidl and G. Andersson, "Optimal power dispatch and conversion in systems with multiple energy carriers," in *15th Power Systems Computation Conference, PSCC*, (Liege, Belgium), 2005.

[90] M. Geidl and G. Andersson, "Optimal power flow of multiple energy carriers," *IEEE Transactions on Power Systems*, vol. 22, no. 1, pp. 145–155, 2007.

[91] S. An, Q. Li, and T. W. Gedra, "Natural gas and electricity optimal power flow," in *Proceedings of the IEEE Power Engineering Society Transmission and Distribution Conference*, vol. 1, (Dallas, United States), pp. 138 - 143, 2003.

[92] C. Unsihuay, J. Lima, and A. De Souza, "Modeling the integrated natural gas and electricity optimal power flow," in *IEEE Power Engineering Society General Meeting*, pp. 1 –7, June 2007.

[93] Elexon, "Pricing data." Web page. `http://www.elexon.co.uk/marketdata/creditdata/pricingdata.aspx`, Last accessed, March 2010.

[94] The National Grid Company, "Operational data." Web page. `http://marketinformation.natgrid.co.uk/gas/DataItemExplorer.aspx`, Last accessed, March 2010.

[95] "System integration of additional MicroGeneration," tech. rep., The UK Department of Trade and Industry, September 2004. `http://www.berr.gov.uk/files/file15192.pdf`.

[96] G. Moore, *Electric cables handbook / BICC Cables.* Oxford, UK: Blackwell Science, third ed., 1997.

Appendix A

Analysis of Pipe Networks

A.1 Pressure drop in pipes

Figure A.1 shows a water pipe. In this figure, $\dot{m}$ is the water mass flow rate, v is the flow velocity, p is the static pressure, z is the altitude, A is the pipe cross-sectional area, and D is the pipe diameter. The subscripts 1 and 2, where used, denote the point at which these parameters are defined. Steady fully developed flow is assumed.

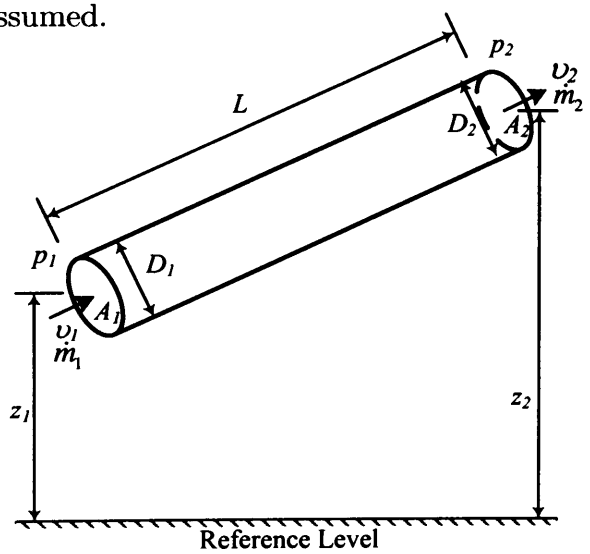

Figure A.1: Steady Incompressible Viscous Flow in a Pipe

Fluid flow in this pipe is subject to Bernoulli Equation. This is illustrated by Equation A.1 where h_l is the static head loss due to friction and viscosity.

$$\left(p_1 + \frac{1}{2}\rho v_1^2 + \rho g z_1\right) - \left(p_2 + \frac{1}{2}\rho v_2^2 + \rho g z_2\right) = p_l \qquad \text{(A.1)}$$

Reynolds number, Re, is used to determine the nature of the flow in this pipe. This number is calculated by Equation A.2 ρ is the density of the fluid, μ is its dynamic viscosity, and v is its kinematic viscosity. The flow is laminar at low values of Reynolds number, $Re \leq 2320$; turbulent at high values, $Re \geq 4000$; and transitional between these two ranges [50].

$$Re = \frac{\rho V D}{\mu} = \frac{V D}{v} \tag{A.2}$$

Head and pressure loss in this pipe, h_l and p_l, are functions of the Darcy friction factor,f. The Darcy friction factor for laminar flow is determined by Reynolds number only, equation A.3. For turbulent flow the value of the friction factor depends on Reynolds number, the pipe diameter, and the roughness of the internal surface of the pipe, ϵ. This is shown by equation A.4. For transitional flow, a linear interpolation between the values calculated from equations A.3 and A.4 is used to determine the friction factor. The plot of these relations, the Moody Chart, is shown in Figure A.2.

$$f = \frac{64}{Re} \tag{A.3}$$

$$\frac{1}{\sqrt{f}} = -2 \log \left(\frac{\epsilon}{3.71D} + \frac{2.51}{Re} \frac{1}{\sqrt{f}} \right) \tag{A.4}$$

As shown in A.2, as the turbulence increases, the Darcy friction factor saturates. At high turbulence, which is often the case encountered in district heat systems, this value becomes constant. This is shown by Equation A.5.

$$f = \left(\frac{1}{-2 \log \left(\frac{\epsilon}{3.71D} \right)} \right)^2 \tag{A.5}$$

The static head loss is calculated from Darcy's equation, equation A.6. As the mass flow rate, $\dot{m}$, is a function of the flow velocity, the water density, and the pipe diameter, Darcy's equation is re-written as Equation A.7.

$$h_l = f \frac{L}{D} \frac{1}{2g} V^2 \tag{A.6}$$

$$h_l = f \frac{8L}{\pi^2 \rho^2 g D^5} \dot{m}^2 \tag{A.7}$$

The equivalent static pressure loss, p_l, associated with this head loss is given

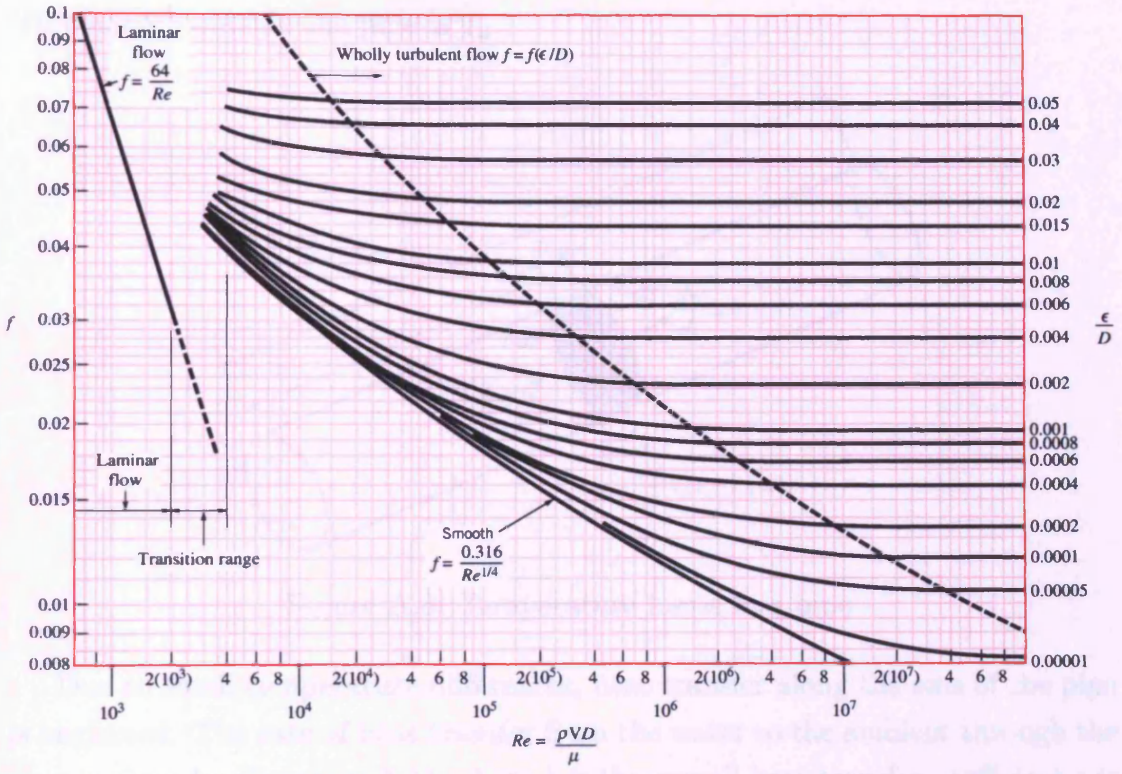

Figure A.2: The Moody chart [50]

by equation 2.3. This is expressed as a function of the flow rate by equation A.9 where r_l is a factor expressing the hydraulic resistance of the pipe. This factor, calculated from equation A.10, is constant at high turbulence.

$$p_l = \rho g h_l \tag{A.8}$$

$$p_l = r_l \dot{m}^2 \tag{A.9}$$

$$r_l = \left(\frac{1}{-2 \log\left(\frac{\epsilon}{3.71D}\right)} \right)^2 \frac{8L}{\pi^2 \rho D^5} \tag{A.10}$$

A.2 Temperature drop in pipes

Figure A.3 shows a cylindrical element of water in a water pipe. The element length is dx. The temperature of the water in this element is T, The temperature of the water at both sides of this element are $T + dT$ and $T - dT$. The ambient

temperature outside the pipe is T_a.

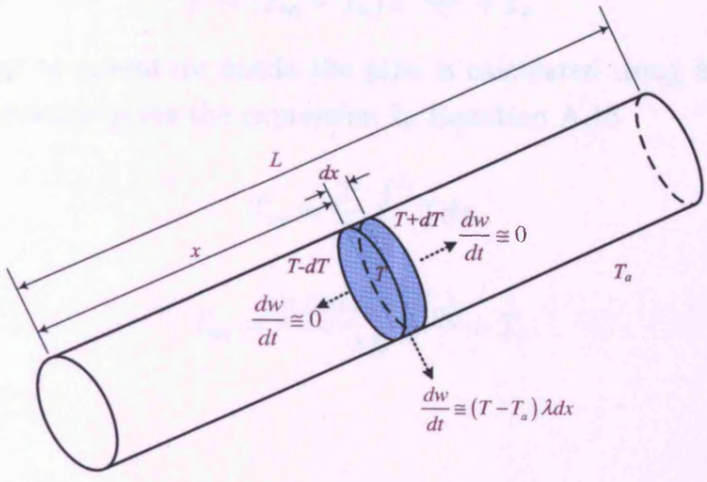

Figure A.3: Temperature losses in a pipe

Due to small temperature differences, heat transfer along the axis of the pipe is neglected. The rate of heat transfer from the water to the ambient through the pipe is given by Equation A.11 where λ is the overall heat transfer coefficient per unit length of the pipe, measured in W/m°C.

$$\frac{dw}{dt} = (T - T_a)\,\lambda dx \tag{A.11}$$

This heat transfer will cause the temperature of the water to change as shown in Equation A.13 where c_p is the specific heat of water and dm is the mass of the water in this element.

$$dw = -c_p dm dT \tag{A.12}$$

Solving the two equations, Equation A.11 and Equation A.13, gives the temperature of water as a function of time. This is shown by Equation

$$T = (T - T_a)\,e^{-\frac{\lambda dx}{c_p m}t} + T_a \tag{A.13}$$

In a pipe in a district heat system, this element enters the pipe at temperature T_{in} and exits it at temperature T_{out}. The time required for the element to travel from the entrance to the exit is determined by the velocity of the water, dx/dt, and the length of the pipe, L. This time is then given by $\frac{L}{dx/dt}$.

The temperature at the exit of the pipe is then given by Equation A.16 where $\dot{m} = \frac{dm}{dt}$ is the mass flow rate of the water.

$$T = (T_{in} - T_a)\, e^{-\frac{\lambda L}{c_p \dot{m}}} + T_a \tag{A.14}$$

The average temperature inside the pipe is calculated using Equation A.15. Solving this equation gives the expression in Equation A.16

$$T_{av} = \frac{1}{L} \int_0^L T dx \tag{A.15}$$

$$T_{av} = \frac{c_p \dot{m}\,(T_i - T_o)}{\lambda L} + T_a \tag{A.16}$$

Appendix B

Data for the Energy MicroGrid Model

Table B.1: Data of the lines in the CIGRÉ benchmark network lines

Line type	R_{ph} Ω/km	X_{ph} Ω/km	$R_{neutral}$ Ω/km	R_0 Ω/km	X_0 Ω/km
OL-Twisted cable 4×120mm^{2}Al	0.284	0.083		1.136	0.417
OL-Twisted cable 3×70mm^{2}Al + 54.6mm^2 AAAC	0.497	0.086	0.630	2.387	0.447
OL-Al conductors 4×50mm^2 equiv. Cu	0.397	0.279			
OL-Al conductors 4×35mm^2 equiv. Cu	0.574	0.294			
OL-Al conductors 4×16mm^2 equiv. Cu	1.218	0.318			
UL-3×150mm^{2}Al + 50 mm^{2}Cu	0.264	0.071	0.387		
SC-4×6mm^{2}Cu	3.690	0.094		13.64	0.472
SC-4×16mm^{2}Cu	1.380	0.082		5.25	0.418
SC-4×25mm^{2}Cu	0.871	0.081		3.48	0.409
SC-3×50mm^{2}Al + 35mm^{2}Cu	0.822	0.077	0.524	2.04	0.421
SC-3×95mm^{2}Al + 34mm^{2}Cu	0.410	0.071	0.524		

Table B.2: Data of the Pipes of the District Heat System

From node	To node	Length	Diameter	Roughness	Conductivity
1	2	140	0.3	0.00125	0.00025
2	3	70	0.3	0.00125	0.00025
3	4	70	0.3	0.00125	0.00025
2	5	70	0.2	0.00125	0.00035
3	6	30	0.2	0.00125	0.00035
4	7	70	0.2	0.00125	0.00035
4	8	30	0.2	0.00125	0.00035

Appendix C

Derivation of The OLTC Deadband

To calculate the reactive power deadband, the MicroGrid was simlified into the approximate system shown in figure C.1 where all MicroSources and loads were lumped into one equivalent MicroSource and one load connected at the same busbar. This busbar is connected to an MV network via an LV feeder and and an ideal transformer.

The total load power $P_{L_t} + jQ_{L_t}$ and MicroSource output is $P_{MS_t} + jQ_{MS_t}$. The inverse of the droop line slope of the equivalent MicroSource, k_{MS_t} is given by equation C.1 where $\mathbb{MS}$ is the set of all MicroSources in the MicroGrid. The parameters of the feeder connecting them to the transformer were assumed to be equal to the total resistance, R, and reactance, X, of the path from the Control MicroSource, MS_C, to the MV network.

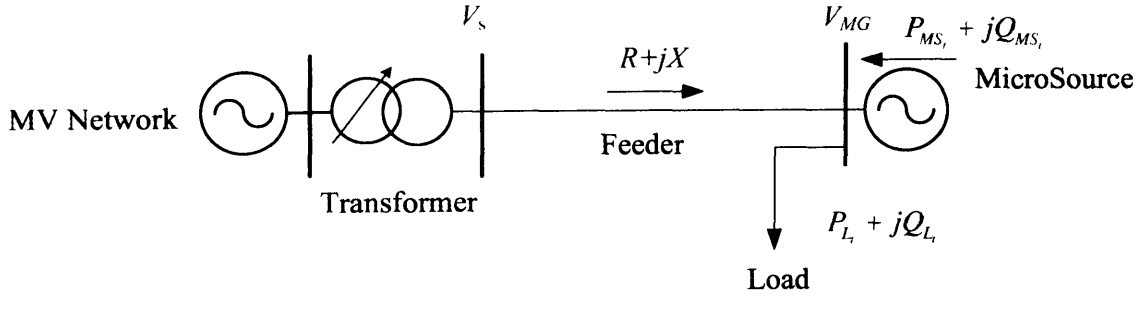

Figure C.1: Simplified MicroGrid

$$k_{MS_t} = \sum_{i \in \mathrm{MS}} k_i \tag{C.1}$$

The approximate value of the voltage V_{MG} is given by equation C.2.

$$V_{MG} = V_s + \frac{(P_{MS_t} - P_{L_t})\,R + (Q_{MS_t} - Q_{L_t})\,X}{V_L} \tag{C.2}$$

As the equivalent MicroSource is controlled by droop, its reactive power output is given by equation C.3 where V_0 is the nominal voltage.

$$Q_{MS_t} = -k_{MS_t}\,(V_{MG} - V_0) \tag{C.3}$$

Solving equations C.2 and C.3, the load voltage will be given by equation C.4 and its derivative with respect to the supply voltage, V_s by equation C.5.

$$V_{MG} = \frac{V_s - k_{MS_t}X}{2} + \sqrt{\left(\frac{V_s - k_{MS_t}X}{2}\right)^2 + (P_{MS_t} - P_{L_t})\,R - Q_{L_t}X + k_{MS_t}V_0X} \tag{C.4}$$

$$\frac{dV_{MG}}{dV_s} = \frac{1}{2} + \frac{\frac{V_s - k_{MS_t}X}{2}}{2\sqrt{\left(\frac{V_s - k_{MS_t}X}{2}\right)^2 + (P_{MS_t} - P_{L_t})\,R - Q_{L_t}X + k_tV_0X}} \tag{C.5}$$

Assuming no load and no active power generation, equation C.5 is rewritten as:

$$\frac{dV_{MG}}{dV_s} = \frac{1}{2} + \frac{\frac{V_s - k_{MS_t}X}{2}}{2\sqrt{\left(\frac{V_s - k_{MS_t}X}{2}\right)^2 + k_{MS_t}V_0X}} \tag{C.6}$$

Since $\frac{dQ_{MS_t}}{dV_{MG}} = -k_{MS_t}$, $\frac{dQ_{MS_t}}{dV_s}$ will be given by

$$\frac{dQ_{MS_t}}{dV_s} = -k_{MS_t}\left(\frac{1}{2} + \frac{V_s - k_{MS_t}X}{2\sqrt{(V_s - k_{MS_t}X)^2 + 4k_{MS_t}V_0X}}\right) \tag{C.7}$$

And the change in reactive power generation ΔQ_{MS_t} due to a change in source power ΔV_s is

$$\Delta Q_{MS_t} = -k_{MS_t}\left(\frac{1}{2} + \frac{V_s - k_{MS_t}X}{2\sqrt{(V_s - k_{MS_t}X)^2 + 4k_{MS_t}V_0X}}\right)\Delta V_s \qquad \text{(C.8)}$$

As this change is shared among all MicroSources according to their droop line slopes, the corresponding change in the reactive power output of the control MicroSource is

$$\Delta Q_{MS_C} = -\frac{k_{MS_C}}{2}\left(1 + \frac{V_s - X\sum_{i\in\mathbf{MS}} k_i}{\sqrt{\left(V_s - X\sum_{i\in\mathbf{MS}} k_i\right)^2 + 4V_0X\sum_{i\in\mathbf{MS}} k_i}}\right)\Delta V_s \qquad \text{(C.9)}$$

Appendix D

Data for the Voltage Control Case Study

The active and reactive power limits that were used for the MicroSources in the MicroGrid system for the case study in Chapter 3 are given in Tables D.1 and D.2. The thermal limits of the cables connecting the MicroSources in MG_1 as calculated from [96] are given table D.1. Table D.3 shows the parameters used for the voltage control system as well as the normalisation and weighing factors for both MicroGrids.

Table D.1: Active and reactive power limits for MicroSources in MG_1

Busbar to which the MicroSource is connected	P_{max} kW	Q_{max} kVAr	Thermal limit of the service cable kW
14	150	±10	80
15	100	±3	46
16	250	±20	104
17	200	±30	104
19	250	±30	80

The thermal limits and the maximum possible voltage for different sections of the MicroGrid MG_1 are given in Table D.4. The maximum possible voltage difference between each two MicroSources in this MicroGrid are calculated in Table D.5. The mean value and the standard deviation of these voltage differences are given in the same table. Based on these values, MS_{16} was chosen to be the Control MicroSource for MG_1

Table D.2: Active and reactive power limits for MicroSources in MG_2

Busbar to which the MicroSource is connected	P_{max} kW	Q_{max} kVAr	Thermal limit of the service cable* kW
24	300	±60	80
28	150	±20	80
30	150	±20	80
31	300	±30	80

* MicroSources are assumed to be connected to the MicroGrid through a 4×16mm^2 Cu.

Table D.3: The parameters of the voltage control system

			MG_1	MG_2
Control MicroSource at busbar			16	24
Deadband		kVAr	±4.5	±9.8
Power compensation factor	p_{cf}	kVAr/kW	0.0752	0.0417
Normalisation factor	n		$\frac{80}{30}$	$\frac{50}{30}$
Weighing factor	w		$\frac{93}{213}$	$\frac{120}{213}$

Table D.4: Maximum voltage drop across links of cables and feeders in MG_1

Line		Resistance R_l	Thermal limit P_{l-max}	Maximum voltage drop ΔV_{l-max}
From	To	p.u.	p.u.	p.u.
1	4	0.07455	0.455	0.03392
4	6	0.0497	0.455	0.022614
6	8	0.07455	0.315	0.023483
8	14	0.1532	0.200	0.03064
8	15	0.27675	0.115	0.031826
6	16	0.065325	0.260	0.016985
4	17	0.192111	0.260	0.049949
4	19	0.1035	0.200	0.0207

Table D.5: Maximum voltage difference between MicroSources in MG_1

	MS_1	MS_{14}	MS_{15}	MS_{16}	MS_{17}	MS_{19}
MS_1		0.1107	0.1118	0.0735	0.0839	0.0546
MS_{14}	0.1107		0.0625	0.0711	0.1267	0.0974
MS_{15}	0.1118	0.0625		0.0723	0.1279	0.0986
MS_{16}	0.0735	0.0711	0.0723		0.0896	0.0603
MS_{17}	0.0839	0.1267	0.1279	0.0895		0.0706
MS_{19}	0.0546	0.0974	0.0986	0.0603	0.0706	
$\overline{\Delta V}_{MS_iMS_j-max}\big\vert_{MS_i}$	0.0869	0.0937	0.0946	0.0734	0.0997	0.0763
$\sigma\left(\Delta V_{MS_iMS_j-max}\right)\big\vert_{MS_i}$	0.0220	0.0240	0.0243	0.0094	0.0233	0.0185
$\overline{\Delta V}_{MS_iMS_j-max}\big\vert_{MS_i}$ $+2\,\sigma\left(\Delta V_{MS_iMS_j-max}\right)\big\vert_{MS_i}$	0.1309	0.1416	0.1432	* 0.0921	0.1464	0.1132

* MS_{16} was chosen as the Control MicroSource
Values are in p.u.

Appendix E

Calculation of Load Profiles for Individual Consumers

The CIGRÈ MicroGrid benchmark model [21] includes a set of daily load curves for different types of loads. Since the Energy MicroGird considered in this research was assumed to be serving a residential area, only the residential load profile was considered.

Each set of consumers connected to the same busbar in the CIGRÈ benchmark MicroGrid was described by two values. The first value is S_{max} which defines the maximum possible demand for this set of consumers. The other value is S_0 which defines the average demand of this set of consumers around 9pm when the total electricity demand in the MicroGrid exhibits its maximum value. In cases where more than one consumer was connected to the same busbar, these values were assumed to be shared equally among the consumers.

The peak demand in the MicroGrid in this case will be given by Equation E.1.

$$S_{Peak} = \sum S_0 \tag{E.1}$$

The daily load curve described in [21] for residential loads specifies the 1-hour averages for the aggregated demand as a percentage of the peak demand. This curve was used to produce individual load curves for each consumer using the following steps.

The 1-hour average value for the aggregated load was used to calculate a 1-hour average value for individual loads. In this case, at any time t, the 1-hour average for the demand of the consumer$i$ is given by Equation E.2 where $L_f(t)$

is the percentage loading at this time as defined on the daily load curve.

$$S_i(t)|_{1-hour} = L_f(t) \times \frac{S_{0_i}}{S_{Peak}} \tag{E.2}$$

To calculate the 15-minute average demand for each consumer a random number, R_{1i}, was generated for each consumer. R_{1i} was chosen from a normal distribution with average value of 1 and a standard deviation of 0.2. These numbers were chosen arbitrarily. This choice guarantees that $0.4 \leq R_{1i} \leq 1.6$ for 99.5% of the cases. The 15-minute average was calculated using Equation E.3

$$S_i(t)|_{15-min} = R_{1i}\, S_i(t)|_{1-hour} \tag{E.3}$$

The 1-minute average demand for each consumer was calculated in the same way as the 15-minute average demand. A number R_{2i} was chosen randomly from a normal distribution with an average value of 1.0 and a standard deviation of 0.2. This number was used to calculate a 1-minute average demand for the consumer using Equation E.4.

$$S_i(t)|_{1-min} = R_{1i}\, S_i(t)|_{15-min} \tag{E.4}$$

A power factor of 0.85 for all domestic loads in the MicroGrid was specified in [21]. This power factor was used to calculate the active and reactive power demand of each consumer.

$$P_i(t)|_{1-min} = 0.85\, S_{2i}(t)|_{1-min} \tag{E.5}$$

$$Q_i(t)|_{1-min} = 0.53\, S_{2i}(t)|_{1-min} \tag{E.6}$$

The 1-min average of the demand of critical loads, $P_{i-critical}|_{1-min}$, was chosen from a uniform random distribution with a minimum of 0.2kW and a maximum of 0.3kW.

The 1-min average of the demand of non-critical loads was calculated using Equation E.7.

$$P_{i-non-critical}(t)|_{1-min} = P_i(t)|_{1-min} - P_{i-critical}(t)|_{1-min} \tag{E.7}$$

An example of the 1-min average demand for a single consumer in the MicroGrid is shown in Figure consumers is shown in Figure E.1. The total demand

variations in the MicroGrid are shown in Figure E.2.

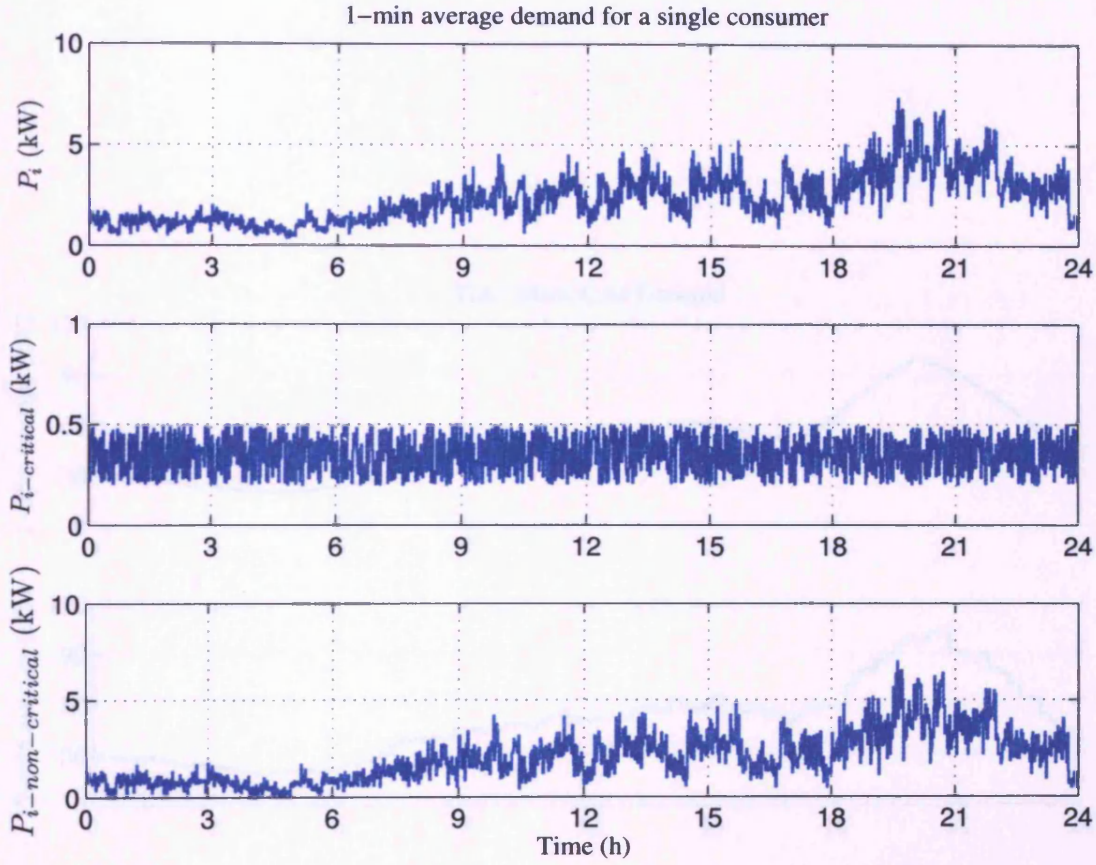

Figure E.1: Electricity demand of one consumer the MicroGrid

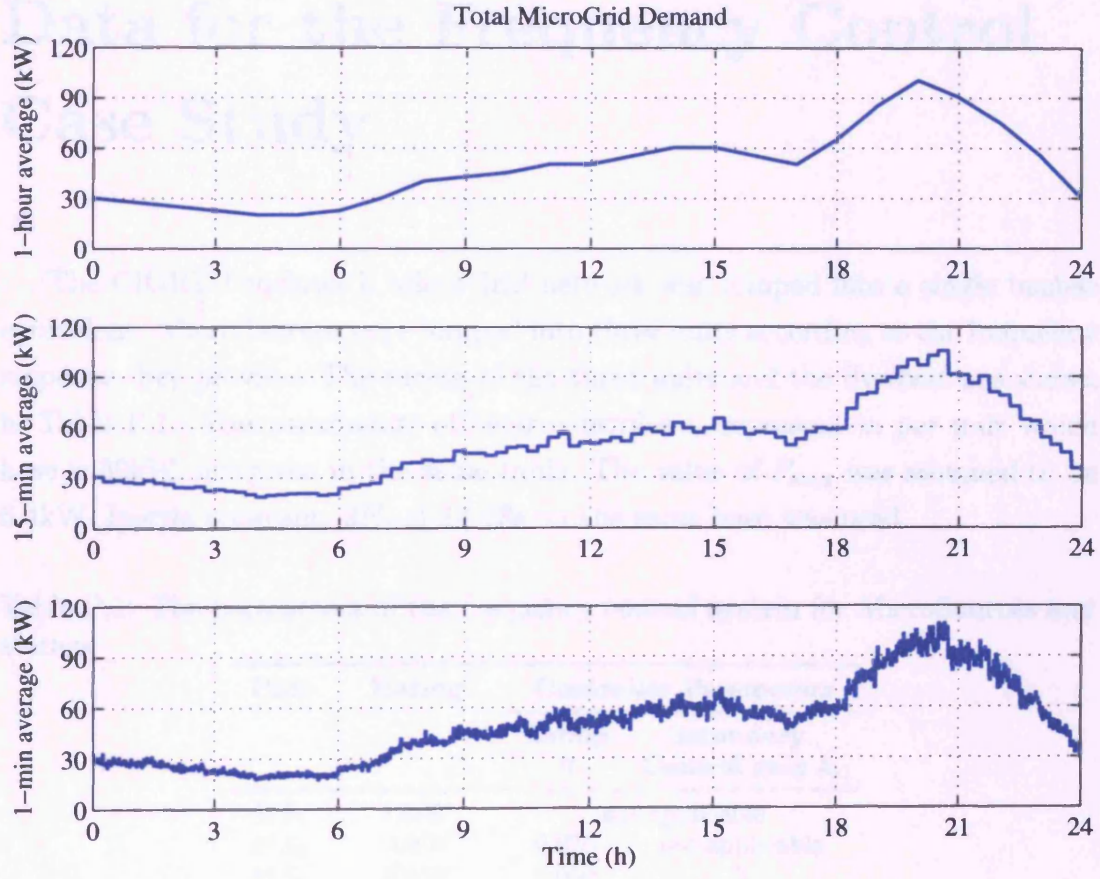

Figure E.2: Total electricity demand in the MicroGrid

Appendix F

Data for the Frequency Control Case Study

The CIGRÉ benchmark MicroGrid network was lumped into a single busbar equivalent. MicroSources were lumped into three units according to the frequency response they provide. The rating of the three units and the flywheel are shown in Table F.1. The parameters of their controllers, expressed in per unit which base is 30kW, are given in the same table. The value of P_{max} was assumed to be 6.4kW. Inertia constant, $2H_t$ of 14.43s on the same base was used.

Table F.1: The parameters of the frequency control system for MicroSources and storage

Unit	**Rating**	**Controller Parameters**	
		Droop R	**Secondary Control gain** k_s
MS_1	13kW	not applicable	
MS_2	20kW	0.075	not applicable
MS_3	30kW	0.050	3
FW	30kW/14MJ	0.050	0.3333×10^{-3}

The demand of different consumers used in Case study 4.5.2 is given in Table F.2. The initial values of the output of the three MicroSources used in this simulation are listed in table F.3.

The initial values of the historical unserved energy for different consumers that was used in section 4.5.3 are given in tale F.4. The initial output of MicroSources given in Table F.3 was used.

Table F.2: Demand used in Case study 4.5.2

Consumer	P_{nc} kW	P_c kW	Consumer	P_{nc} kW	P_c kW
1	5.0236	0.3299	14	1.6173	0.2178
2	7.7876	0.2678	15	2.0275	0.3809
3	5.4747	0.3739	16	3.0290	0.2151
4	4.4300	0.4281	17	3.9289	0.3246
5	4.8254	0.3589	18	3.8836	0.2915
6	2.0777	0.3922	19	2.8517	0.4623
7	3.3303	0.2627	20	3.6419	0.2045
8	2.6591	0.3139	21	2.5807	0.4304
9	3.8835	0.4350	22	2.9355	0.4913
10	2.2252	0.4043	23	3.7892	0.4970
11	2.9640	0.3383	24	3.1010	0.4367
12	2.3286	0.3703	25	3.6377	0.3316
13	4.2694	0.4383	26	5.5446	0.3495

Table F.3: Initial output of MicroSources for Case studies 4.5.2 and 4.5.3

Unit	Output kW
MS_1	0
MS_2	6
MS_3	6

Table F.4: Initial values the Historical Unserved Energy for Case study 4.5.3

Consumer	E_{us} kWh	Consumer	E_{us} kWh
1	11.7343	14	18.1473
2	7.51970	15	13.6963
3	8.35940	16	8.37650
4	15.0717	17	3.45180
5	6.18610	18	1.06080
6	18.0869	19	0.51740
7	0.43580	20	11.2340
8	8.27160	21	4.21670
9	12.5009	22	18.3749
10	0.15110	23	6.67480
11	12.6655	24	5.63240
12	0.43030	25	15.7310
13	10.9842	26	5.08960